Precise Motion Control of Hybrid Hydraulic Electric Architecture (HHEA)

A DISSERTATION

SUBMITTED TO THE FACULTY OF THE GRADUATE SCHOOL

OF THE UNIVERSITY OF MINNESOTA

BY

Arpan Chatterjee

IN PARTIAL FULFILLMENT OF THE REQUIREMENTS

FOR THE DEGREE OF

DOCTOR OF PHILOSOPHY

Dr. Perry Li

July, 2023

Acknowledgements

I am grateful to have the opportunity to pursue my Ph.D. at this prestigious institution and would like to take this opportunity to express my heartfelt gratitude to the people who have supported me throughout this journey.

First and foremost, I would like to thank my advisor, Dr. Perry Li, for his guidance, support, and encouragement throughout my research. His deep expertise, insights, and attention to detail have been invaluable to me, and I have learned so much from him. His enthusiasm for research has been infectious, and I am deeply grateful for the opportunity to work with him. Without his persuasion, I would have never been able to pursue this journey.

I would like to express my sincere gratitude to my committee members, Dr. Jim Van de Ven, Dr. Kim Stelson, and Dr. Donatello Materassi, for their valuable guidance and input throughout this project.

I would also like to extend my heartfelt thanks to our industry partner, Danfoss, for their collaboration and support. In particular, I am deeply grateful to Dr. Rachel Wang for her industry insights, collaboration, and guidance throughout the entire duration of the project. I would also like to acknowledge the contributions

of Aaron Jagoda and Dr. Mohd Zulkefli Azrin for their collaboration in building a high-pressure testbed at their facility.

I am grateful to the U.S. Department of Energy for their funding support for both projects: EE0008384 and EE0009875.

A special note of appreciation goes to my fellow lab members for their camaraderie, assistance, and stimulating discussions.

I would like to extend my heartfelt gratitude to all the friends I made in Minneapolis, whose presence has been invaluable in helping me navigate life in a new country. Their support, kindness, and friendship have played an instrumental role in helping me adjust and feel at home. A sincere thank you goes to my friends back in India, who have always believed in me, and no matter the physical distance, they have always been there for me, cheering me on and sharing in my accomplishments.

I am immensely grateful for Sneha's unwavering support and encouragement during my Ph.D. journey. She has been a trusted friend and companion with whom I've shared countless adventures and joyful experiences. I am thankful to her for always having my back; her words of motivation, and positive energy have been invaluable sources of inspiration.

I am deeply grateful for the presence of my twin brother, Arkan, in my life. He has been more than just a sibling; he has been my confidante, a source of fun and laughter, and someone who I can rely on. His unwavering support and genuine friendship have been instrumental in shaping who I am today, and I am incredibly thankful to have him by my side. I am also thankful to his wife, my sister-in-law,

Beepa, for the love, warmth, and care she brings to our family.

I am deeply grateful to my cousins, uncles, and aunts for their unwavering belief in me and I cherish the strong bond that we share. The love and camaraderie we share create a sense of belonging and make life's joys even sweeter. I am thankful for their presence in my life and the lasting impact they have had on my personal growth.

Lastly, I am profoundly indebted to my parents and both grandmothers for their immeasurable contributions to my life. Their unwavering love, support, and endless encouragement have been the bedrock of my achievements. Their selfless prayers, sacrifices, and dedication have shaped the person I am today, and I will forever be grateful for the boundless love and support they have bestowed upon me. Their presence in my life is a constant reminder of the strength and resilience that comes from a nurturing and supportive family, and I am eternally thankful for their unwavering belief in me.

Dedication

This thesis is dedicated to my grandmothers, Geeta Chattopadhyay and Rina Chowdhury, and my grandfathers, Sagar Chandra Chattopadhyay and Nirmalendu Chowdhury. Their unwavering love, support, and encouragement have been instrumental in shaping who I am today and have inspired me to pursue my dreams. My grandfathers were extraordinary role models of hard work and perseverance, and their unwavering determination to succeed has been a constant source of inspiration to me. They believed in the power of education as the greatest tool for personal and societal advancement, and their unrelenting hope for a better generation motivates me to work harder every day. Their dreams for me have always been bigger than what I could envision for myself, and their support and encouragement have been instrumental in shaping my aspirations and ambitions. I owe them an immeasurable debt of gratitude for the values they instilled in me and the opportunities they made possible. Their legacy will live on through my pursuits, and I am honored to dedicate this thesis to them. May their love continue to inspire me and guide me in all my future endeavors.

Abstract

Off-highway heavy-duty vehicles have been long-standing users of hydraulic systems for power transmission and control. However, traditional hydraulic systems suffer from significant energy losses which lead to increased operating costs and a larger carbon footprint due to higher CO_2 emissions. Improving the efficiency of these mobile machines is crucial not only for reducing their environmental impact but also for saving billions of dollars in operating costs. Currently, the state-of-the-art Load Sensing Architecture uses throttling valves for control, which significantly reduces its efficiency and does not recuperate energy from over-running loads. Researchers have developed several architectures such as Common Pressure Rail systems, Displacement Control, STEAM, and Electrohydraulic Architecture to improve the efficiency of off-road mobile machines. However, each of these architectures has its drawbacks. To increase system efficiency and take advantage of electrification benefits, our research group has developed a novel Hybrid Hydraulic-Electric Architecture (HHEA). The HHEA can significantly improve efficiency, decrease the size of electrical components, and maintain control performance. This new architecture has the potential to revolutionize the off-highway mobile machine industry and lead to a more sustainable future. The HHEA uses a set of common pressure rails to provide the majority of power to the actuators via power-dense hydraulics and uses electric motors for precise control and power modulation.

In the context of off-road mobile machines, energy savings are undoubtedly important but it is equally important to consider the machines' ability to perform tasks with precision and accuracy according to given commands. Therefore, precise motion control is of utmost importance to maintain the utility of Hybrid Hydraulic-Electric Architecture (HHEA). The HHEA presents a unique challenge to motion control due to the discrete pressure changes that occur when the system switches between selected pressure rails. These changes are made to minimize system inefficiencies or to keep the system within the torque capability of the electric motor. Hence, it is important to solve the motion control challenges for HHEA. This thesis aims at developing an effective motion control strategy for HHEA.

The dissertation presents a two-tiered control strategy for HHEA, comprising a high-level and a low-level controller. The primary responsibility of the high-level controller is to optimize energy efficiency by making informed pressure rail selections. On the other hand, the low-level controller is focused on achieving precise motion control of the HHEA, which is crucial for realizing the desired reference trajectories. To achieve this, the low-level controller utilizes a passivity-based backstepping integral controller as the nominal control, which handles the motion control between two pressure rail switches. Additionally, a separate least norm controller is utilized as a transition controller to manage motion control during pressure rail transitions. The effectiveness of the combined control strategy is demonstrated through experiments conducted on two hardware-in-the-loop testbeds.

Furthermore, the HHEA is installed on the boom and stick actuators of a

backhoe arm to build a Human-in-the-Loop system that a human operator can control. A real-time rail switching algorithm is developed to determine pressure rail switching based on present duty cycle information from the operator. Modifications have been made to the human-machine interface to achieve more intuitive control. Modifications include performing control in the task-oriented coordinates, incorporating pressure feedback to enhance control with physical interaction, and using velocity field control to simplify multi-degree-of-freedom tasks and to enable novice operators to perform them with reduced risk, improved efficiency, and productivity.

The research in this dissertation makes significant contributions to the field of off-road mobile machine control, providing a novel and effective control strategy for the HHEA, and demonstrating the potential for simplified machine operation.

Contents

List of Tables

List of Figures

Chapter 1

Introduction

Mobile hydraulics are extensively used in the construction and agriculture industry, which results in the emission of more than 26.32 million metric tons of CO_2 annually in the US alone [9]. The reduction of CO_2 emissions from these machines will be crucial in helping nations fulfill their obligations under the Paris Agreement in 2015 to substantially reduce global greenhouse gas emissions. Off-road mobile vehicles alone account for 9% of the total energy consumed in the U.S. transportation sector, out of which 70% belongs to the construction and agricultural sector [10]. However, the average efficiency of these machines is only 21% with respect to engine power output, dropping down to a mere 7% with engine efficiency consideration [9]. Given the rising fuel prices and the implementation of stringent emission regulations, it is crucial to improve the efficiency of these mobile machines.

To evaluate the impact of these inefficiencies, the Oak Ridge National Laboratory conducted an assessment focusing exclusively on mobile hydraulics in the United States [9]. They found that each year, at least 0.362 quadrillions of British Thermal Units (Quads) of energy are consumed. With an assumed average efficiency of 21% (without considering engine efficiency) across all applications, only 0.076 Quads of work are produced. However, if we could increase the efficiency number to 50%, the same amount of work could be generated while saving 0.21 Quads. Considering diesel's energy density of 138,700 BTU per gallon and the current cost of diesel fuel assumed to be USD 5 per gallon, these efficiency improvements could save about USD 7.61 billion per year. This substantial operating cost-saving potential highlights the need to make mobile machines more efficient.

In this chapter, several efforts to improve the efficiency of off-road mobile machines are reviewed and compared to state-of-the-art systems. The drawbacks of contemporary solutions to improve system efficiency have also been discussed to establish the need for a new architecture. Additionally, a review of the control systems used for hydraulic systems has been provided to define the scope and objectives of this thesis. An organizational framework has been included in this chapter to provide ease of maneuverability throughout the thesis.

1.1 Review of architectures

1.1.1 Hydraulic system architectures

Conventional heavy-duty off-highway vehicles, such as excavators, wheel loaders, and mowers have multiple degrees of freedom and are primarily hydraulically actuated to take advantage of hydraulics' unsurpassed power density. The majority of these vehicles use throttling valves to control the motion of hydraulic actuators. The adoption of throttling control methodology as well as the inefficiency of hydraulic components are the prime reasons for the increase in fuel consumption and harmful emissions making mobile machines inefficient.

Load Sensing Aechitecture

A state-of-the-art architecture very commonly used in mobile machines is the Load Sensing (LS) system ([11], [12]). In this system, as shown in figure 1.1, a pressure-compensated pump provides a common pressure (p_{in}) at a level that is slightly higher than the highest pressure requirement among all the services (p_1, p_2, p_3). Then, throttling valves are used to drop the pressure as required by the services. This can only be efficient if the pressure drops are kept low, which means the services would require nearly the same pressure levels (this is unlikely). However, the energy saving potential is reduced due to significant throttling losses in systems where the instantaneous pressure requirement for different services differ significantly as can be seen from the power distribution of a Load Sensing architecture with 3 actuators having different instantaneous pressures shown in

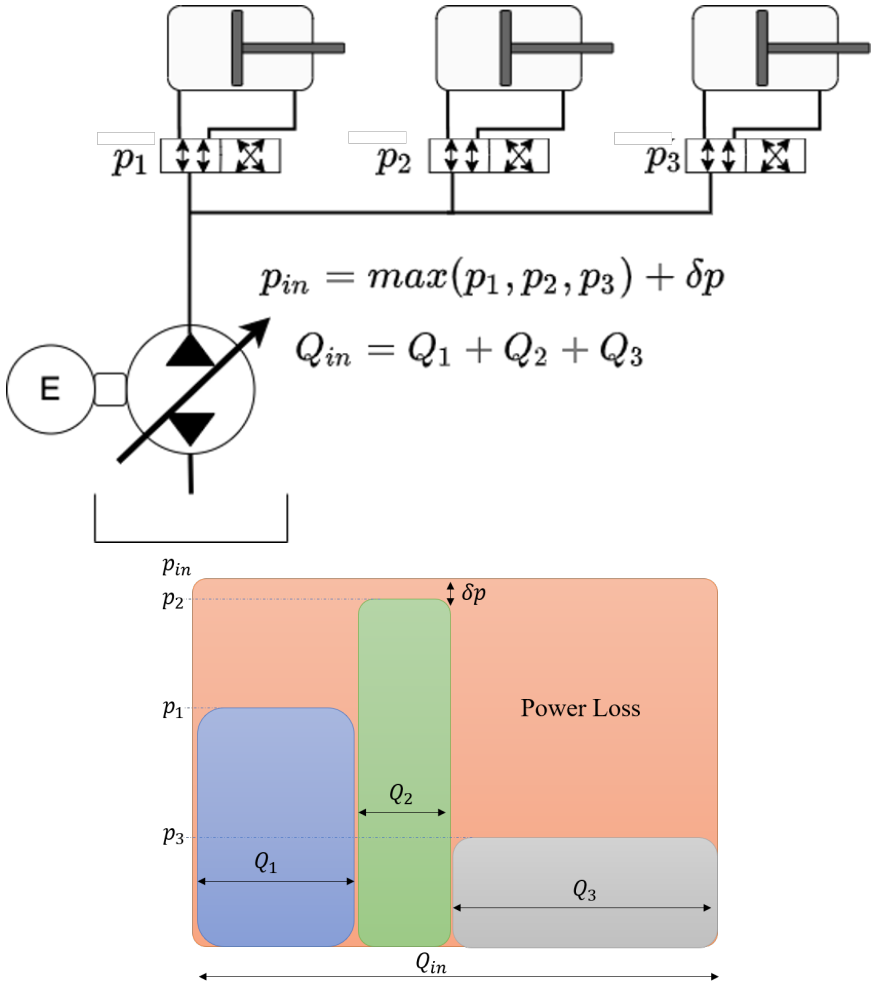

Figure 1.1: A Load-Sensing architecture with power distribution

figure 1.1. The inability to recuperate energy from over-running loads due to the mismatch in pressure of the accumulator and the load also adds to the energy losses.

There are many potential areas where the Load Sensing architecture can be improved to increase efficiency. Throttling has been known to have a major impact on efficiency hence, throttling valves can be replaced as the primary means of

control. Any opportunity to recuperate energy from regenerative loads should be effectively capitalized. Hydraulic component inefficiencies are also a major source of system inefficiency. Components should work under more efficient conditions or be made more efficient. It would be beneficial to avoid using hydraulic pumps and motors at partial displacements since their efficiency tends to decline when operating at low displacements. The operation of the engine should not be restricted and be permitted to run at its most efficient regime.

Displacement Control

Researchers from all around the world have proposed various methods to improve the energy-saving potential of these heavy-duty vehicles. An efficient approach is to use Displacement Control (DC). Displacement-controlled actuation, is a type of throttle-less hydraulic actuation, using one (or multiple) variable displacement pumps to directly control the motion of the hydraulic linear or rotary actuator. There is no throttling because actuators do not share flows and each actuator has its own flow source. The pressure is automatically built and subjected to the actuator load. A simplified closed circuit for a single DC actuator is shown in figure 1.2. Rahmfeld and Ivantsysnova developed and tested this circuit for a wheel loader [1]. The circuit can be powered by a constant or variable speed power source and utilizes a variable displacement pump to control the velocity of the cylinder. The pump's speed, displacement, or both can be manipulated to regulate the cylinder velocity. The pilot-operated check valves are essential to account for the flow differences between the two cylinder chambers. A prototype of

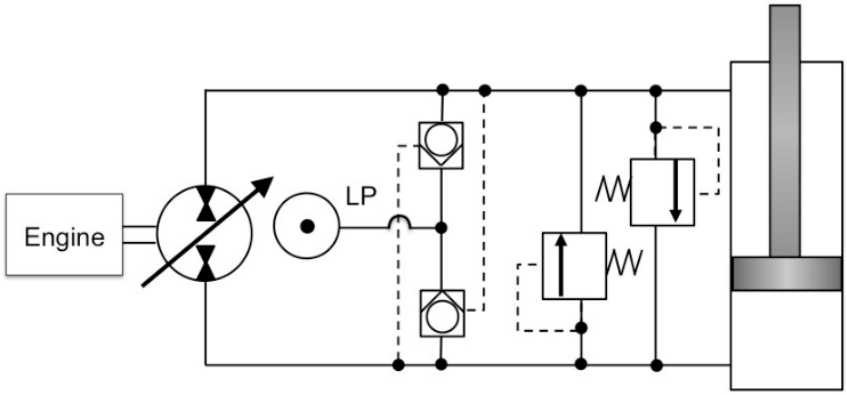

Figure 1.2: Basic closed circuit Displacement control for a linear actuator [1]

the closed circuit solution implemented in a wheel loader showed a saving of 15% in fuel consumption compared to a standard loader equipped with a conventional load-sensing hydraulic system.

Heybroek proposed a novel open circuit Displacement Control solution as shown in figure 1.3. The concept of an open circuit is proficient in achieving four-quadrant actuation through the utilization of four individual valves incorporated within the circuit. The inclusion of additional valves enables the amalgamation of certain benefits derived from distributed valve technology with those derived from displacement control. He demonstrated 20 % energy saving potential for the working hydraulics in a medium-sized wheel loader compared to a Load Sensing system [2]. Hippalgaonkar et al. have developed a Hydraulic Hybrid Displacement Controlled system for a 5t mini-excavator [13]. They have been able to show 40% fuel saving in a side-by-side comparison with Load sensing architecture. They were able to downsize the engine by 50 %. Ivantysyn et al. have demonstrated 35%

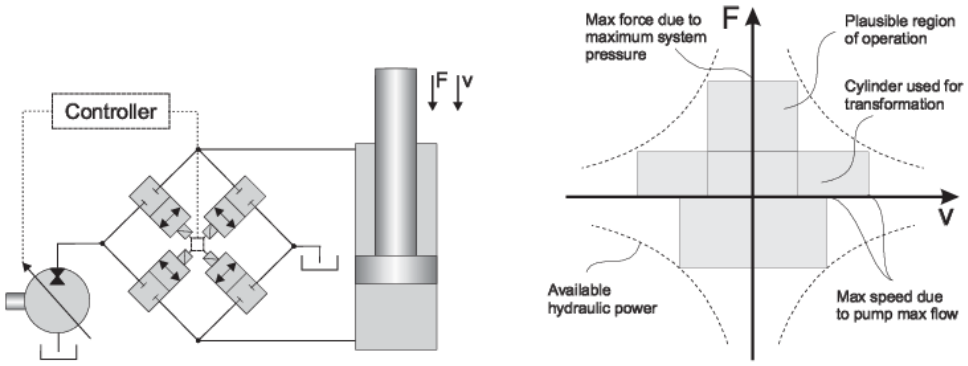

2.10(a) Displacement control in an open circuit solution.

2.10(b) Region of operation.

Figure 1.3: Open circuit Displacement control for a linear actuator [2]

improvement in cycle energy by using a novel open circuit Displacement Control architecture for a 290t mining excavator [14]. Zimmerman et al. [15] implemented Displacement Control in a compact excavator and demonstrated a 50 % reduction in engine-rated power. They also showed that the use of displacement-controlled actuation offers a distinct advantage in reducing the cooling power requirements of hydraulic systems and, consequently, minimizing the parasitic losses associated with them.

Although Displacement control is promising, this potential solution suffers from bulkiness as each service requires a variable displacement pump, which needs to be driven on a common shaft by the engine. The variable displacement pump might need to operate at lower displacements for partial load thereby becoming inefficient. Also, the control bandwidth is limited to control the displacement of the pump/motor.

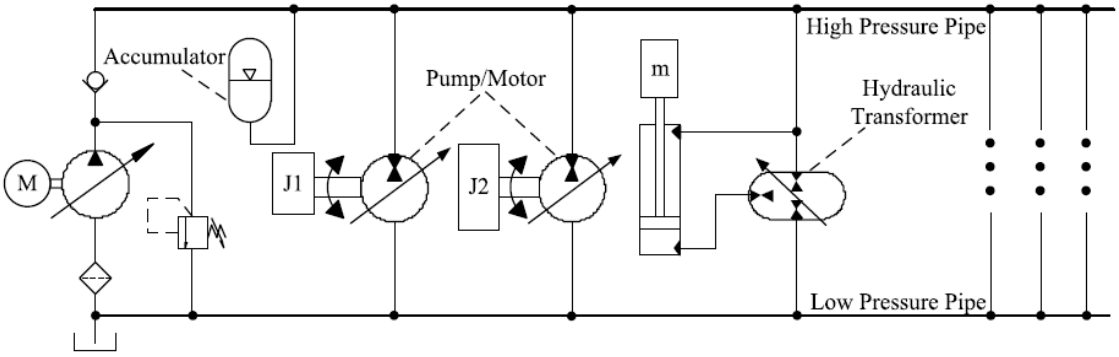

Figure 1.4: A CPR based architecture [3]

Common Pressure Rail Systems

The concept of the Common Pressure Rail (CPR) system provides a promising direction for building a highly efficient, modular, and reliable hydraulic system [3]. The hydraulic system based on CPR can be divided into a high-pressure side (HP) and a low-pressure side (LP), as shown in figure 1.4. In order to ensure that the pressure remains constant for HP, a constant pressure regulating variable displacement pump is used as the main pump and coupled with a hydraulic accumulator. Rotary loads can be controlled by a Variable Hydraulic Pump/Motor and the linear load is controlled by using a Hydraulic Transformer which bucks or boosts the CPR pressure to achieve the desired pressure on the linear actuators. As the throttling valves are replaced by a hydraulic transformer the CPR-based system becomes throttle-less. Energy recovery is also possible with components like the variable displacement pump and hydraulic transformers working in all four quadrants. Shen et al. have developed a Hydraulic Hybrid Excavator based on Common pressure Rail [16] architecture. They have shown that a common

pressure rail-based architecture is able to reduce the fuel consumption of an excavator by 21 % when compared to a Load Sensing based architecture. Reduction of metering losses and recuperating regenerative loads allows them to improve fuel efficiency over Load Sensing architecture. They have further shown that the engine can be downsized to improve fuel efficiency by 32 %. But there are some disadvantages to the CPR-based system. One of the key components - the hydraulic transformer - hinders the application range and they tend to be quite bulky and expensive. Hydraulic Transformers have limited efficiency at partial loads as one of the pumps/motors require to operate at low displacement. Since the late 1990s, the Dutch company INNAS has been developing the Innas Hydraulic Transformer (IHT) which allows the transformer ratio to vary by rotating a 3-ported port plate. The IHT is still in the prototyping stage. S. Lee et al. at the University of Minnesota have developed a switched-mode hydraulic transformer [17, 18]. Unlike the IHT, the switched mode hydraulic transformer uses a traditional transformer topology consisting of a pair of hydraulic pumps and motors but uses switching valves to configure itself as either the common input, common output, or common tank configuration. Depending on the operating condition, the configuration that is most efficient can be chosen. In addition to being efficient, the switched-mode hydraulic transformer can effect precise motion and force control [19, 20, 21] Despite these developments, hydraulic transformers are still not commercially available.

Multiple Common Pressure Rail Systems

An obvious direction for the common pressure rail architecture is to drop the use of transformers and still be able to reduce throttling losses and recover energy. A new common pressure rail architecture STEAM with multiple common pressure rails (MPR) has been proposed by the Institute of Fluid Power Drives and Controls at RWTH Aachen University. A comparison of the STEAM architecture with Load Sensing on a hydraulic excavator has been shown in figure 1.5. STEAM [4] is a hydraulic hybrid system that uses three pressure rails along with a series of valves to reduce major sources of loss found in mobile hydraulic circuits. The accumulators take care of peak power demands enabling more efficient engine operation. To reduce throttling losses while driving the linear actuators, a system of switching valves connect both pressure rails and the tank line to the cap and rod chambers of each actuator. Depending on the current load this configuration generates a system of nine different pressure combinations which is employed to reduce throttling losses by selecting the pressure rail closest to the required service pressure while simultaneously recovering energy. The engine and the pump are decoupled from the actuators, unlike the Load Sensing architecture. This helps the engine and pump to operate more efficiently. They have demonstrated that STEAM consumes 27 % less fuel than Load Sensing despite having a lower engine speed and the same cycle time. According to measurements, around half of the gain in fuel saving is attributable to enhanced engine performance. The reduced throttling and energy recovery in hydraulics is directly responsible for the rest. STEAM has shown a significant energy-saving potential but it still involves

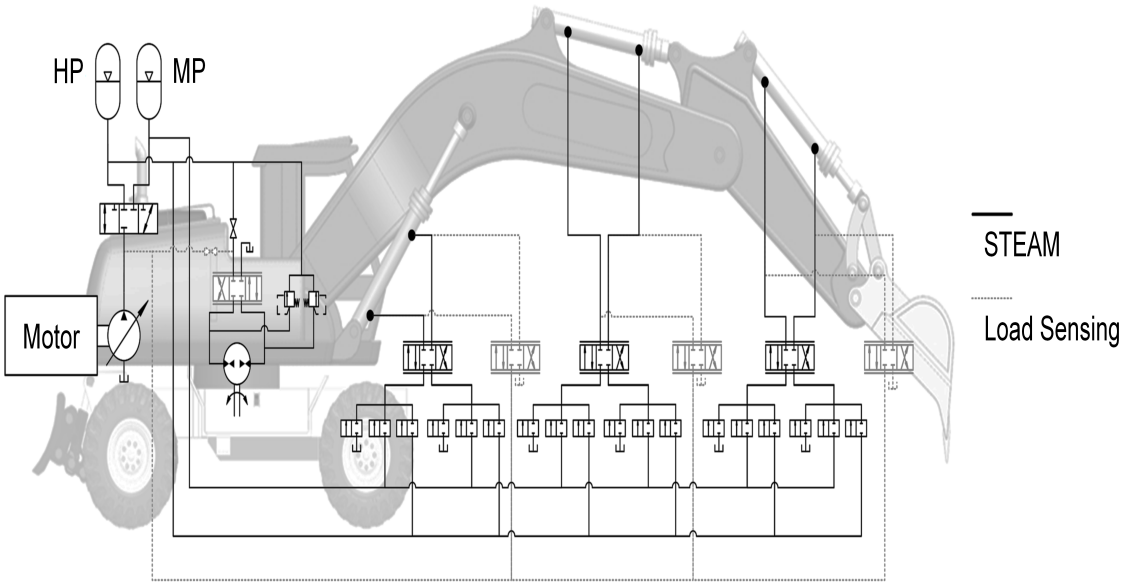

Figure 1.5: Circuit layout of an excavator comparing STEAM with state of the art Load Sensing architecture [4]

throttling losses which cut into the efficiency gains.

Another multi-Pressure Rails (MPR) system was proposed recently for agricultural applications by Vacca et al. in [5]. This system employs individual variable displacement pumps for each pressure rail, allowing for independent variable pressure control. A merging valve is used to combine the flow from two pumps to one rail, allowing for more efficient operation by downsizing the pumps and operating at higher displacements. Figure 1.6 shows how the three rails are connected to a hydraulic actuator via pressure select and control valves (PSCV). The pressure selection stage is used to select the optimized pressure rail, and the metering stage is used for actuator control to minimize throttling losses. The MPR's ability to use various inlet/outlet pressure level combinations provides each actuator with access to a range of output torque and force. The highest-pressure rail is chosen slightly

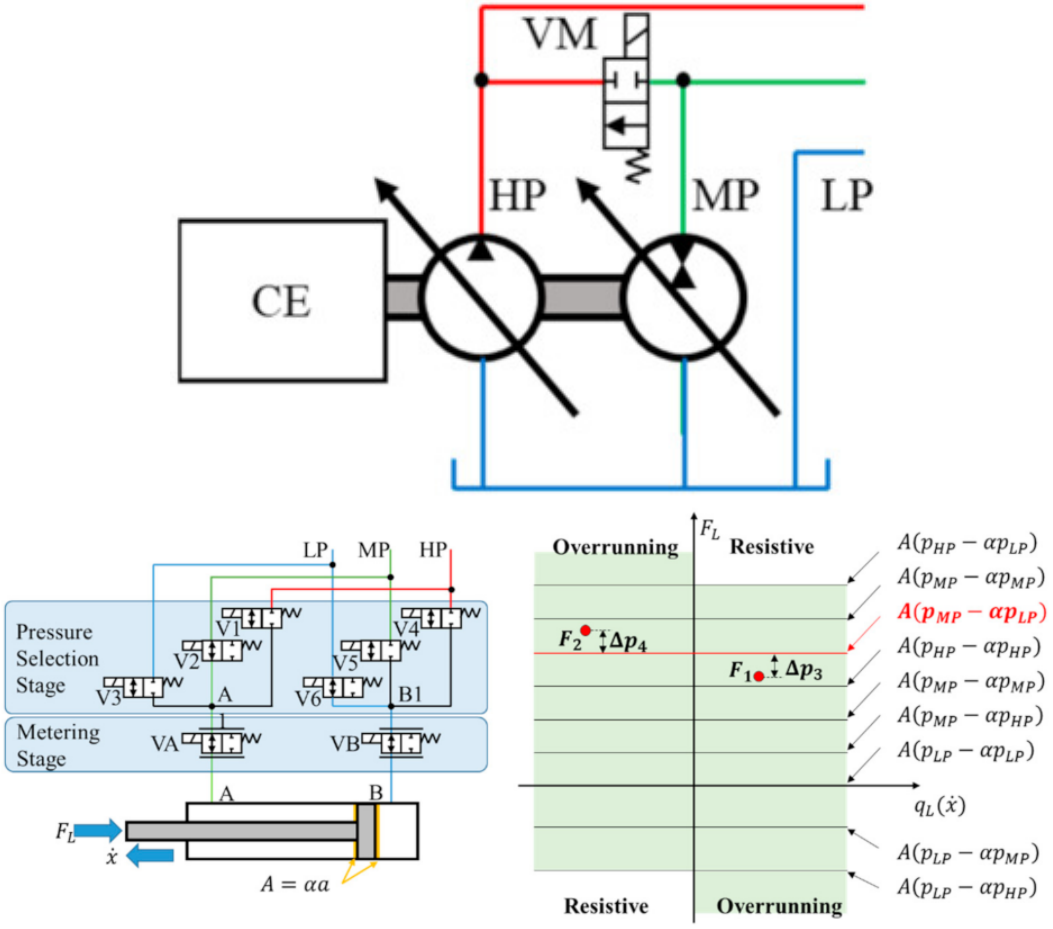

Figure 1.6: A variable rail multi-pressure rail (MPR) system [5]

above the highest actuator pressure, and the middle-pressure rail pressure continuously adjusts with respect to the actuator's load pressures. The corresponding mode for each actuator switches to minimize power loss due to throttling.

The MPR architecture has been implemented on a tractor powering a 16-row planter, resulting in a 58% reduction in total power at the pump shaft and an 89% increase in system efficiency from the baseline machine. However, this approach may prove challenging for duty cycles with fast dynamics, which is often

the case for construction machines. In summary, the MPR system with variable pressure rails in [5] shows promising results for agricultural applications, but its effectiveness for other types of duty cycles need to be further investigated.

The focus of this dissertation, the Hybrid Hydraulic-Electric Architecture (HHEA) proposed by Li et al. at the University of Minnesota in [22], is also based upon multiple common pressure rails with constant pressure but it does not rely on throttling. Details will be provided in chapter 2.

1.1.2 Electrification

Over the past few years, there has also been a growing trend toward complete electrification in off-road vehicles. This trend is being driven by a variety of factors, including increasing environmental concerns, advances in battery technology, and improvements in electric motor performance. One of the key benefits of electrification in off-road construction vehicles is reduced emissions. Many construction sites are located in urban areas where air pollution is a major concern. By switching to electric vehicles, construction companies can help reduce emissions and improve air quality in these areas. Another benefit of electric construction vehicles is their reduced noise pollution. Construction sites can be very noisy, and electric vehicles are much quieter than their diesel counterparts, which can help improve the quality of life for workers and nearby residents. In addition, electric construction vehicles can also be more efficient than diesel vehicles, as they do not waste energy idling or when performing low-load tasks. This can help reduce operating costs and improve productivity on construction sites. Battery technology

is a key driver in the trend toward electrification in construction vehicles. The development of high-capacity batteries and improved charging infrastructure can make it possible to use electric construction vehicles for longer periods of time and in more remote locations.

While the trend toward complete electrification of off-road construction vehicles is gaining momentum, there are a number of challenges that make this transition difficult.

One of the main challenges is that these vehicles require a lot of power to operate. This means that they need large and heavy batteries to provide enough energy for a full day's work. As battery technology continues to improve, the weight and size of batteries will likely become less of an issue, but it is still a challenge for the time being.

Another challenge is the ruggedness of construction sites. Off-road construction vehicles are designed to operate in harsh environments and under tough conditions. These conditions can be hard on batteries and electric motors, which can lead to reduced performance and reliability. Special considerations need to be made for the design and manufacturing of electric construction vehicles to ensure they are durable and can withstand the rigors of the construction site.

Another challenge is power density. Unlike on-road consumer vehicles, where energy density is the main concern, off-road vehicles require high power density due to their reliance on hydraulic counterparts, which are significantly more power dense than electric machines. Even though electric motors can deliver high levels of torque, they are generally more expensive than hydraulic counterparts, and the

power density of batteries is also limited. As a result, construction companies may need to invest in larger and more powerful batteries, which can be costly.

The adoption of electric construction vehicles faces a significant hurdle in the form of cost. While the potential long-term savings stemming from reduced fuel consumption and maintenance expenses are substantial, the initial investment required to purchase electric construction vehicles tends to exceed that of their diesel-powered counterparts. This higher upfront cost is primarily attributed to the expenses associated with high-powered electric machines and the utilization of more power-dense batteries. This can make it difficult for construction companies to justify the initial investment. Lewis et al. [23] conducted a study to assess the feasibility of electrifying a large mobile crane. The study found that the current state of energy storage technology is not yet capable of feasibly replacing traditional crane systems in terms of cost, size, and reliability.

An efficient electric and hydraulic approach to improve the efficiency of these mobile machines is to utilize an electro-hydraulic actuator (EHA) setup (Fig 1.7). This actuation system is based on the use of an electric motor as the prime driver which drives a fixed-displacement pump to regulate the flow going to a single actuator. The advantages of EHA are that it's throttle-less, regenerative, efficient, and also has good control performance.

The high efficiency of the system is due to the efficient components and the electric drives. A fixed displacement pump is always running at full displacement making it more compact and cost-effective than variable displacement pumps/motors. Various EHA solutions have been proposed by researchers around

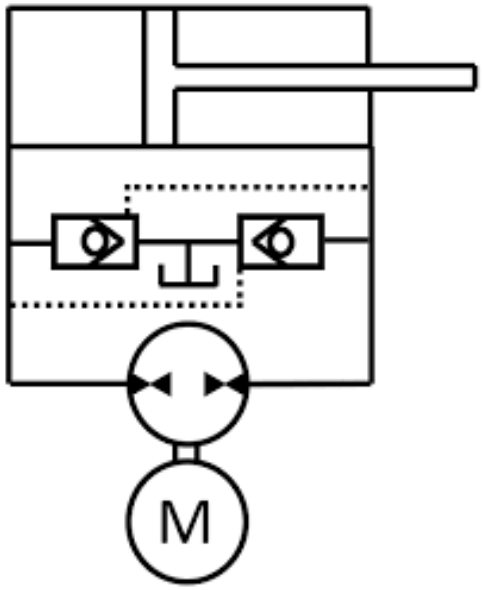

Figure 1.7: An Electro-hydraulic Actuator for a single service

the globe. Schmidt et al. put forward multiple proposals for pump control systems that include load-holding characteristics [24]. They describe the energy distribution and energy recovery potential for each of these solutions and compare the results to those obtained from conventional valve-controlled hydraulic systems. Niraula et al. and Zhang et al. conducted research on 1-ton mini excavators and demonstrated that implementing an electro-hydraulic actuation system could lead to an energy consumption reduction of up to 50 % compared to traditional load sensing circuit architecture-based systems [25][26]. Qu et al. [27] have recently developed a highly efficient Electro-hydraulic Actuator system. They tested an open-circuit and a closed-circuit EHA architecture on a 20KW system. They have been shown to increase the efficiency of fluid power actuation systems from 21 % to 80% in their study. The team further extended their open circuit EHA

design by building an Electro-Hydraulic Unit which is an integrated electric motor and pump. They were able to demonstrate system efficiency of up to 54% [28]. Padovani et al. proposed an electro-hydraulic drive system for single-rod cylinders with passive load-holding capability. The research aims to evaluate the performance of this architecture in a single-arm crane application. The experimental results demonstrated that the final position error of the arm remained within a range of ±2 mm, and the overall energy efficiency during handling was approximately 60% [29]. Casoli et al. [30] implemented an open circuit and two closed-circuit EHA layouts on a 9-ton excavator. They compared all the layouts with Load Sensing Architecture and have shown 30-32 % improvement in fuel saving potential.

However, there are some drawbacks to EHA. Since all the power is provided electrically the electrical components become bulky and expensive. The power densities of electric drives are one or two orders of magnitude lower than hydraulic counterparts. Hence EHA is practical for low-power applications like aerospace. A system greater than 20kW would become very expensive with an EHA.

1.1.3 Key takeaway

The current state-of-the-art approach for hydraulic systems in off-road machines is Load Sensing (LS), which suffers from inefficiencies due to throttling losses and the inability to recover energy from over-running loads. To address these issues, several alternative approaches have been proposed in the literature, such as hydraulic-only and electric-only architectures. While these approaches have

been successful in improving system efficiency, each has its own drawbacks that have prevented their adoption in the industry.

Despite the limitations of these approaches, their success in improving hydraulic system efficiency highlights the potential for further advancements in this area. The development of a hybrid solution that combines the benefits of hydraulic and electric technologies may provide a more efficient and economically feasible solution for industry adoption. Such a hybrid solution could leverage the high power density and efficient energy transfer of hydraulic systems while also incorporating the energy recovery and control capabilities of electric systems. The resulting architecture could improve the overall efficiency of off-road machines and reduce their environmental impact. This drives the development of a new architecture called Hybrid Hydraulic Electric Architecture (HHEA) within our research group [22, 6]. HHEA provides the majority of the power through hydraulics and uses electric only for modulation, hence keeping the size of electric components small. This will be discussed in detail in chapter 2.

1.2 Review of control systems

Ensuring energy efficiency is undoubtedly a crucial aspect when it comes to off-road machines. However, it is equally essential to acknowledge that the utility of such machines is heavily dependent on their ability to execute tasks with precision and accuracy, in accordance with the given commands. Hence, the role of precise motion control in determining the acceptance of an architecture cannot be

overstated. Hydraulic systems are inherently highly non-linear and linear methods have limited performance. The nonlinear dynamics of hydraulic systems, as established by Merritt [31], presents a significant challenge when it comes to controlling these systems. This challenge arises from the nonlinearities that are inherent in the system, which is rooted in fundamental properties like fluid compressibility (due to entrained air, dependence on pressure and temperature), complex flow properties of hydraulic valves (such as pressure losses, transient flow conditions), and nonlinear friction characteristics in hydraulic actuators (due to the combined properties of static, coulomb, and viscous friction). Additionally, the system may be subject to non-smooth and discontinuous nonlinearities due to the directional change of the pump rotation or valve opening, valve overlap, and pump/motor deadband [32].

Hydraulic systems are characterized by nonlinear behavior, making advanced control schemes necessary for high-performance control. Conventional hydraulic control designs rely on linear approximations that may not accurately capture system dynamics. This can result in crude approximations of component and fluid parameter values. Advanced control schemes that consider nonlinear behavior and uncertainties can improve control performance and efficiency in hydraulic systems.

One of the most widespread controllers being used in the industry is Proportional-integral-derivative (PID) control. PID control has been proven to be reliable, and easier to implement and understand. Several modifications of PID controllers have been used in hydraulic control systems. Zhang et al. [26] implemented PID control

for trajectory tracking of the excavator bucket. They found out that the straightness error was 4.8 %, but the maximum straight-line error was 112mm comparing this to an average operator. Skarpetis et al. implemented a robust proportional-integral-derivative (PID) controller for the purpose of regulating the position of an electro-hydraulic actuator (EHA) under the presence of physical uncertainties and external disturbances. Hanh et al. [33] implemented two fuzzy logic-based controllers on an EHA excavator -the fuzzy PID controller and the fuzzy self-tuning controller with a neural network. The experimental results demonstrated that both the fuzzy PID controller and the fuzzy self-tuning controller with neural network yielded superior control performance compared to the conventional PID. The fuzzy self-tuning controller with a neural network exhibited greater flexibility due to the ability to tune the control output signal online through the neural network update process. The tracking performance of the fuzzy self-tuning controller with the neural network was superior to that of the conventional PID, attributable to its superior adaptability to disturbances and nonlinear systems. Van et al. [34] conducted a study in which they implemented fuzzy feedback control for Electro Hydraulic Actuators (EHA). The authors proposed a control algorithm called Fuzzy feedback control (FLFC) which combined fuzzy logic and linear feedback controller (LFC) to improve the control performance of the EHA system. The study compared FLFC with two other control algorithms, namely PID and Fuzzy PID (FPID). The authors reported that FLFC outperformed PID and FPID in terms of control performance for low-power applications. The analysis showed that FLFC was 99% superior to PID and 77 % superior to feedback algorithms.

However, the study did not include any experimental results.

Anderson et al. [35] have shown that for hydraulic systems linear controllers in their standard form are not generally sufficient to obtain acceptable performance. Hence, a non-linear control strategy needs to be developed that can capture the non-linear dynamics of the system. In the field of hydraulic systems, other than approaches based on linearization and linear system assumption, there are many advanced non-linear control approaches that have been demonstrated.

According to Yang's work [32], two control strategies were implemented for an electro-hydrostatic actuator (EHA) system with a nonlinear model: H_∞ proportional integral (PI) with feedforward control, and robust discrete-time sliding mode control design. The performance of the controllers was evaluated, and it was found that the robust sliding mode control was superior, exhibiting tracking errors of less than 1 mm.

Wang et al. [36] developed a sliding mode control with an extended state observer for an EHA (electro-hydraulic actuator) system. They utilized an exponential approach law to attenuate perturbations inherent in SMC (sliding mode control) and created a variable damping sliding surface for their controller design. The proposed SMC controller was tested in experiments and compared to a traditional PID controller. The results show that the damping variable sliding mode control reduces tracking error by 50% and improves settling time. However, chattering of control input remains an issue for sliding mode controller designs with a wide operating range.

Another common non-linear control approach is based on back-stepping [37]

[38]. In this approach, the desired force from the actuator is first designed, and then the actuator force is controlled successively by back-stepping through a cascade structure. This structure can be modified to add robustness and performance enhancements. Generally, a quadratic term in the actuator force error is used in the Lyapunov function, and non-linearities are canceled out to preserve stability. The natural and physical energetic structure of the actuator pressure dynamics are not being considered [39]. The back-stepping controller needs to be augmented to include the intrinsic energy of the system in the design process. Tri et al. [40] have developed an iterative back-stepping control scheme for a symmetrical pump controlled EHA. There is an iterative learning control signal with a backstepping modifier to deal with uncertainties and nonlinearities in EHA. They have shown good tracking performance with constant load. They haven't shown trajectory tracking performance with variable load.

Yang et al. [41] propose a nonlinear adaptive output feedback robust control scheme for a double-rod hydraulic actuator-driven electro-hydraulic servo motion system. The control strategy simultaneously handles parameter uncertainties and matched and mismatched disturbances under output feedback conditions. The proposed control scheme employs observers to estimate system states and disturbances. An adaptive law is synthesized using the backstepping methodology. Experimental results show that the proposed control scheme outperforms the PI controller in terms of tracking performance. However, the proposed controller requires the desired trajectory to be third-order continuous differentiable, which limits its applicability.

Zhang et al. [42] have compared three controllers Integral sliding mode Back-stepping control (ISMBC), Back-stepping control, and PID for an asymmetric EHA. They have shown that the backstepping controller does a better job at trajectory tracking than simple PID but it is not very robust. The ISMBC shows the best tracking results and stronger robustness to parameter changing among the three controllers compared. Although, the Lyapunov function devised here fails to incorporate the natural physical property of the system.

Rachel Wang and P. Li has shown hydraulic actuators to be a passive two-port system [43]. They have devised an innovative passivity control framework for the mechanical-pressure dynamics of a hydraulic actuator, leveraging the inherent physical energy of the system. By integrating this framework with the widely recognized back-stepping technique, they successfully account for the system's natural physical properties [44]. As a result, the back-stepping approach is significantly enhanced, offering improved stability and performance for the hydraulic actuator system.

Since these mobile machines are operated by human operators it is also essential to explore the interaction of HHEA with human operators. Zhang et al. [45] shows how a hybrid control scheme for velocity and position control has been adopted for an Excavator boom operated by an operator. The HHEA can explore the hybrid control strategy for interacting with the operator. Elton [46] has proposed various mapping for joystick commands vs. rate or position reference commands for position control of the dynamic system and rate control of dynamic systems. These mappings were used to build a ghost interface. Such a relationship

between the joystick and the reference trajectories can be explored.

Overall, the backstepping control design methodology has been shown to have better motion control performance than the PID controller for EHA systems. While this design methodology is prevalent and has been tested on EHA systems, an augmented form of backstepping control design may be more suitable for the HHEA system, given its unique characteristics and special circumstances. Subsequent chapters will explore these issues in more detail to identify the most effective control design for the HHEA system.

1.3 Research objective

Hydraulic systems are widely used in mobile machines such as construction equipment, agricultural machinery, and material handling equipment. These systems provide high power density and efficient energy transfer, making them suitable for heavy-duty applications. However, hydraulic systems also suffer from energy inefficiencies due to throttling losses and other factors. These inefficiencies lead to increased fuel consumption and environmental impact.

To address these issues, there have been significant efforts to improve the efficiency of hydraulic systems in recent years. The Load Sensing architecture is currently considered state-of-the-art and is widely used in mobile machines. However, Load Sensing suffers from throttling losses and is unable to recover energy from over-running loads. Several other architectures have been proposed, such as the Hydraulic-only and Electric-only architectures, to improve system

efficiency, but each has its own drawbacks.

The Hybrid Hydraulic-Electric Architecture (HHEA) [6] is a promising new architecture that combines the benefits of hydraulic and electric technologies (chapter 2. HHEA enables the electrification of high-power machines using small electrical components, resulting in significant energy savings. However, for HHEA to be widely adopted, controllability is critical, particularly for mobile machines that require accurate and responsive motion control. Thus, understanding the dynamics of HHEA and devising a control strategy is essential for effective motion control.

Developing a control strategy for HHEA involves understanding the dynamics of the system and designing a controller that can effectively control the system's behavior. This control strategy must consider limited torque availability to reduce the size of electric components. Several control approaches have been discussed in the literature, such as model-based control, fuzzy logic control, PID control, backstepping control, robust control, and sliding mode control. However, none of these approaches fit the unique needs of HHEA. Thus, the primary objective of this thesis is to develop a control strategy specifically designed for HHEA.

The first specific objective is to understand the dynamics of HHEA and develop a control strategy for precise motion control of HHEA. This objective involves studying the behavior of the system and developing a model that represents its dynamics. Based on this model, a control strategy can be designed to achieve precise motion control.

The second specific objective is to validate the control performance of the developed control strategy using off-the-shelf components at modest (200 bar) and realistic pressure (300 bar). This objective involves implementing the developed control strategy on a test rig and evaluating its performance under different operating conditions.

The third specific objective is to explore retrofitting HHEA onto an existing machine and understand human interaction with real-world operation. This objective involves retrofitting HHEA onto an existing mobile machine and evaluating its performance in real-world conditions. This evaluation considers human interaction with the system using a joystick, where the future duty cycle and the pressure rail selection are unknown.

Achieving these objectives will validate the control performance of HHEA and bring this new architecture one step closer to commercialization. In the future, HHEA has the potential to become a widely adopted architecture for mobile machines, resulting in significant energy savings and reduced environmental impact. The contribution of this thesis would play a key role in its adoption.

1.4 Organization of thesis

The thesis at hand introduces a novel architecture that amalgamates the benefits of hydraulic and electric systems. The primary objective of this research work is to develop and validate a motion control solution specifically tailored to HHEA. The thesis is structured into eight comprehensive chapters, providing a comprehensive

understanding of the architecture and developing a control solution to demonstrate its controllability.

Chapter 1 commences by providing a comprehensive overview of the existing architectures and identifying the need for a new hybrid architecture. This chapter highlights the deficiencies in the existing architectures and establishes the necessity for a new architecture that overcomes these limitations. Additionally, the chapter outlines the objectives and scope of the thesis, along with an examination of various control strategies from the literature.

In Chapter 2, a detailed discussion of the proposed Hybrid Hydraulic Electric Architecture (HHEA) is presented. The chapter describes the components of the system and their interactions, both physical and mathematical. Furthermore, the governing equations that serve as the basis of the proposed model are elaborated upon.

In Chapter 3, the overall control architecture of HHEA is presented. The motion control objectives are formulated and the control strategy is discussed catering to the unique challenges faced by HHEA.

Chapter 4 formulates a nominal control strategy for the HHEA, and the control law is derived using the chosen control strategy. This chapter also discusses the implementation of the control strategy and its effectiveness in regulating the system. Additionally, the chapter elaborates upon the constraints imposed on the control system and how they are managed.

In Chapter 5, the need for transition control to improve tracking performance during a pressure rail switch is highlighted, and a control law based on Least

Norm Control is proposed for HHEA. The chapter illustrates the effectiveness of the transition control and its contribution to improving the performance of the HHEA.

Chapter 6 validates the developed motion control strategy using two test rigs with 200-bar and 300-bar maximum pressure capacities respectively. The chapter demonstrates the trajectory tracking performance of the proposed motion control strategy, thus establishing its effectiveness.

In Chapter 7, the HHEA is retrofitted onto a backhoe arm to evaluate the human interaction with the architecture. The chapter presents the results obtained from the human operator's control of the backhoe arm using a joystick and discusses the implications of these results.

Finally, Chapter 8 presents concluding remarks, summarizes the overall contribution of the thesis, and discusses the future scope of the proposed architecture. This chapter highlights the potential impact of the HHEA in various industries and applications and the possible avenues for further research in this field.

In conclusion, this thesis presents a comprehensive study of Hybrid Hydraulic Electric Architecture (HHEA) and its control strategy. The proposed architecture combines the best of both hydraulic and electric systems while minimizing their individual drawbacks. This research work contributes to the development of a precise motion control strategy that is specifically tailored to the needs of HHEA. The control strategy is validated experimentally to demonstrate the controllability of HHEA.

1.5 Chapter summary

Off-road mobile hydraulics are a significant contributor to CO2 emissions and energy consumption. It is extremely important to improve the efficiency of these machines to reduce emissions and save operating costs. The state-of-the-art Load Sensing architecture suffers from significant throttling losses and is unable to recuperate energy from regenerative loads. The literature review discusses several architectures (hydraulic only, electric only, hybrid) that are more efficient than Load Sensing but there are still some drawbacks. This leads to the development of a Hybrid Hydraulic Electric Architecture that combines the benefits of hydraulic and electric technologies in a cost-efficient package to improve system efficiency.

Despite the excellent energy-saving potential of HHEA, the precise motion control of mobile machines is crucial for their effective utilization. This thesis recognizes the potential of HHEA and focuses on developing control strategies specifically tailored to its unique architecture. The literature review on various control strategies discussed points to a general framework for similar architectures but HHEA requires a tailored motion control solution. By devising and implementing an effective control strategy, this thesis aims to demonstrate the controllability of HHEA which will help to reap the energy-saving benefits along with the effective utilization of off-road mobile machines.

Chapter 2

The Hybrid Hydraulic Electric Architecture (HHEA)

The Hybrid Hydraulic-Electric Architecture (HHEA) proposed by Li et al. [6] represents an innovative approach that combines hydraulic and electric components, providing throttle-less and regenerative flow control in mobile machines. This architecture presents several advantages, such as improved energy efficiency, regeneration capabilities, and control performance, while also being cost-effective and utilizing smaller electric components.

This chapter aims to provide a comprehensive description of the HHEA and its main components, which include the Common Pressure Rails (CPRs) and the Hydraulic Electric Control Module (HECM). Furthermore, the performance of HHEA concerning other architectures has been reviewed, highlighting its potential for adoption in off-road mobile machines.

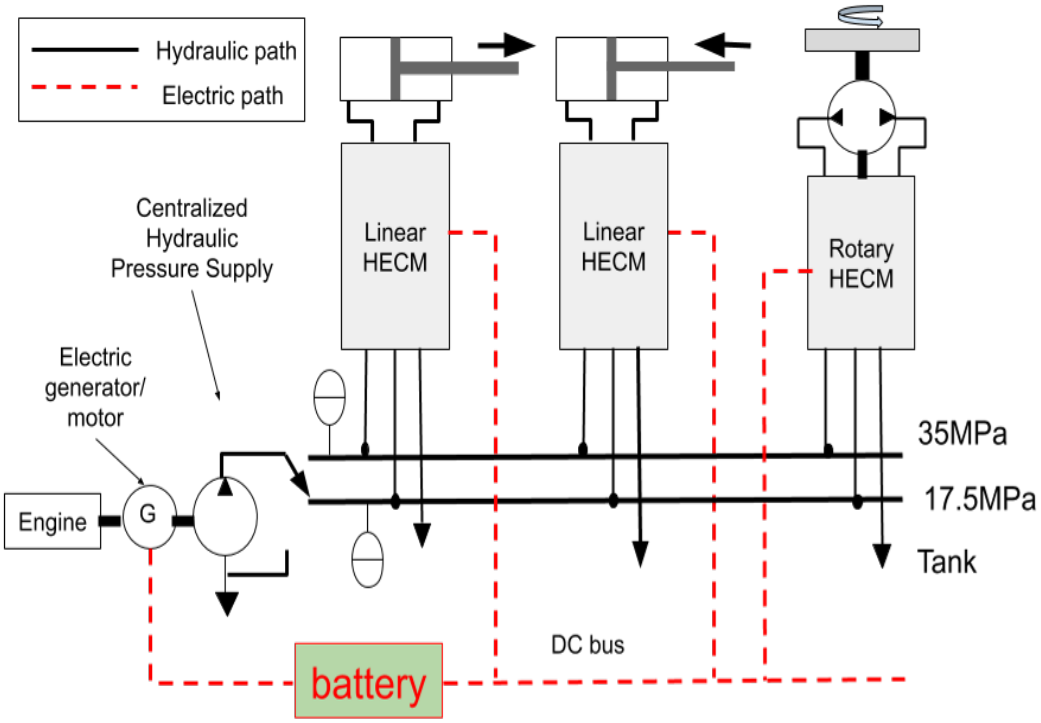

Figure 2.1: The hybrid hydraulic-electric architecture (HHEA) with 3 services and 3 pressure rails at 0 MPa, 17.5 MPa, and 35 MPa. The electric generator/motor at the engine is optional [6].

To better understand the HHEA system, a mathematical model based on the governing dynamic equations has been formulated. This will enable us to define the control objective of the architecture more precisely. Overall, this chapter aims to provide a thorough understanding of the HHEA architecture and its benefits, thereby facilitating its adoption in the industry.

2.1 Architecture

The HHEA architecture is designed to provide the majority of the system power hydraulically and efficiently, while electric drives are used to modulate the power. The foundation of the architecture lies in a set of Common Pressure Rails (CPRs) and a Hydraulic Electric Control Module (HECM) that controls each degree of freedom.

2.1.1 Common Pressure Rails

The multiple common pressure rails as shown in figure 2.1 act as the source and sink for hydraulic power. The common pressure rails are generated efficiently by a single centralized hydraulic power supply consisting of a fixed displacement pump and an electric motor/generator. This supply can be used to alternately connect the outlet, and possibly the inlet as well, of the fixed displacement pump to multiple pressure rails or unload it. This approach enables the pump to always operate efficiently at full displacement. Frequent switching of the supply pump or large variations in the pressure levels of the pressure rails can be avoided by installing accumulators on each rail with sufficient capacities. The accumulators also allow for efficient regeneration to occur without first motoring the power supply, thus avoiding the conversion losses associated with power cycling [47].

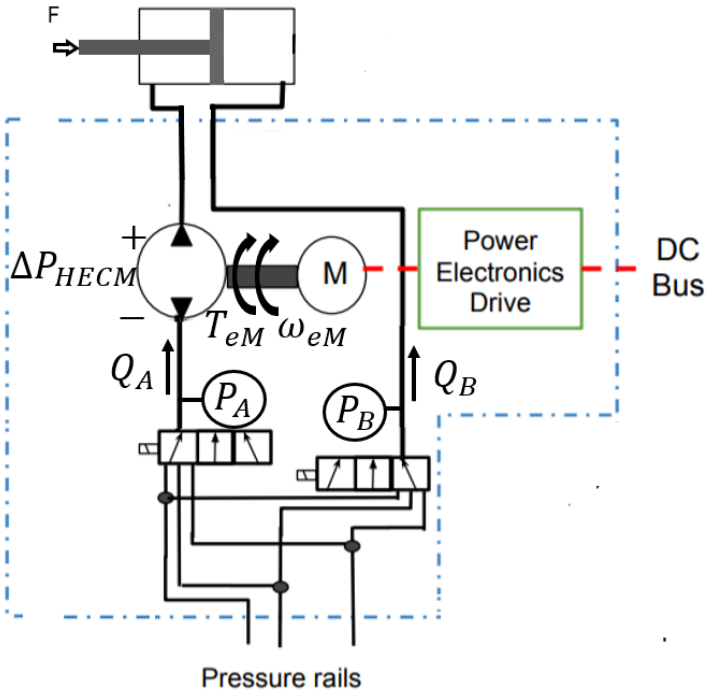

Figure 2.2: Hydraulic Electric Control Module for Linear Actuator [6].

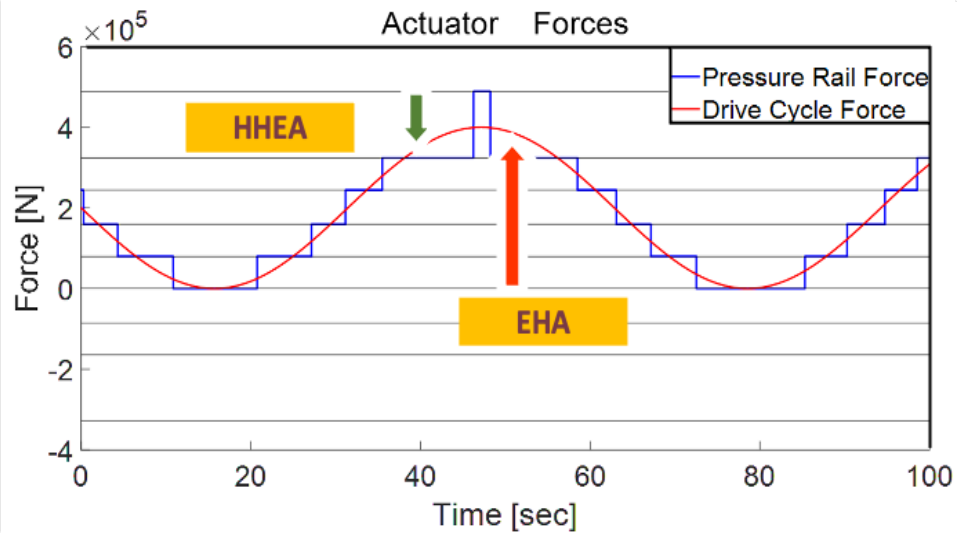

Figure 2.3: Illustration of hydraulic forces generated using common pressure rails, electric actuation force (from HHEA or EHA), and the desired actuator force

2.1.2 Hydraulic Electric Control Module

The Hydraulic Electric Control Module (HECM), as depicted in figure 2.2, comprises a fixed displacement hydraulic pump/motor mechanically coupled to an electric motor/generator and a set of switching valves. The switching valves selectively connect the pump/motor and the cap side of the actuator to the Common Pressure Rails (CPR). The electric motor-driven pump/motor is connected in series with the selected CPR and the hydraulic actuator. The HECM controls the flow and direction of the hydraulic power to the actuators and helps in power modulation. This configuration allows for precise control of the actuator's flow by regulating the HECM pump/motor speed. For rotary actuators, the pump/motor and electric drive can be directly coupled to the load, offering a more efficient path for actuation and energy recovery.

2.1.3 Working principle

The linear actuator connected to the HECM as shown in figure 2.2 had to satisfy desired load and speed requirements during a duty cycle operation. To generate the necessary hydraulic force for each degree of freedom, a pair of pressure rails is chosen using the switching valves for the pump/motor inlet and the actuator's return port. A combination of CPRs is selected and the HECM's electric motor torque is used to provide the desired actuator force. To control the actuator's motion, the HECM regulates the speed of the electric motor, which in turn corresponds to the actuator's speed. By adjusting the electric motor speed, the flow of hydraulic fluid to the actuator can be precisely controlled, allowing for smooth

and accurate actuation.

In the case of linear actuators, with three Common Pressure Rails (CPRs), there are $3^2 = 9$ possible combinations for connecting the pressure rails to each side of the actuator. The hydraulic force produced by each combination is determined by the equation:

$$F_{hyd} = P_A A_{cap} - P_B A_{rod} \tag{2.1}$$

where P_A and $P_B \in [P_{tank}, P_{mid}, P_{high}]$ and A_{cap} and A_{rod} are the capside and rodside areas of the actuator. The hydraulic force can be modulated by bucking or boosting the selected pressure by actuating the electric motor. The force provided by the electric motor is given by:

$$F_{elec} = A_{rod} \frac{2\pi}{D} T_{elec} \tag{2.2}$$

where T_{elec} is the electric motor torque and the total force of the actuator is $F_{act} = F_{hyd} + F_{elec}$. The HHEA system utilizes the electric motor torque (T_{elec}) and the hydraulic force (F_{hyd}) to produce the required actuator force (F_{act}). The 9 possible hydraulic forces that the common pressure rails can produce are represented by the horizontal lines in figure 2.3. The actuator force requirement (represented by the red curve) can be achieved by selecting the CPRs that correspond to a hydraulic force close to the desired actuator force. In this way, the electric actuation only needs to provide the difference between the hydraulic force and the desired actuator force. In contrast, an electric-hydraulic actuation

(EHA) system would require the electric motor to provide the entirety of the desired actuator force as shown in figure 2.3, without the benefit of hydraulic force assistance. Therefore, the HHEA approach can significantly downsize the electric motor compared to an EHA.

The utilization of only 2 common pressure rails (CPRs), which includes the return CPR, in the Hybrid Hydraulic-Electric Architecture (HHEA) can result in a reduction of 50% in the required torque and hence the size of the electric drive, compared to a conventional electrically driven Electro-Hydrostatic Actuation (EHA) without any hydraulic support (as depicted in figure 1.7). With the inclusion of three or four CPRs, the electric motor can be significantly downsized and CPRs pressure levels can be also optimized to reduce electric motor torque even further [48][49].

2.2 HHEA benifits

The proposed Hybrid Hydraulic-Electric Architecture (HHEA) combines electrical actuation and hydraulic actuation in a complementary manner to improve efficiency, performance, and compactness simultaneously. This architecture is expected to have the following features:

1. Hydraulics as the majority means of power transmission: In the HHEA, hydraulics is used as the primary means of power transmission. This means that hydraulic power is used to transmit power between the engine and the hydraulic motors, and between the hydraulic motors and the machine's

actuators.

2. Centralized hydraulic power supply: The HHEA uses a centralized hydraulic power supply to feed the pressure rails. This is a more efficient method than having individual pumps for each hydraulic actuator.

3. Since the hydraulic system is more efficient the engine does not need to do as much work. Also, with the accumulators, the instantaneous engine operation can be decoupled from that of the rest of the circuit thus allowing the engine operation to be optimized.

4. Throttle-less control: Throttling is not used for control in the HHEA. Instead, precise control of hydraulic power is achieved via the electric power inverter and the electric drive. This allows for better control and improves efficiency. This is in contrast to other common pressure rail systems [50].

5. Reduced size of electric drives: The HHEA reduces the size of the electric drives (motor/generator and inverter) compared to systems with only electric actuation. This is because the hydraulic system takes over most of the load from the electric drives, reducing their workload.

6. Fixed displacement hydraulic pump/motors: The HHEA uses fixed displacement hydraulic pump/motors, which ensure high hydraulic efficiency. These pumps/motors are more efficient than variable displacement pumps/motors.

7. Recuperation of regenerative energy: The HHEA can recuperate regenerative energy either electrically or hydraulically. This means that the energy

generated by the machine during deceleration or braking can be stored and reused.

8. Energy storage: Energy can be stored either in hydraulic accumulators or electric batteries. This allows the machine to store energy and use it when needed.

9. Highly modular: The HHEA is highly modular and applicable to many platforms. This means that it can be used in a wide range of machines, including excavators, wheel loaders, skid steer-loaders, mowers, etc.

10. Integration of electric motor and hydraulic pump: The integration of the electric motor and hydraulic pump in the HHEA improves power density and reduces cost [51][52]. This is because it eliminates the need for additional bearings and shaft seals, reduces the number of energy conversion stages, improves the power density of the electric motor and motor drive electronics enabled by hydraulic cooling of the electric components, and improves control response by reducing the rotational inertia of the integrated electric-hydraulic machine.

In summary, the proposed HHEA combines electrical and hydraulic actuation in a complementary manner to improve efficiency, performance, and compactness. By using hydraulics as the primary means of power transmission, a centralized hydraulic power supply, and fixed displacement hydraulic pumps/motors, the HHEA can achieve higher efficiency and power density than systems with only electric actuation. Moreover, by using both electric and hydraulic energy storage, it can

recuperate regenerative energy and store energy for later use. The HHEA is highly modular and applicable to a wide range of machines, and its integration of the electric motor and hydraulic pump can improve power density and reduce cost.

2.3 HHEA compared with other architectures

Siefert et al. [7] has compared the HHEA with STEAM [50] (popular multiple CPR-based architectures) and the Load Sensing Architecture discussed in chapter 1 for a 5-ton excavator and a 20-ton wheel-loader. The Load Sensing architecture is used as the baseline for this study. The STEAM architecture also uses common pressure rail like HHEA but instead of HECM it uses throttling valves to throttle to required service pressure. Figure 2.4 compares the energy distribution in the Load Sensing Architecture with HHEA for a 5 ton excavator using 3 pressure rails. As it can be seen almost 50% of the energy is lost in throttling which reduces the efficiency of load sensing architecture. While in HHEA there is 58% energy saving when compared to load sensing. There is also a reduction in main pump losses. Based on the comparison results presented in figure 2.5, it was observed that the HHEA and the STEAM architecture both offer energy-saving benefits in comparison to a load-sensing baseline.

For a system with three common pressure rails (CPRs), the HHEA was found to save between 62-70% of input energy in comparison to the load-sensing baseline, while STEAM saved 34-43%. In a system with five CPRs, the HHEA saved between 69-81% of input energy compared to the load-sensing baseline, while

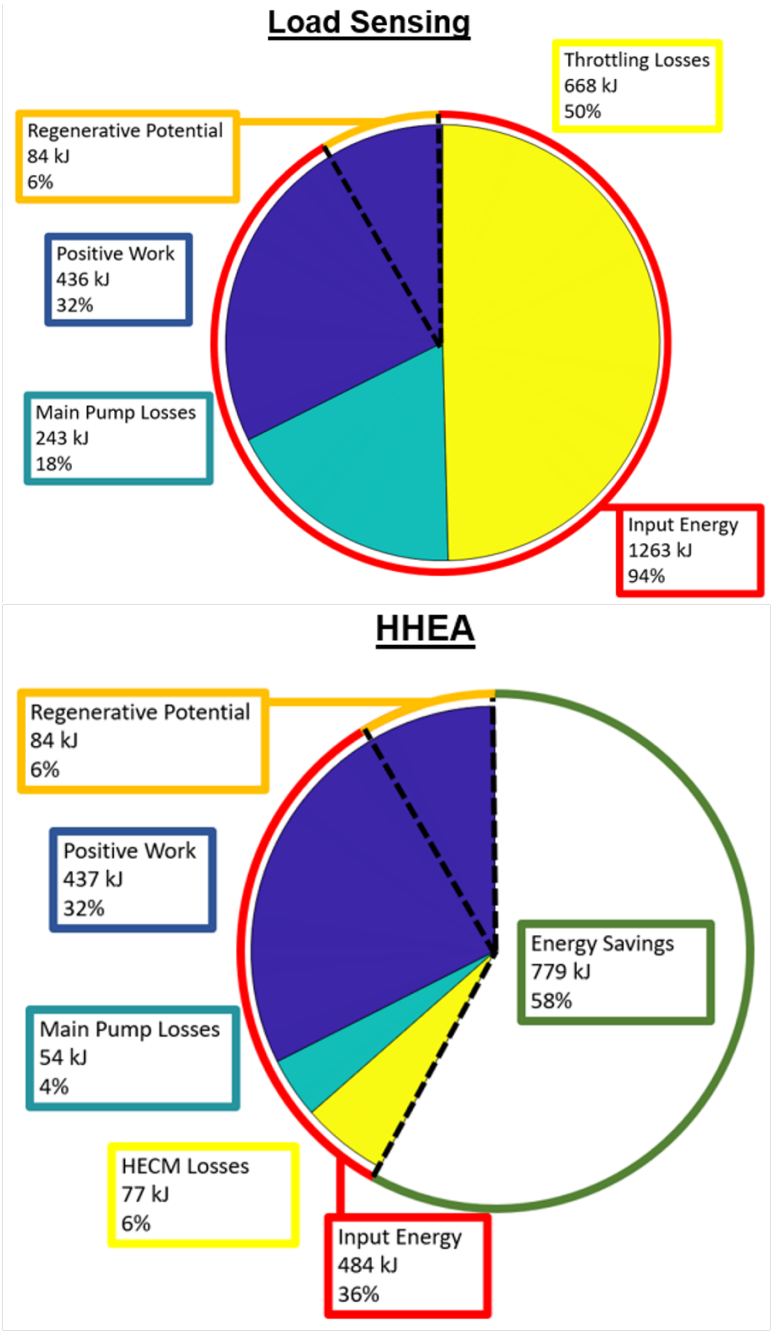

Figure 2.4: Comparison of Load sensing with HHEA for 5t excavator [7]

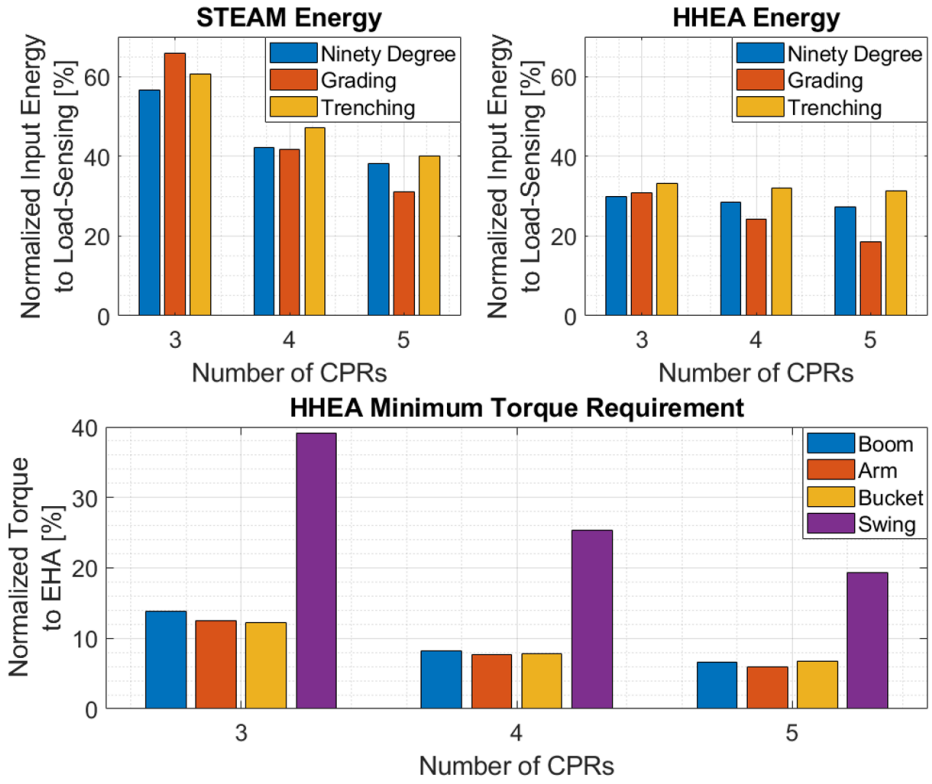

Figure 2.5: Trade-off studies for a 22-ton excavator comparing HHEA with STEAM for different numbers of common pressure rails [7]

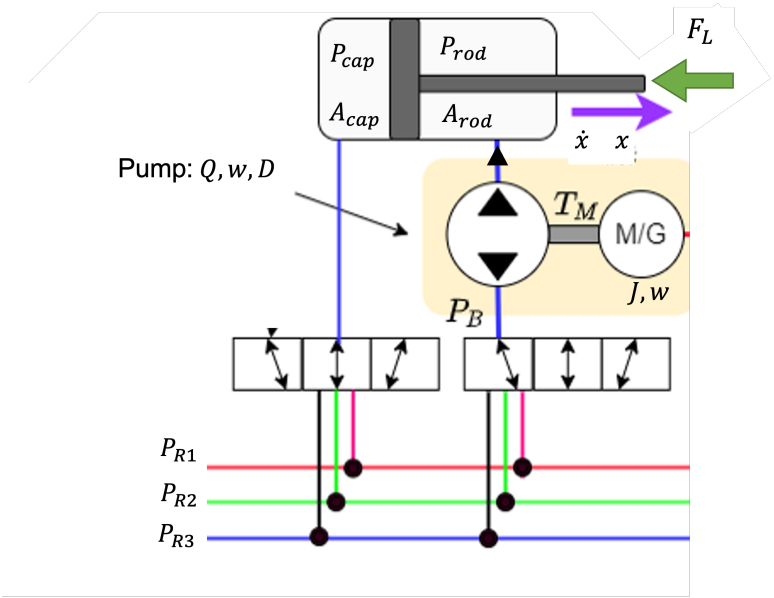

Figure 2.6: Hydraulic Electric Control Module

STEAM saved 60-69%. Furthermore, it was shown that the HHEA utilized approximately 30% less energy than STEAM. This shows that HHEA has great energy-saving potential. The incremental energy saving potential of moving to higher common pressure rails is better for STEAM than HHEA. It has also been shown in figure 2.5 that the torque requirement for the electric motor used in the HHEA architecture is 70-85% smaller than a similarly sized EHA. This shows how HHEA can significantly downsize electric components thereby saving cost.

2.4 System modeling

In this section, a dynamic model of the HHEA has been built based on the governing equations. All the components of the HHEA as shown in Fig. 2.1 has

been modeled and simulated in Matlab Simulink. In HHEA, there are N common pressure rails which are at different nominal pressures ($P_{R1}, \ldots, P_{RN}$). The pressure on these rails is regulated by an accumulator and they are fed by a common pump/motor. For the system model, it is assumed that the rails are at constant pressure. For each degree-of-freedom, there is a hydraulic-electric control module (HECM figure 2.6) that combines hydraulic power from the pressure rails with electric power to actuate the linear degree of freedom. The actuator with which the HECM is connected can be modeled as follows:

$$M\ddot{x} = P_{cap}A_{cap} - P_{rod}A_{rod} - F_L - f \tag{2.3}$$

where $\ddot{x}$ is the acceleration of the actuator. P_{cap} is the cap side pressure of the actuator and P_{rod} is the rod side pressure. A_{cap} and A_{rod} are the respective cap and rod side areas. F_L is the load force acting on the actuator and f accounts for viscous friction and static friction of the actuator. The pressure dynamics for the actuators can be modeled as:

$$\dot{P}_{rod} = \frac{\beta}{V_{rod}(x)}(Q_{HECM} + A_{rod}\dot{x}) \tag{2.4}$$

$$\dot{P}_{cap} = \frac{\beta}{V_{cap}(x)}(Q_{cap} - A_{cap}\dot{x}) \tag{2.5}$$

Here β is the bulk modulus of the fluid and it can be assumed to be constant. V_{rod} and V_{cap} are the volumes of fluid on the cap and the rod side of the actuator and they are a function of the position of the actuator(x). $V_{rod}(x) = V_{or} - A_{rod}x$

and $V_{cap}(x) = V_{oc} + A_{cap}x$, where V_{or} and V_{oc} is the initial volume in the rod and the cap side of the actuator. The flow on the rod side of the actuator is supplied from the HECM pump which is driven by an electric motor. The HECM pump flow can be modeled as :

$$Q_{HECM} = \frac{Dw}{2\pi} \tag{2.6}$$

Here D is the displacement (per revolution) of the HECM pump and w is the angular speed of the pump and of the motor as they are coupled together. The torque from the electric motor drives the pump and this can be modeled as:

$$J\dot{\omega} = \frac{(P_B - P_{rod})D}{2\pi} + T_m \tag{2.7}$$

Here J is the inertia of the electric motor and the hydraulic pump/motor. P_B is the pressure at the inlet of the HECM pump. T_m is the torque from the electric motor. Unlike the rod side, the cap side of the actuator is directly connected to the switching valves. The HECM pump inlet is also connected directly to the switching valves. The switching valve needs to be modeled in order to determine the flow coming in the cap side of the actuator and the inlet of the HECM pump/motor, The switching valve can be modeled by considering the spool dynamics of the

valve and the orifice equation.

$$x_s(s) = \frac{w_n^2}{s^2 + 2\epsilon w_n s + w_n^2} \tag{2.8}$$

$$Q_{cap} = k_v x_s \sqrt{|P_{Rc} - P_{cap}|} sign(P_{Rc} - P_{cap}) \tag{2.9}$$

$$Q_{Rr} = k_v x_s \sqrt{|P_{Rr} - P_B|} sign(P_{Rr} - P_B) \tag{2.10}$$

Here x_s is the valve spool position, w_n is the natural frequency and ϵ is the damping ratio. The valve constant k_v is a valve parameter. The valve constant determines the sizing of the valve.P_{Rc} and P_{Rr} are the cap and rod side pressure rail selection and they belong to the set $\{P_{R1}, \ldots, P_{RN}\}$. Q_{Rr} is the flow from the rails on the inlet of the pump. The pressure dynamics between the pump and the switching valve can be modeled as :

$$\dot{P}_B = \frac{\beta(Q_{Rr} - Q_{rod})}{V_{rail}} \tag{2.11}$$

The mathematical model and equations presented here provide a foundation for analyzing and controlling the HHEA system. By using these equations, we can optimize the system design and control parameters to achieve the desired control objectives. Ultimately, a better understanding of the HHEA system dynamics can lead to the development of more efficient and reliable hydraulic systems.

2.5 Chapter summary

The proposed Hybrid Hydraulic-Electric Architecture (HHEA) combines electrical and hydraulic actuations to improve efficiency, performance, and compactness. The HHEA uses hydraulics as the primary means of power transmission, a centralized hydraulic power supply, and fixed displacement hydraulic pumps/motors to achieve higher efficiency and power density. It can also recuperate regenerative energy and store energy for later use. The HHEA is highly modular and applicable to a wide range of machines, and its integration of the electric motor and hydraulic pump can improve power density and reduce cost. HHEA saves more energy than both Load Sensing and STEAM. For a system with three CPRs, HHEA saved 62-70% of input energy compared to the load-sensing baseline, while STEAM saved 34-43%. For a system with five CPRs, HHEA saved 69-81% of input energy compared to the load-sensing baseline, while STEAM saved 60-69%. HHEA also has the potential to downsize electric components and save costs. The HHEA system has been modeled with pressure and inertial dynamics, and the motion control system will be designed based on these governing equations. In the next chapter the dynamics equations would be used to formulate the control objective and develop the control architecture.

Chapter 3

Control Architecture

The Hybrid Hydraulic Electric Architecture (HHEA) offers significant potential for energy savings compared to state-of-the-art systems. However, precise motion control is imperative for the scalability and utility of this architecture. It is essential to note that a major part of the everyday utility of off-road mobile machines depends on their motion control capabilities.

This chapter provides a high-level understanding of the control objectives and a preview of the proposed control strategy. The HHEA has unique requirements for control compared to the Electro-Hydraulic Actuator (EHA), which was discussed in the review of control systems provided in the introductory chapter. Therefore, a core contribution of this thesis is to demonstrate the controllability of HHEA, and this chapter lays out the high-level design of the motion control system.

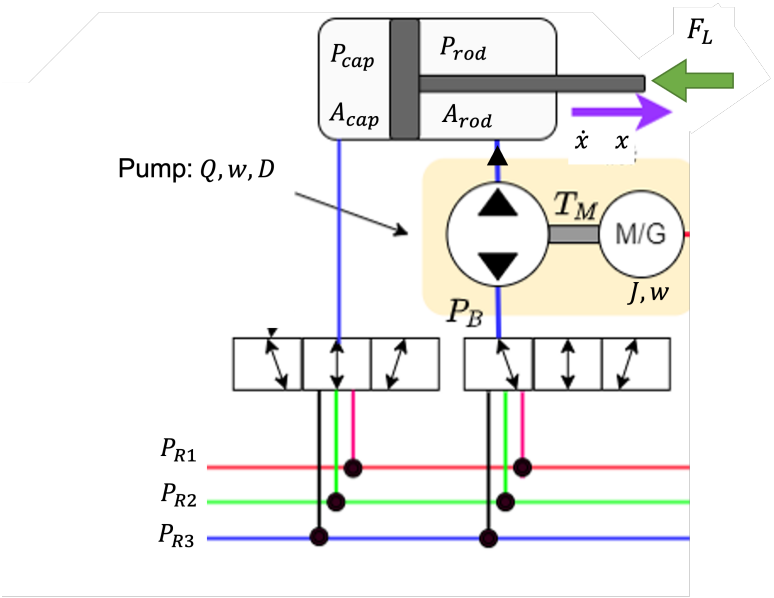

Figure 3.1: Hydraulic Electric Control Module

3.1 Control objective

Before designing the controller for the Hybrid Hydraulic Electric Architecture (HHEA), it is crucial to establish the motion control goals of the system. The HHEA consists of a Hydraulic Electric Control Module that can be retrofitted to an existing hydraulic actuator. The motion of the hydraulic actuator is controlled by an operator. Therefore, the primary goal of the motion control system is to ensure that the motion of each actuator follows the operator's commands precisely. The control system should be able to achieve this goal reliably and efficiently. To better understand the control objective here are the system dynamic equations which are discussed in detail in chapter 2 :

$$M\ddot{x} = P_{cap}(t)A_{cap} - P_{rod}(t)A_{rod} - F_L(t) - f(t) \tag{3.1}$$

$$\dot{P}_{rod} = \frac{\beta}{V_{rod}(x(t))}(Q(t) + A_{rod}\dot{x}(t)) \tag{3.2}$$

$$Q = \frac{D}{2\pi}\omega(t) \tag{3.3}$$

$$J\dot{\omega} = \frac{(P_B(t) - P_{rod}(t))D}{2\pi} + T_M(t) \tag{3.4}$$

In figure 3.1 the inlet of the pump-e-motor unit and the cap side of the actuator are connected to the selected pressure rails. Because these selections can change discretely $P_B(t)$ and $P_{cap}(t)$ can undergo rapid changes in pressure. In between a pressure rail transition $P_B(t)$ and $P_{cap}(t)$ are constant. The electric motor can buck or boost the pressure from P_B to P_{rod} to meet the duty cycle requirements. The motion control objective of HHEA is then to utilize the motor torque T_M to make the actuator position (x) track the desired position $x_d(t)$ trajectory specified by the operator. It is assumed that $x_d(t)$, $\dot{x}_d(t)$, $\ddot{x}_d(t)$ and as well as the external load acting on the actuator $F_L(t)$ are known as of now. In addition, the desired rail selections at any time are assumed to have been determined by another controller concerned with maximizing energy saving [48][53].

Although the HHEA offers numerous benefits, its reliance on downsized electric motors as a core principle can present limitations in terms of available torque for control. Hence, the control objective needs to be achieved with limited electric motor torque T_M. It is important to note that the operator expects the actuator to move exactly as commanded, making the control system responsible for achieving

this. With this objective in mind, the motion control system is designed to ensure precise motion control for HHEA

3.2 Control strategy

The HHEA control strategy incorporates two levels of control design, namely the high-level controller and the low-level controller. The primary responsibility of the high-level controller is to select the appropriate pressure rail for the system. The pressure rail selection plays a crucial role in both reducing the size of electric components and maximizing the energy-saving potential of the architecture. To achieve this, the high-level controller determines the pressure rail choices through an optimization process (currently offline when the desired trajectory is known), which is carried out over a known drive cycle. The objective of this optimization is to minimize losses in the system. A detailed study of the optimization method used to choose the optimal pressure rails has been discussed in [48] [53]. Furthermore, the rail switch decision also considers the switching losses [49]. The output of the high-level controller includes the pressure rail selections on both the cap and rod side of the actuator, which are then fed to the low-level controller.

The low-level controller plays a critical role in the motion control of HHEA. Although some of the control strategies discussed in chapter 1 have been implemented on EHA systems, the HHEA system poses a unique challenge to motion control. This is due to the discrete pressure changes that occur when the pressures for the pump/motor inlet (P_B) and the cap side of the actuator P_{cap} switch

from one selection to another. These changes are necessary to either maximize system efficiency or keep the system within the torque capability of the electric motor. The sudden jump in $P_B(t)$ and $P_{cap}(t)$ can cause jerks in the position of the actuator (x) as it can be seen from equation (3.1).

Compared to EHA systems, the discrete nature of the pressure changes in HHEA adds complexity to the motion control process. The low-level controller must be able to quickly and accurately adjust the system to the changing pressure rails while maintaining the desired performance specifications. This requires a precise understanding of the dynamics of the HHEA system and careful consideration of the system's energy consumption, response time, and stability. Overall, the unique challenges posed by HHEA require a specialized approach to motion control that accounts for the system's discrete pressure changes. However, with an effective low-level controller, HHEA can achieve improved performance, energy efficiency, and overall system reliability.

The control of the HHEA system in the presence of discrete pressure switches is a challenge that has also been encountered in other systems, such as the switched mode hydraulic transformer. In the control of the switched mode hydraulic transformer by Lee et al [20], a bumpless transfer strategy was implemented by delaying the mode switch such that the controller could know about the switch slightly before the actual switch occurred. This allowed for a smooth transition between different modes and helped to maintain stability in the system.

There are other studies with similar bumpless transfer concepts. Ding et al. proposed a bumpless mode switch approach for independent metering systems

that can solve the instability and chattering problems caused by the discrete switches [54]. The proposed approach includes a dynamic dwell-time switch and a bidirectional latent tracking loop. This strategy is verified by a mini-excavator and shown to improve energy efficiency without reducing motion control performance compared to conventional valve control systems.

Malloci et al. [55] presents a bumpless transfer controller for discrete-time switched linear systems that reduce the transient behavior by activating at every switching time. The controller is designed using a linear quadratic optimization problem and provides dwell time conditions for assessing the asymptotic stability of the closed-loop switched system. Herbst et al. [56] examined discrete-time variants of active disturbance rejection control (ADRC) and extended them to meet practical requirements such as bumpless transfer and control signal limitations. This idea is very commonly used in power electronics mode switching.

Heybroek et al. [57] implemented a Model Predictive Controller (MPC) on a multi-chamber actuator, which has a design similar to HHEA in that it is able to generate discrete hydraulic forces. The MPC controller was implemented on an excavator and used solely for mode switching. The results of their study demonstrated that the MPC controller was able to effectively reduce force spikes during discrete force level switches. Although the primary focus of Heybroek's study was on force control rather than motion control, the reduction of force spikes during mode switches can also contribute to smoother transient motion. The reduction of these spikes can help to improve the overall performance and stability of the system by minimizing the impact of discrete force changes on the system's

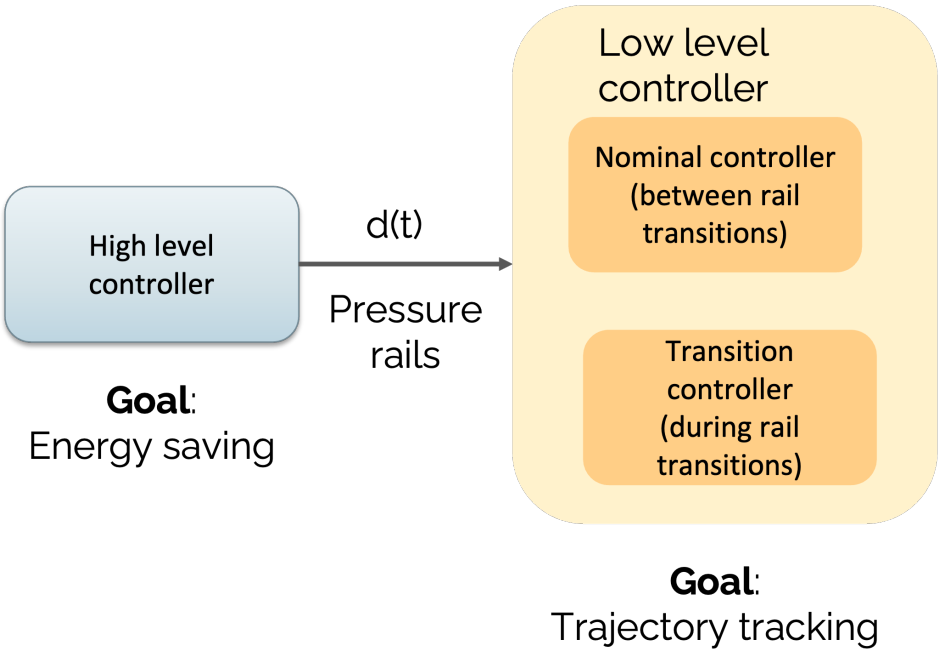

Figure 3.2: Overview of control strategy for HHEA

response. A major limitation of using MPC controller is that it is computationally very expensive. Many other approaches to using bumpless transfer in hydraulics and aerospace applications have been explored by researchers around the world [58] [59] [60].

In the context of the HHEA system, similar strategies to those discussed earlier can be utilized to design a separate transition controller that can anticipate discrete pressure changes occurring during pressure rail switching, leading to smoother transitions and better overall system performance. By using a predictive control strategy, the transition controller can adjust the system's behavior accordingly. Additionally, a nominal controller can be designed to maintain desired performance specifications under normal operating conditions. The nominal

controller is used in between two pressure rail switches which accounts for the majority of operating time. The combined control strategy is shown in figure 3.2, where the high-level controller aims to save energy while the low-level controller is responsible for motion control. The low-level motion control strategy in turn uses two different controllers: a nominal and a transition controller to handle motion control between pressure rail switches and during pressure rail switches respectively. The nominal and transition controllers will be discussed in detail in chapter 4 and chapter 5, respectively.

3.3 Chapter summary

This chapter highlights the crucial role that motion control performance plays in the effectiveness of off-road mobile machines. The specific focus is on defining the motion control objectives for HHEA, which is achieved by tracking a predetermined position trajectory using electric motor torque as the primary control input. The trajectory's duty cycle is predetermined, and the actuator is subject to a load, while pressure rails switch on the cap side of the actuator and inlet of the HECM pump. By successfully achieving these objectives, the HHEA can operate at its optimal level, delivering the required performance for its intended application. The control strategy for HHEA is designed with a two-tiered approach, consisting of a high-level and a low-level controller. The high-level controller is primarily responsible for optimizing energy efficiency within the system by making informed pressure rail selections. On the other hand, the low-level controller

focuses on motion control of the HHEA, which is essential for achieving the desired position trajectory. To accomplish this, the low-level controller employs a nominal controller that handles the motion control between two pressure rail switches. Additionally, a separate transition controller is used to manage motion control during pressure rail transitions. The combination of both high and low-level controllers allows for efficient and precise motion control while also achieving maximum energy efficiency, resulting in optimal performance of the HHEA.

Chapter 4

Nominal Controller

The proposed control design for the HHEA system involves a main controller that comprises two levels of control: a high-level controller and a low-level controller. The high-level controller focuses on the optimal selection of pressure rails to minimize energy losses [48], and the low-level control is used for motion control. The pressure rail configurations selected by the high-level controller are then fed to the low-level controller. The high-level control strategy is not the subject of the proposed research.

Since the switching of pressure rails is an essential aspect of the HHEA architecture, it is vital to understand the dynamics involved during a pressure rail switch. There are three possible pressure rail switches for a linear hydraulic actuator: cap-side pressure rail switch only, rod-side pressure rail switch only, and both cap and rod-side pressure rail switch. In cases where both pressure rails are changing, the pressure on the cap side of the actuator will change faster than

the rod-side pressure, which is limited by the pump flow from the HECM. This pressure mismatch can lead to tracking errors that the controller needs to address. The low-level controller involves two different controllers for tackling a nominal case and a transition case.

This chapter will provide a comprehensive explanation of the design process for the nominal controller, which is utilized during the periods between pressure rail switches. Additionally, we will investigate the potential outcomes of using the nominal controller during a pressure rail switch. To achieve this goal, a passivity-based backstepping control approach has been selected for the nominal controller. A step by step derivation of the control law is discussed and the controller performance is evaluated. The next chapter, Chapter chapter 5, will explain the transition controller.

4.1 Nominal control design

Between two pressure rail switches, a constant pressure rail is selected on both the cap and the rod side of the actuator. The pump can buck or boost pressure on the rod end of the actuator to extend or retract the cylinder based on the load force applied. Passivity property has been used in many non-linear systems to get robust control laws [61]. Using the mechanical systems' physical energy functions and their change incorporated into Lyapunov functions, a passivity property (with mechanical power input being the supply rate) can be derived. A whole class of fixed and adaptive control laws with extensive analysis and arbitrary gains

have been obtained from the passivity property [62]. The passivity property of a mechanical system is an extension of the Euler-Lagrange structure, controls based on such structure have been developed in other domains [63]. A hydraulic actuator has been shown to be a passive two-port system [43]. Wang et al. [64] have developed a passivity control framework for mechanical-pressure dynamics in a hydraulic actuator which is based on the natural physical energy of the system. This has been incorporated into the popular back-stepping technique so that the natural physical property of the system can be taken into consideration. With this, the back-stepping approach can be enhanced so that it is more robust, easier to tune, and less sensitive to velocity measurement error.

Passivity-based back-stepping control has been used for trajectory tracking of the hydraulic actuator using hydraulic Transformer [19]. For HHEA, the controller proposed in [43, 44] where flow is the control input can be extended to make torque from the electric motor as the control input. For the nominal control, we propose to use passivity-based back-stepping with an integral controller. The integral controller with a back-stepping design would improve the system's robustness against modeling uncertainties and external disturbances [65].

Referring to the system dynamics for HHEA as shown:

$$M\ddot{x} = P_{cap}A_{cap} - P_{rod}A_{rod} - F_L - f \tag{4.1}$$

$$\dot{P}_{rod} = \frac{\beta}{V_{rod}(x)}(Q + A_{rod}\dot{x}) \tag{4.2}$$

$$Q = \frac{D}{2\pi}\omega \tag{4.3}$$

$$J\dot{\omega} = \frac{(P_B - P_{rod})D}{2\pi} + T_M \tag{4.4}$$

the control design would proceed successively by assuming P_{rod}, Q_{HECM} and T_m as the control inputs. At each step, the Lyapunov function for proving stability is successively extended to include additional states by adding the energy associated with that state [19]. The process for the design is as follows:

Consider a system in which the control input is the velocity, $\dot{x}$, and the output is the actuator position. To track a known desired position trajectory x_d, let the position tracking error e be defined as $e := x - x_d$. Now, let us define the reference velocity as the control input to achieve stable dynamics :

$$r := \dot{x_d} - \lambda_p e; \tag{4.5}$$

Next, since velocity $\dot{x}$ cannot be adjusted directly, we consider the control input to be the rod side chamber pressure P_{rod} and the actuator position x as the output. Let us define an additional state variable, the reference velocity error, e_v

as:

$$e_v = \dot{x} - r \tag{4.6}$$

An integral term e_I defined as

$$\dot{e}_I = e_v \tag{4.7}$$

is also introduced to compensate for any steady-state errors that may arise due to factors such as model uncertainties, disturbances, or parameter variations. Now, the desired rod side pressure can be designed as :

$$P_d = \frac{1}{A_{rod}} \left(P_{cap} A_{cap} - F_L - f - M\dot{r} + K_v e_v + K_I e_I \right) \tag{4.8}$$

where $K_v > 0$ and $K_I > 0$. Then the reference velocity error dynamics becomes:

$$\begin{aligned} M\dot{e_v} &= M(\ddot{x} - \dot{r}) \\ &= P_{cap} A_{cap} - (P_d + \tilde{P}) A_{rod} - F_L - f - M\dot{r} \\ &= -K_v e_v - K_I e_I - \tilde{P} A_{rod} \end{aligned} \tag{4.9}$$

where $\tilde{P} = P_{rod} - P_d$. The Lyapunov function can be defined as :

$$V_2 = \frac{1}{2} M e_v^2 + \frac{1}{2} K_I e_I^2 \tag{4.10}$$

Now we can show that the time derivative of the Lyapunov function on simplification becomes:

$$\dot{V}_2 = -K_v e_v^2 - \tilde{P} A_{rod} e_v \tag{4.11}$$

Note that from (4.10) and (4.11), the mechanical system is passive with respect to the supply rate $\tilde{P} A_{rod} e_v$. As $\dot{V}_2$ is negative semi-definite when $\tilde{P} = 0$, by applying Barbalat's lemma, we can show e_v converges to zero asymptotically. However, since P_{rod} cannot be manipulated directly, the design needs to be further extended.

In the next step, we take into account pressure dynamics in the system and consider the output flow Q_{HECM} from the pump/motor as the control input. Following [43], we define an augmented Lyapunov function using the pressure error energy function

$$W_p(x, \tilde{P}, P_d) := V_{rod}(x) W_V(\tilde{P}, P_d) \tag{4.12}$$

$$W_V(\tilde{P}, P_d) := \int_{P_d+\tilde{P}}^{P_d} [e^{g(P_d+\tilde{P}, P')} - 1]\, dP' \tag{4.13}$$

where $W_V(\tilde{P}, P_d)$ is the energy density associated with compressing the fluid from P_d to $P_{rod} = P_d + \tilde{P}$ with

$$g(P_d + \tilde{P}, P_d) = \int_{P_d+\tilde{P}}^{P_d} \frac{dP'}{\beta(P')} \tag{4.14}$$

and $\beta(P')$ is the bulk modulus at that pressure. For details, please see [43]. This

is where the passivity-based approach differs from a conventional backstepping approach where a quadratic pressure error term is typically used instead of a physically motivated Lyapunov function. The augmented Lyapunov function then becomes :

$$V_3 := V_2 + W_p(x, \tilde{P}, P_d) \tag{4.15}$$

The derivative of the Lyapunov function is given by :

$$\dot{V}_3 = -K_v e_v^2 - \tilde{P} A_{rod} e_v + \dot{W}_p(x, \tilde{P}, P_d) \tag{4.16}$$

It has been shown in [43] that:

$$\dot{W}_p(x, \tilde{P}, P_d) = \left[\tilde{P} + W_V(\tilde{P}, P_d)\right] Q - \tilde{P} A_{rod} \dot{x} - V(x) \left[e^{g(P,P_d)} - 1\right] \dot{P}_d \tag{4.17}$$

We define Q_d to cancel out the trajectory terms and to make the system stable:

$$Q_d = -A_{rod}\, r + \frac{V_{rod}(x)\dot{P}_d}{\beta} - \lambda_3 \tilde{P} \tag{4.18}$$

where β is the bulk modulus. Using bounds on

$$\left| \frac{\tilde{P}}{[e^{g(P_1,P_d)} - 1]} - \frac{1}{\beta(P_d)} \right|, \quad \text{and} \quad \frac{W_V \tilde{P}, P_d}{\tilde{P}^2}$$

it can be shown (see [43]) that with λ_3 chosen to be sufficiently large, $\dot{V}_3$ satisfies

:

$$\dot{V}_3 :\leq -\begin{bmatrix} e_v & \tilde{P} \end{bmatrix} \mathcal{M} \begin{bmatrix} e_v \\ \tilde{P} \end{bmatrix} + \Psi(\tilde{P}, P_{rod,d})\tilde{Q} \tag{4.19}$$

Here,

$$\Psi(\tilde{P}, P_{rod,d}) := \tilde{P} + W_v(\tilde{P}, P_{rod,d}) \tag{4.20}$$

is the hydraulic effort (conjugate to hydraulic flow Q), $\tilde{Q} = Q - Q_d$ is the flow error, and $\mathcal{M}$ is a positive definite matrix. Eq.(4.19) signifies that with the control design, the system is passive with respect to the supply rate, $\Psi(\tilde{P}, P_{rod,d})\tilde{Q}$.

The desired pump flow can be converted to the desired shaft speed command for the HECM's e-motor and pump combination as:

$$Q_d = \frac{D}{2\pi}\omega_d \tag{4.21}$$

Here, D represents the displacement for the pump, and ω_d is the desired angular speed of the electric motor.

If the electric motor is capable of accepting a speed reference, the solution described up to this point is sufficient. In such a case, the electric motor would have an internal speed control loop or an inner PID control loop. This control loop enables the electric motor to receive the commanded electric motor torque as the input and the desired speed as the reference. By utilizing this control loop, the electric motor can adjust its torque output to achieve the desired speed.

It is also possible to expand the existing backstepping framework by utilizing

the torque generated by the electric motor, T_m, as a control input to operate the HECM pump/motor. This is the final step with an assumption that the response of the power electronics is fast enough to generate the desired torque command as requested. The Lyapunov function for this step includes the rotational kinetic energy term, which is used to model the dynamics of the combined pump and electric motor unit. The angular velocity error is defined as the difference between the actual and desired angular velocities and is denoted by $\tilde{\omega}$ then the desired electric motor torque can be defined as:

$$T_m = \frac{D}{2\pi}(P_{rod} - P_B - \tilde{P}) - \lambda_4 \tilde{\omega} \tag{4.22}$$

This makes the angular velocity error dynamics as :

$$J\dot{\tilde{w}} = -\frac{D}{2\pi}\tilde{P} - \lambda_4 \tilde{w} \tag{4.23}$$

where J is the inertia of the combined pump and electric motor unit and λ_4 is a positive control parameter. The Lyapunov function is defined as :

$$V_4 := V_3 + \frac{1}{2}J\tilde{\omega}^2 \tag{4.24}$$

Substituting the desired control input in the time derivative of the Lyapunov function we can show that the time derivative is negative definite implying that

the Lyapunov function decreases with time.

$$\dot{V}_4 \leq -\begin{bmatrix} e_v & \tilde{P} \end{bmatrix} \mathcal{M} \begin{bmatrix} e_v \\ \tilde{P} \end{bmatrix} - \lambda_4 \, \tilde{\omega}^2 \tag{4.25}$$

This indicates that V_4 and the errors e_I, e_v, $\tilde{P}$, $\tilde{\omega}$ all converge to 0 asymptotically. The block diagonal matrix $diag(\mathcal{M}, \lambda_4)$ is positive definite with a strictly positive lower bound for its eigenvalues, and V_4 is positive definite, which ensures the stability of the control system. Although the current control input achieves asymptotic convergence, with slight modification to the Lyapunov function (4.10), exponential convergence can be proved. One such modification is to redefine the Lyapunov function (4.10) as:

$$V_2 = \frac{1}{2} M e_v^2 + 2\epsilon e_I e_v + \frac{1}{2} K_I e_I^2 \tag{4.26}$$

where $\epsilon > 0$ is a small constant.

The conventional back-stepping approach which employs a quadratic pressure error term differs from passivity-based backstepping control in terms of the requirements for system parameters, parameter uncertainty, and the treatment of the piston velocity.

Firstly, the actuator volume and bulk modulus are needed only for the feedforward term in the passivity-based backstepping approach, while both feedback and feedforward terms in the basic backstepping control equation require knowledge of these parameters. This makes the passivity-based approach more immune to

measurement noises and parameter uncertainty.

Secondly, there is a different treatment of the piston velocity between the two control approaches. The passivity-based approach uses only the reference velocity, while the traditional backstepping approach actively cancels the actual piston velocity and feeds back a velocity error.

Finally, the conventional backstepping approach which uses a quadratic energy function requires tuning additional gain to achieve the required performance. Moreover, if the gain is not tuned properly, it may lead to unstable or undesirable control behavior. The passivity-based control strategy discussed in this section also involves gain tuning that plays a very crucial role in dictating the performance of the system. The state error dynamics of the system can be represented as :

$$\begin{bmatrix} K_I \dot{e}_I \\ M \dot{e}_v \\ \frac{V_{rod}(x)}{\beta} \dot{\tilde{P}} \\ J \dot{\tilde{\omega}} \end{bmatrix} = \begin{bmatrix} 0 & K_I & 0 & 0 \\ -K_I & -K_v & -A_r & 0 \\ 0 & A_r & -\lambda_3 & \frac{D}{2\pi} \\ 0 & 0 & -\frac{D}{2\pi} & -\lambda_4 \end{bmatrix} \begin{bmatrix} e_I \\ e_v \\ \tilde{P} \\ \tilde{\omega} \end{bmatrix} \tag{4.27}$$

The system matrix consists of different gains such as K_I, K_v, λ_3, and λ_4 which need to be tuned. The goal of tuning these gains is to ensure that the eigenvalues of the linearized dynamics are real and negative with all the eigenvalues close to each other. Once the gains are tuned, they can be used to calculate the control inputs required to achieve a desired state. Specifically, the gains K_I and K_v are used to compute the integral and derivative gains for the velocity and position

controllers, respectively. The gain λ_3 is used to calculate the feedback gain for the pressure controller, and λ_4 is used to determine the feedback gain for the motor velocity controller

To tune the gains, the eigenvalues of the linearized dynamics at typical chamber volume are evaluated. The gains are then adjusted until all the eigenvalues are real and negative, and all the eigenvalues are close to each other. This ensures that the system is stable and that the response to disturbances is well-damped. This methodology can be used to tune the nominal controller for different systems.

4.2 Modified control with exponential convergence

The control law formulated in the preceding section establishes asymptotic stability. This section derives an alternative algorithm such that exponential convergence can be demonstrated directly from the Lyapunov analysis. The key difference lies in the way that integral error is handled. Due to the integral error, the previous control algorithm only shows asymptotic stability, not exponential stability, using direct Lyapunov analysis.

Similar to the previous analysis let us consider a system with velocity as the control input and position as the control output. Let us define position tracking error as $e = x - x_d$, where x_d is the desired position. This time, let us define the

integral error as $\dot{e_I} = e$. The reference velocity can be designed as:

$$r := \dot{x_d} - 2\zeta\omega_n e - \omega_n^2 e_I \tag{4.28}$$

Here $\omega_n \geq 0$ and $\zeta \geq 0$. With this reference velocity, e_v defined in equation (4.6) can be written as:

$$\begin{aligned} e_v &:= \dot{x} - r \\ &:= \dot{e} + 2\zeta\omega_n e + \omega_n^2 e_I \\ &:= \ddot{e_I} + 2\zeta\omega_n \dot{e_I} + \omega_n^2 e_I \end{aligned} \tag{4.29}$$

Note that this represents an exponentially stable system driven by e_v.

With the rod side pressure as the control input, the desired pressure can be defined as:

$$P_d = \frac{1}{A_{rod}} \left(P_{cap} A_{cap} - F_L - f - M\dot{r} + k_v e_v \right) \tag{4.30}$$

where $k_v > 0$ and the reference velocity error dynamics is:

$$M\dot{e_v} = -k_v e_v - \tilde{P} A_r \tag{4.31}$$

where $\tilde{P} = P_{rod} - P_d$. The Lyapunov function can be defined as :

$$V_2 = \frac{1}{2} M e_v^2 \tag{4.32}$$

Now we can show that the time derivative of the Lyapunov function on simplification becomes:

$$\dot{V}_2 = -k_v e_v^2 - \tilde{P} A_{rod} e_v \tag{4.33}$$

Since $\dot{V}_2$ is negative definite when $\tilde{P} = 0$, we can show $e_v \to 0$ exponentially when $\tilde{P} \to 0$. As $e_v \to 0$ exponentially, we can show from equation (4.29) that $e_I \to 0$ exponentially also. This indicates that the system has achieved its desired state. The rest of the proof is similar to the previous analysis from equation (4.11) - equation (4.24). The Lyapunov function for the final step is defined as :

$$V_4 := \frac{1}{2} M e_v^2 + V_{rod}(x) W_V(\tilde{P}, P_d) + \frac{1}{2} J \tilde{\omega}^2 \tag{4.34}$$

The time derivative of the Lyapunov function becomes:

$$\dot{V}_4 \leq - \begin{bmatrix} e_v & \tilde{P} \end{bmatrix} \mathcal{M} \begin{bmatrix} e_v \\ \tilde{P} \end{bmatrix} - \lambda_4 \, \tilde{\omega}^2 \tag{4.35}$$

Compared with (4.34), since there exists $\gamma > 0$ such that :

$$\dot{V}_4 \leq -\gamma V_4$$

we can show V_4 and the errors e_v, $\tilde{P}$, $\tilde{\omega}$ all converge to 0 exponentially. The block diagonal matrix $diag(\mathcal{M}, \lambda_4)$ is positive definite with a strictly positive lower bound for its eigenvalues, and V_4 is positive definite, which ensures the stability

of the control system. Since e_v converges to 0 exponentially from equation (4.29) we can also show e_I to converge exponentially. Hence the system converges exponentially. The state error dynamics of the system can be represented as :

$$\begin{bmatrix} \dot{e}_I \\ \dot{e} \\ M\dot{e}_v \\ \frac{V_{rod}(x)}{\beta}\dot{\tilde{P}} \\ J\dot{\tilde{\omega}} \end{bmatrix} = \begin{bmatrix} 0 & 1 & 0 & 0 & 0 \\ -\omega_n^2 & -2\zeta\omega_n & 1 & 0 & 0 \\ 0 & 0 & -k_v & -A_r & 0 \\ 0 & 0 & A_r & -\lambda_3 & \frac{D}{2\pi} \\ 0 & 0 & 0 & -\frac{D}{2\pi} & -\lambda_4 \end{bmatrix} \begin{bmatrix} e_I \\ e \\ e_v \\ \tilde{P} \\ \tilde{\omega} \end{bmatrix} \tag{4.36}$$

Similar to the previous analysis the gains ζ,w_n, k_v, λ_3, and λ_4 are tuned to make the eigenvalues real and negative. It is worth highlighting that, despite the successful demonstration of exponential convergence in this section, the subsequent content of the thesis employs the control law established in section 4.1 for all experimental and simulation results related to the nominal controller.

4.3 Simulation results

The control strategy developed in section 4.1 is implemented on a 21-ton wheel loader using the HHEA model. This study aimed to evaluate the performance of the lift cylinder of the wheel loader in tracking a given duty cycle, which was used to provide reference trajectories and load force. Based on the load force, pressure rail switches were employed and the tracking performance of the lift cylinder was observed.

Table 4.1: Simulation Parameters

Parameter	**Symbol**	**Value**
Cap Area	A_{cap}	0.0101 m^2
Rod Area	A_{rod}	0.0075 m^2
HECM pump displacement	D	107 $\frac{cc}{rev}$
e-motor-pump inertia	J	0.004 Kgm^2
Mass	M	1200 Kg
Bulk Modulus	β	1.6GPa
velocity error dynamics gain	λ_p	20
Reference velocity error gain	K_v	1000
Pressure feedback gain	λ_3	10^{-9}
angular velocity feedback gain	λ_4	0.1

The results of the study using the parameters shown in table 4.1 showed that the controller was able to track the duty cycle with a maximum error of 0.2mm as shown in figure 4.1. This indicates that the controller was effective in maintaining the desired position of the lift cylinder throughout the duty cycle. However, it is important to note that the controller required a peak control input of 2000 Nm of torque. This suggests that the controller had to exert a significant amount of effort to maintain the desired position of the lift cylinder when the pressure rails were switching.

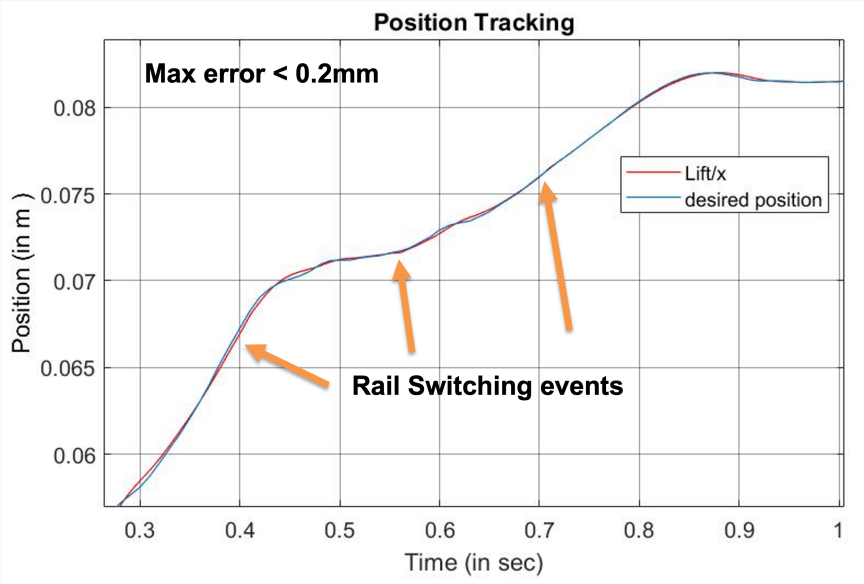

Figure 4.1: Position tracking with pressure rail switches

The HHEA architecture is designed to make the electric components smaller, which implies that the peak available torque for control is limited. This approach is based on the core principle that smaller electric components lead to a more compact and cost-effective hydraulic hybrid system. However, it is important to analyze the effects of torque saturation on the position-tracking performance of the system.

To investigate the impact of torque saturation on the performance of the HHEA system, a single switch was demonstrated where the cap side pressure rail switches from 30 Mpa to 40 Mpa and the rod side pressure rail switches from tank to 20 MPa. This switch was designed to simulate the real-world operating conditions of the wheel loader during a typical duty cycle. The position tracking error during this switch was demonstrated in figure 4.4, which shows that the peak error is 0.3

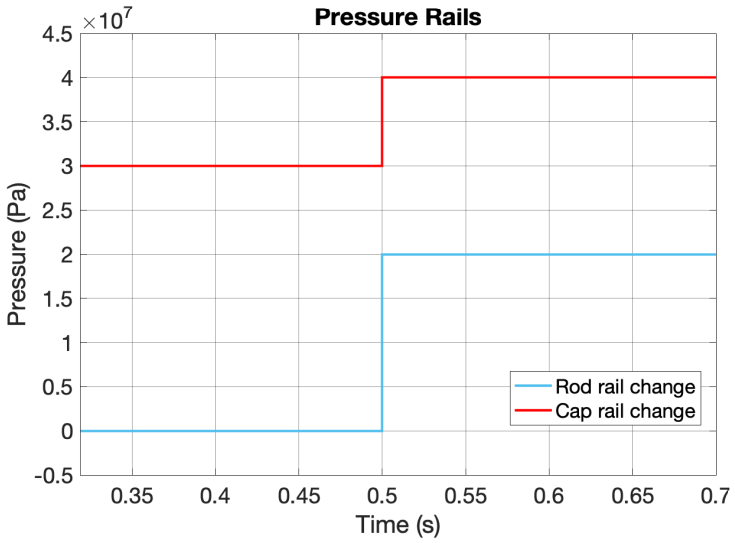

Figure 4.2: Pressure rail switches

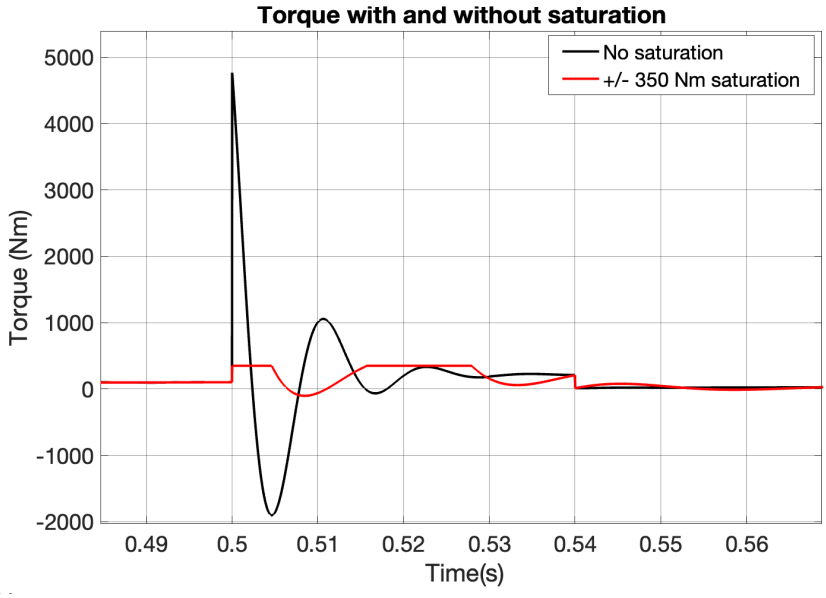

Figure 4.3: Electric motor torque with and without saturation

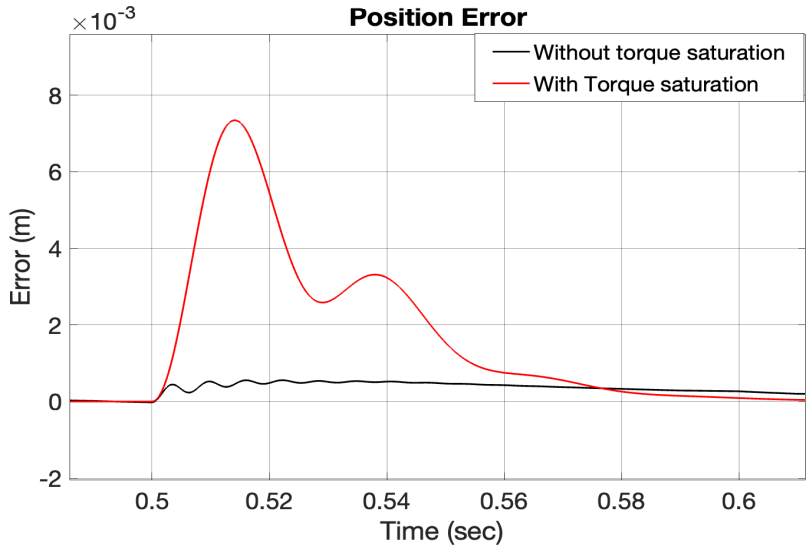

Figure 4.4: Position tracking error with and without electric motor torque saturation

mm when a peak torque of 4500 Nm is applied at the start of the rail switch, as shown in figure 4.3.

However, when the motor torque is limited to 350 Nm, the position-tracking performance is affected. The peak tracking error increases to 7.1 mm, as depicted in figure 4.4. These results indicate that while the passivity-based integral backstepping controller can provide excellent trajectory tracking performance when the electric motor torque is not limited, it is affected when the motor torque is limited during a pressure rail switch. Therefore, a separate controller is required that can take over control during a pressure rail switch to improve the tracking performance when a pressure rail switch takes place.

The nominal conditions are defined between two consecutive switches and this condition prevails for a majority of the trajectory. The passivity-based integral

controller serves as the nominal control for the HHEA motion control system. In the following chapter, we will delve into the specifics of designing a separate controller to manage pressure rail switches.

4.4 Effect of parameter uncertainty

Table 4.2: Model paramters

Parameter	**Symbol**	**Value**
Cap Area	A_{cap}	0.002 m^2
Rod Area	A_{rod}	0.0012 m^2
HECM pump displacement	D	8 cc/rev
e-motor-pump inertia	J	0.0024 Kgm^2
Mass	M	5 Kg
Bulk Modulus	β	$1.3GPa$
Velocity error dynamics gain	λ_p	15
Reference velocity error gain	K_v	100
Integral gain	K_I	300000
Pressure feedback gain	λ_3	10^{-10}
Damping coefficient	B	1000 N/m
Stiction	F	600 N

An investigation was conducted to assess the robustness of the passivity-based integral backstepping controller against parameter uncertainties in mass, viscous damping coefficient, and stiction in a hydraulic cylinder. The controller was intentionally unaware of the correct model parameters (denoted as M, B, and F), and a trapezoidal trajectory was utilized for testing purposes, with varying parameter values provided to the controller. The control gains were maintained at a consistent level across all cases. The specific model parameters are outlined in table 4.2, and an unchanging load force of 14000 N was applied to the hydraulic cylinder throughout the experiments.

As depicted in figure 4.5, the controller demonstrated effective tracking of the desired trajectory even in the presence of parameter variations, exhibiting no steady-state errors. Notably, the influence of uncertainty in stiction became apparent during the actuator's initial movement. Assuming zero stiction resulted in a maximum tracking error of 0.6 mm, while overestimating the stiction by three times led to a peak error of 1.8 mm. Consequently, it can be concluded that uncertainty in stiction affects the initial motion of the actuator, but the controller promptly adapts and achieves accurate tracking within a short period of time.

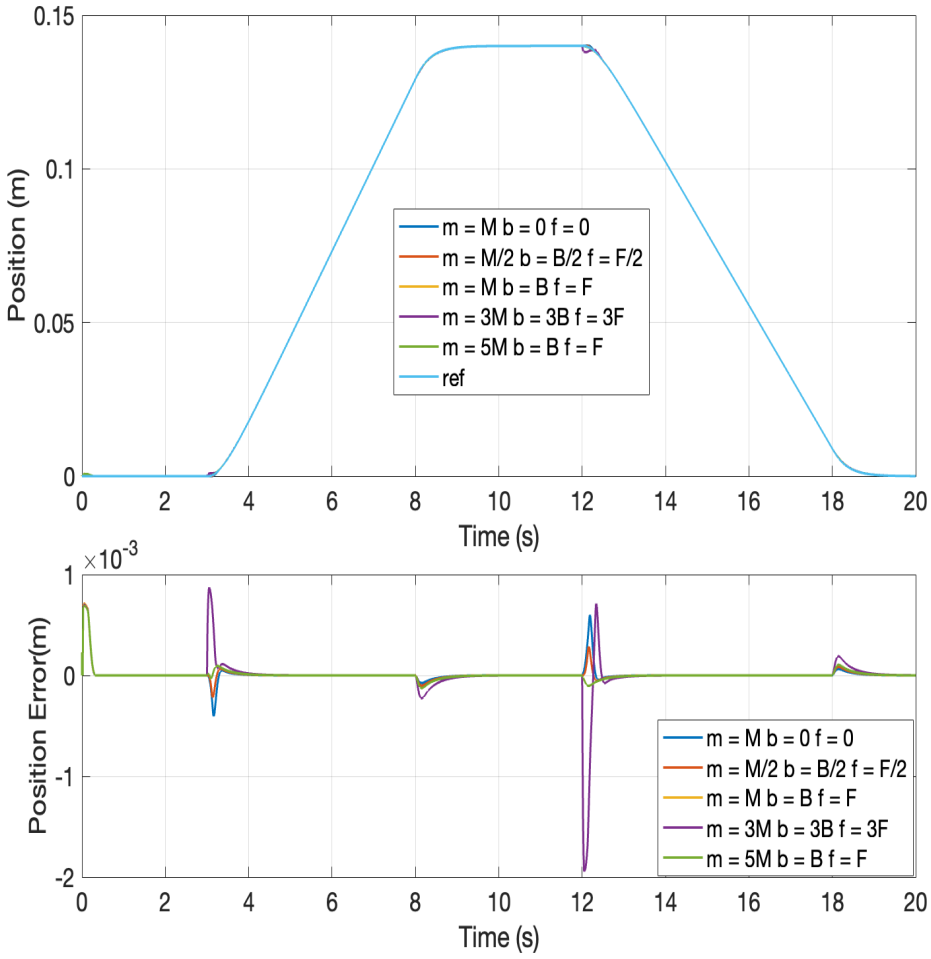

Figure 4.5: Position tracking with parameter uncertainty

4.5 Chapter summary

Pressure rail switches are crucial components in reducing the size of electrical components and improving efficiency in the Hybrid Hydraulic Electric Architecture (HHEA). To handle pressure rail switches, the motion control design employs two different controllers: the nominal controller and the transition controller. The nominal controller is used between two pressure rail switches and utilizes a passivity-based integral backstepping controller, which considers the system's intrinsic energy. This chapter dives into the details of designing the nominal controller.

The passivity-based controller is an improvement over the conventional backstepping design which uses a quadratic energy function. The backstepping design begins with velocity as the control input and progresses to the final stage, where the electric motor torque is the control input. At every step, each additional term in the Lyapunov function is inspired by the different energy storage elements in the system. The nominal controller is capable of tracking the duty cycle even during a pressure rail switch when no torque restrictions are applied. However, the torque required during a switch is very high, which contradicts the core principle of reducing the size of electrical components.

Therefore, a different controller is needed when the pressure rails are switching which can reduce the electric motor torque usage during switching. The tracking accuracy for nominal cases is less than 0.2 mm, making the passivity-based framework an excellent choice for the nominal controller in the architecture.

Chapter 5

Transition Control

The nominal controller is designed to ensure good motion tracking performance under normal operating conditions. However, when the pressure rails switch, the pressure error can suddenly become very large, requiring a significant torque input that exceeds the capabilities of the electric motor/drive. This becomes even more problematic when both pressure rails switch at the same time. This is a significant issue because the system architecture is based on the premise that it requires only small electric machines. Attempting to saturate the torque at its maximum level in response to the pressure rail switch can lead to a significant increase in tracking error and it takes a long time for the controller to recover.

To address this issue, the system design includes a short transition period during which a special transition controller is used. The purpose of this controller is to minimize the effect of the pressure rail changes on motion tracking while keeping the control input within feasible limits. The transition controller aims

to reach a state with zero error at the end of the transition period, after which control is returned to the nominal controller.

This particular approach to managing the transition period between the pressure rail switch is designed to minimize the impact of the pressure rail changes on the motion tracking performance. By keeping the control input within a feasible range and aiming for a state with zero error at the end of the transition, the transition controller helps to ensure that the system remains stable and the motion tracking performance is not significantly impacted.

The nominal controller operates without any knowledge of the pressure rail switches. It has to rely on changes in the desired pressure rate to detect potential switch cases and take action. In this scenario, the nominal controller is reactive rather than proactive. In contrast, the transition controller can be thought of as a proactive control mechanism. This means that the controller has prior knowledge of the pressure rail switch events and is designed to mitigate their impact on motion control performance. By taking control before a switch occurs and minimizing the impact of the switch, the transition controller aims to ensure that the motion control performance remains stable and that the system is not impacted by any sudden changes in pressure.

The current chapter provides an in-depth discussion of the design and requirements of the transition controller [66], with a focus on addressing the control problem that arises during a pressure rail switch. To tackle this problem, a Least Norm Control approach is utilized and the results are presented. Additionally, a comparison of tracking performance is presented, demonstrating the benefits

of using both the nominal and transition controller together, as opposed to relying solely on the nominal controller. This finding reinforces the importance and advantages of incorporating the transition controller during a pressure rail switch.

5.1 Least Norm Control

In order to drive a system from its starting point to its desired end state in a finite duration, multiple control input trajectories can be used. An effective way to calculate the optimal input is through Least Norm Control, which is a control strategy where the control input is selected in a way that minimizes the L_2 norm of the input, while ensuring that the system satisfies a specified desired behavior, such as reaching a target state. In addition, by minimizing the L_2 norm of the control input, the least-norm control approach provides a mathematical optimization problem that can be easily solved using a variety of numerical methods. This makes the approach widely applicable to a variety of control problems and systems and enables researchers to find efficient and effective control solutions for their systems.

The formulation presented in the description is a method to solve the least-norm control problem for the system:

$$\dot{X} = A(t)X + B(t)u \tag{5.1}$$

The goal is to find the control input u(t) that steers the state from $X(t_0) = X_0$ to $X(t_f) = X_f$ at the final time t_f while minimizing the L_2-norm of u(t) [67].

This problem is posed as a reachability problem and the reachability map L_r is used to find the control input that achieves the desired state transition. From the transition map of a linear system:

$$X_f - \Phi(t_f, t_0)X_0 = \int_{t_0}^{t_f} \phi(t_f, \tau)B(\tau)u(\tau)d\tau \tag{5.2}$$

The least norm problem is to find the $u(\cdot)$ with the minimum L_2 norm such that (5.2) is satisfied. Define the reachability map L_r over the period $[0, t_f]$ to be the final state reached from zero initial state ($X_0 = 0$) by applying the control input $u(\cdot)$ to be: $L_r : u(\cdot) \mapsto X(t_f)$,

$$L_r[u(\cdot)] := \int_0^{t_f} \Phi(t_f, \tau)B(\tau)u(\tau)d\tau$$

and let L_r' to be its adjoint for the inner products on the spaces of the input $u(\cdot)$ and of the final states $X(t_f)$. According to the finite rank theorem [68], any input $u(\cdot)$ can be expressed as $u(\cdot) = u_1(\cdot) + u_2(\cdot)$ where $u_1(\cdot)$ is in the range space of the adjoint of the reachability map L_r', and $L_r[u_2(\cdot)] = 0$. Hence, since the $u_2(\cdot)$ component contributes to the L_2 norm of the $u(\cdot)$ but does not contribute to the output of L_r, the optimal input that minimizes the L_2 norm input must not have a $u_2(\cdot)$ component but must be in the range space of L_r'. Hence, the optimal input is given by:

$$u(\cdot) = L_r'\Lambda$$

for some $\Lambda \in \Re^n$. Then the Least Norm Control solution can be derived as :

$$L_r[u(\cdot)] = L_r L_r' \Lambda = (X_f - \Phi(t_f, t_0)X_0) \tag{5.3}$$

From this, we solve for Λ and $u(\cdot)$:

$$\Lambda = (L_r L_r')^{-1}(X_f - \Phi(t_f, t_0)X_0) \tag{5.4}$$

$$u(\cdot) = L_r'(L_r L_r')^{-1}(X_f - \Phi(t_f, t_0)X_0) \tag{5.5}$$

With the inner products applied to states $X_1, X_2 \in \Re^n$ and inputs $u_1(\cdot), u_2(\cdot)$ as

$$\langle X_1, X_2 \rangle := X_1^T X_2;$$
$$\langle u_1(\cdot), u_2(\cdot) \rangle := \int_{t_0}^{t_f} u_1^T(\tau) u_2(\tau) d\tau$$

The adjoint L_r' applied to $X \in \Re^n$ is:

$$(L_r' X)(\tau) = B^T(\tau)\Phi^T(t_f, \tau)$$

Therefore, the optimal control can be written explicitly as:

$$u(\tau) = B^T(\tau)\Phi^T(t_f, \tau)G^{-1}(t_0, t_f)(X_f - \Phi(t_f, t_0)X_0) \tag{5.6}$$

$$G(t_0, t_f) := \int_{t_0}^{t_f} \Phi(t_f, \tau)B(\tau)B^T(\tau)\Phi^T(t_f, \tau)d\tau \tag{5.7}$$

where $G(t_0, t_f) = L_r L_r'$ is the reachability Grammian. This generalized solution

presented above will be applied for HHEA during a pressure rail switch.

5.1.1 Least Norm Control for HHEA

The least norm solution can be used to compute the optimal torque required from the HECM electric motor to minimize any deviation from the desired performance during a pressure rail switch. The dynamics of the system are shown below :

$$M\ddot{x} = P_{cap}A_{cap} - P_{rod}A_{rod} - F_L - f \tag{5.8}$$

$$\dot{P}_{rod} = \frac{\beta}{V_{rod}(x)}(Q + A_{rod}\dot{x}) \tag{5.9}$$

$$Q = \frac{D}{2\pi}\omega \tag{5.10}$$

$$J\dot{\omega} = \frac{(P_B - P_{rod})D}{2\pi} + T_M \tag{5.11}$$

The system dynamics has four states : actuator position (x), actuator velocity($\dot{x}$), rod-chamber pressure (P_{rod}) and HECM e-motor/pump speed (w). The transition period is very short and hence a reasonable assumption of constant rod-side volume $V_{rod}(x)$ and constant bulk modulus (β) during the transition period makes the state dynamics a linear time-invariant system which can be represented as:

$$\dot{X} = AX + B_P \begin{bmatrix} F_L(t) \\ P_{cap}(t) \\ P_B(t) \end{bmatrix} + B_U T_m(t) \tag{5.12}$$

where,

$$X = \begin{bmatrix} x \\ \dot{x} \\ P_{rod} \\ \omega \end{bmatrix}, \quad A = \begin{bmatrix} 0 & 1 & 0 & 0 \\ 0 & 0 & -\frac{A_{rod}}{M} & 0 \\ 0 & \frac{\beta A_{rod}}{V_{rod}} & 0 & \frac{\beta D}{2\pi V_{rod}} \\ 0 & 0 & -\frac{D}{2\pi J} & 0 \end{bmatrix}$$

$$B_P = \begin{bmatrix} 0 & 0 & 0 \\ -\frac{1}{M} & \frac{A_{cap}}{M} & 0 \\ 0 & 0 & 0 \\ 0 & 0 & \frac{D}{2\pi J} \end{bmatrix}, B_U = \begin{bmatrix} 0 \\ 0 \\ 0 \\ \frac{1}{J} \end{bmatrix}$$

The pressure rails $P_{cap}(t)$, $P_B(t)$, and the load force $F_L(t)$ are characterized as input disturbances to the system. We assume for the moment that we know the time course of the input disturbances during the transition period. The goal then is to use the motor torque ($T_M(t)$) to control the system such that it reaches a desired final state (X_f) at the end of the transition period (t_f), starting from the initial state ($X(t_0)$) at the beginning of the transition. The least norm solution makes it possible to efficiently calculate the optimal motor torque ($T_M(t)$) required to reach the desired final state, taking into account the initial state, input disturbances, and desired performance criteria. This allows for precise control of the system, ensuring that the desired final state is reached even in the presence of disturbances.

The solution to the linear system (5.12) with disturbances of pressure rail and

loads, and with electric motor torque input is:

$$X(t_f) = \Phi(t_f, t_0)X(t_0) + \int_{t_0}^{t_f} \Phi(t_f, \tau)B_P \begin{bmatrix} F_L(\tau) \\ P_{cap}(\tau) \\ P_B(\tau) \end{bmatrix} d\tau + \underbrace{\int_{t_0}^{t_f} \Phi(t_f, \tau)B_U T_M(\tau)d\tau}_{L_r[T_M(\cdot)]} \tag{5.13}$$

where $\Phi(t_2, t_1)$ is the state transition matrix of A, $L_r : \Re^{[t_0,t_f]} \to \Re^4$ denotes the reachability map. The input disturbances and the initial conditions can affect the final state of the system, causing deviation from the desired outcome. We first analyze the impact of the disturbances and the initial conditions on the final state X_f of the system without any control effort (T_M). This helps to understand the magnitude of the correction needed. This can be defined as :

$$\Delta x := X_f - \Phi(t_f, t_0)X(t_0) - \int_{t_0}^{t_f} \Phi(t_f, \tau)B_P \begin{bmatrix} F_L(\tau) \\ P_{cap}(\tau) \\ P_B(\tau) \end{bmatrix} d\tau \tag{5.14}$$

where the final state $X(t_f)$ has been substituted by the desired final state X_f. The control input can now be designed to correct the disturbance and guide the system to the desired final state using the least norm solution. The objective function and constraint equations are:

$$\min_{T_M(\cdot)} \int_{t_0}^{t_f} T_M^2(\tau)d\tau \quad , \quad \text{s.t.} \quad \Delta x = L_r[T_M(\cdot)]$$

Since the system (5.12) can be shown to be completely controllable from T_M, the reachability map L_r is surjective and the least norm control can be derived by applying the equations (5.2)-(5.5) [68]:

$$T_M(\cdot) = L_r'(L_r L_r')^{-1}\Delta x \tag{5.15}$$

Explicitly, it is written as:

$$T_M(\tau) = B_U^T \Phi^T(t_f, \tau) G^{-1}(t_0, t_f)\Delta x \tag{5.16}$$

$$G(t_0, t_f) := \int_{t_0}^{t_f} \Phi(t_f, \tau) B_U B_U^T \Phi^T(t_f, \tau) d\tau \tag{5.17}$$

As a reminder, $G(t_0, t_f)$ is the reachability Grammian and L_r' is the adjoint of L_r.

5.2 Scaling the Least Norm Control

The Hybrid Hydraulic Electric Architecture (HHEA) is designed to minimize energy loss by utilizing multiple pressure rail switches throughout its duty cycle. While the least norm control solution described earlier provides an effective way to drive the system to a desired final state in response to a single pressure rail switch, computing this solution for each individual switch would require significant computation and might be challenging to implement in real-time applications. Therefore, it is necessary to scale the solution in a way that it can be applied to all possible pressure rail events, thus making it more practical and efficient for real-world applications. To gain insights into the scalability of the solution for

different switches, we can examine the effect of disturbances on the states and the least norm solution:

$$\Delta x := X_f - \Phi(t_f, t_0)X(t_0) - \int_{t_0}^{t_f} \Phi(t_f, \tau)B_P \begin{bmatrix} F_L(\tau) \\ P_{cap}(\tau) \\ P_B(\tau) \end{bmatrix} d\tau \tag{5.18}$$

$$T_M(\tau) = B_U^T \Phi^T(t_f, \tau) G^{-1} \Delta x \tag{5.19}$$

$$G(t_0, t_f) = \int_{t_0}^{t_f} \Phi(t_f, \tau) B_U B_U^T \Phi^T(t_f, \tau) d\tau \tag{5.20}$$

The transition matrix $\Phi(t_f, \tau)$ can be precomputed as it is dependent only on the system dynamics. Although the rod side chamber volume $V_{rod}(x)$ can be assumed to remain constant during the transition time, it differs for different transitions. Hence $\Phi(t_f, \tau)$ and $G(t_0, t_f)$ need to be parameterized by chamber volume. Furthermore, if the valve dynamics are known, Δx expression can be expressed as a linear function of $X(t_0)$, X_f, the old and new values of P_B and P_{cap} (Rail changes) as seen in (5.18). The behavior of the pressure rail changes in the HHEA system during the transition is linked to the dynamics of the switching valve. Since the previous and current pressure rail selections are known, the pressure rail dynamics can be estimated using a filter. This estimation allows us to determine the exact behavior of $P_B(\tau)$ and $P_{cap}(\tau)$ over time by scaling them with the known magnitude of the current and previous pressure rails. For

example, the cap side pressure time course can be assumed as :

$$P_{cap}(\tau) = P^R_{old} + (P^R_{new} - P^R_{old})H(t) \tag{5.21}$$

where $P_{cap}(\tau)$ is the cap side pressure and P^R_{old} is the cap side pressure rail selection before a rail switch and the P^R_{new} is the cap side pressure rail selection after the rail switch. $H(t)$ is a second-order filter that can be estimated experimentally or from the valve dynamics. In other words, this filter $H(t)$ is a prediction of how the pressure in the rails will change based on the previous and current choices (used for scaling), and the exact course of the pressure changes can be found by adjusting these predictions according to the known magnitude of the pressure rails.

The load force $F_L(t)$ is assumed to vary linearly with time between the initial and final loads that are assumed to be known from the duty cycle for the transition period. The initial states $X(t_0)$ are measured in real-time from sensor measurements and the final states X_f are assumed to be known from the duty cycle data. Therefore, the least-norm control at any time $T_M(\tau)$ can be computed by multiplying a pre-computed kernel $L'_r(L_rL'_r)^{-1}$ with a scaling matrix Δx.

5.3 Simulation Results

To illustrate the transition control, only the transition controller has been applied, in simulations, to the rail switching event where the cap side pressure rail switches from 30 Mpa to 40 Mpa and the rod side pressure rail switches from tank to 20 Mpa

and the same system parameters are used as table 4.1.The simulation used in this investigation is an extreme case, where the pressure rail changes are assumed to a step function. In reality, the pressure rail changes would have associated dynamics that would be favorable for the controller. The dynamics of the cap and rod side pressure rails during the transition process can be modeled and incorporated into the control strategy to improve its performance in real-world applications. The rod side volume is assumed to be 700 ml and the bulk modulus is kept constant. The desired trajectories and the pressure rail switches are assumed to be known ahead of time for these simulations.

The least norm control has been used with motor torque (T_M) as the control input. The cap-side pressure rail switch has been delayed. Delaying the time when the cap-side rail switch takes place allows time for the rod-side pressure to build towards the desired pressure, thus reducing the error during the transition. The time delay shows up in the cap side pressure time course $P_{cap}(\tau)$. All the four states (defined in equation (5.12) tracking errors have been plotted in figure 5.1, where the transition period (t_f) has been varied with a constant 8 ms delay for the cap side pressure rail. If the transition period is short then the control input required is higher which has been shown in figure 5.2. Also, if the transition period is too long then the tracking error increases as it can be seen in figure 5.1. In figure 5.3 the control input (motor torque) is plotted with different cap side pressure rail switch delays. It can be seen that for delays between 7-9 ms the control input is the least.

A comparison between two control strategies: the backstepping controller and

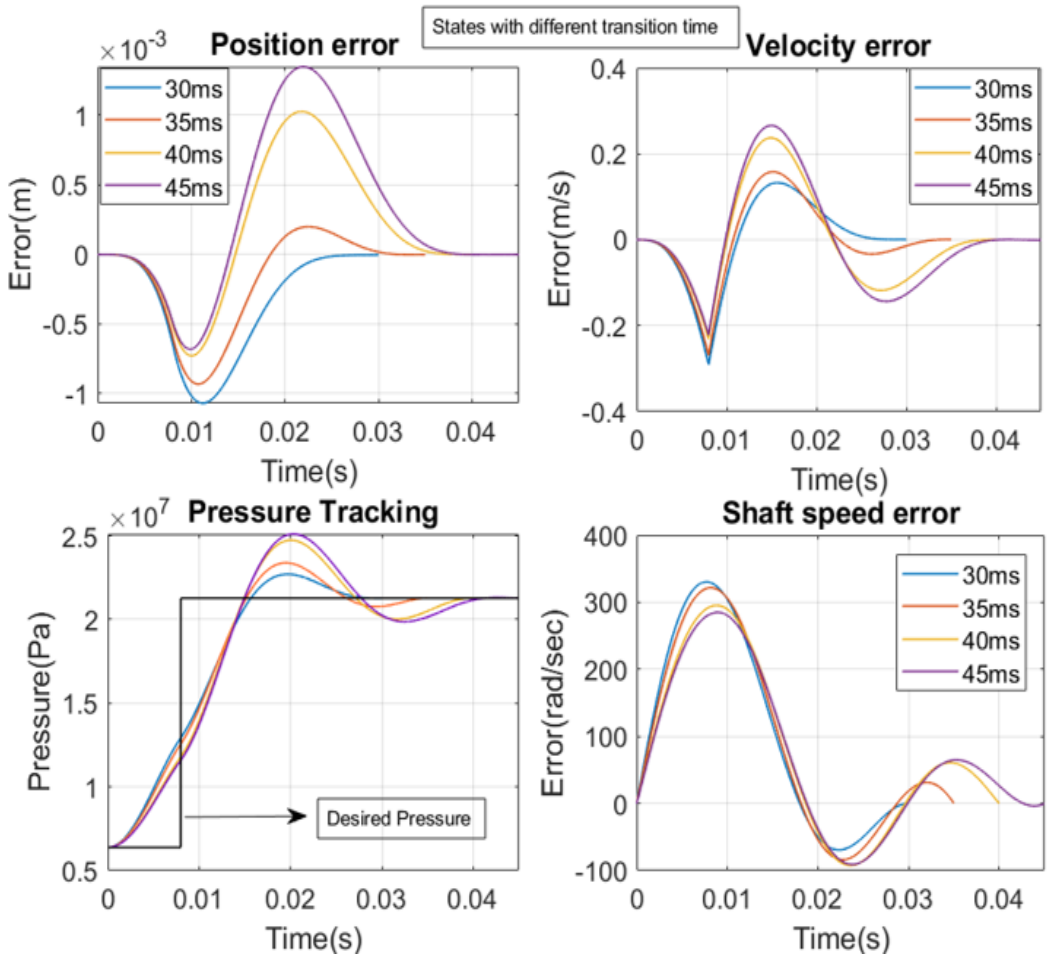

Figure 5.1: Performance for different transition times - Least Norm Control using only motor torque as input. Time delay of the P_A switching is 8 ms

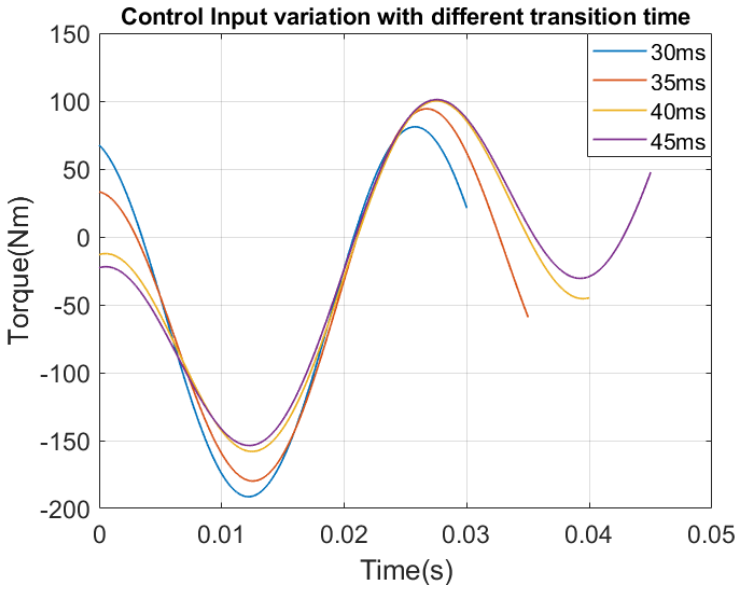

Figure 5.2: Torque inputs for different transition times - Least Norm Control using only motor torque as input. Time delay of the P_A switching is 8 ms.

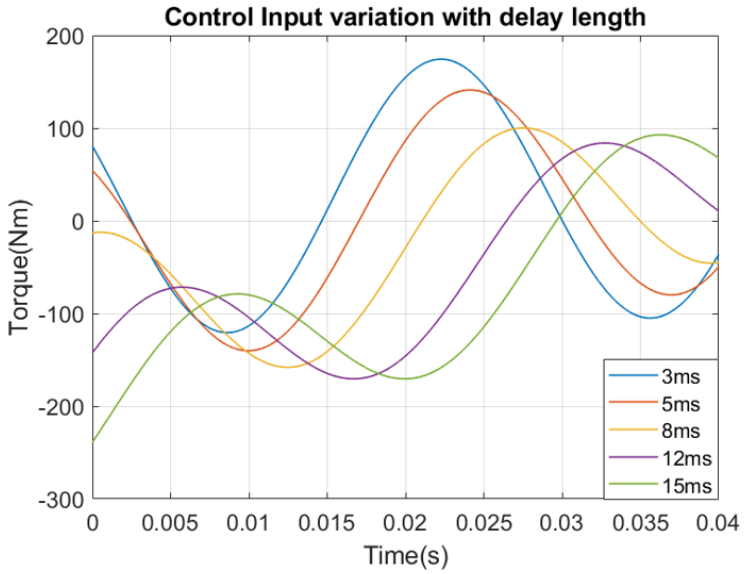

Figure 5.3: Torque input for various cap-side delays - Least Norm Control using only motor torque as input.

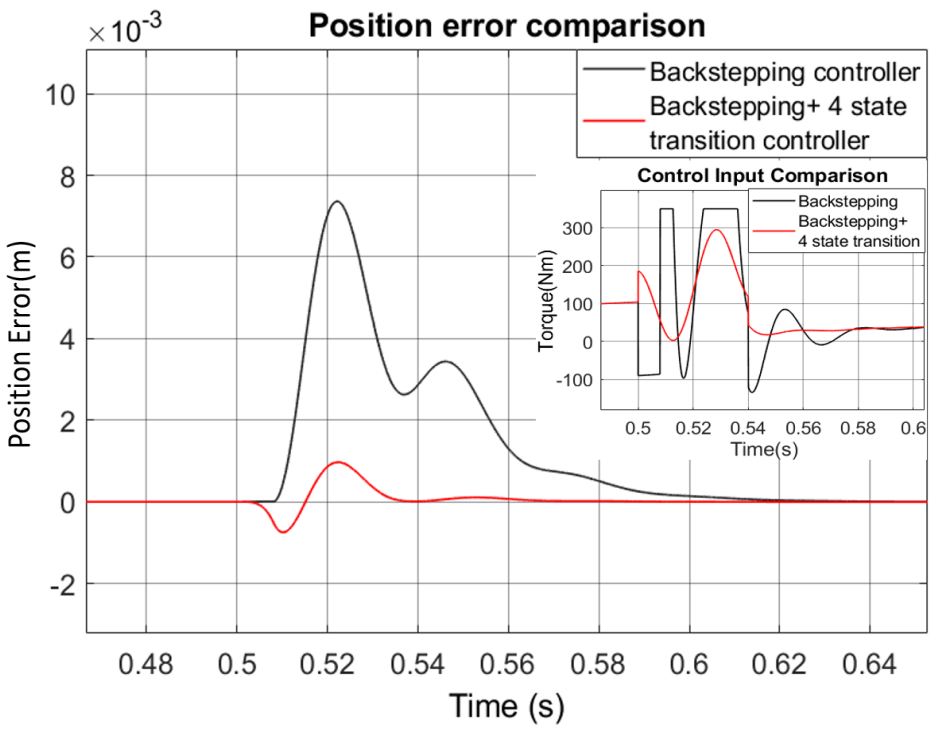

Figure 5.4: Tracking error and control input comparison of nominal controller and the combination of nominal and transition controller

the combination of the backstepping controller and the transition controller has been made. During the transiiton period the the backstepping controller is turned off and the Least Norm Control is switched on. The objective of the comparison is to evaluate how the combination of the two controllers affects the performance of the system. In figure 5.4, the comparison of the two controllers is presented. The plot shows that using just the backstepping controller, the recovery time (the time it takes to return back to its initial tracking error) is 100 ms, and the peak error is 7 mm. However, when the combination of the two controllers is used, the peak error is less than 1 mm, reducing the peak error by 7 folds, and the recovery

time by 60 ms. This result indicates that the combination of the two controllers significantly improves the system's performance.

In addition to the improvement in the tracking error and recovery time, the combination of the two controllers also reduces the control effort. This means that the control inputs required to achieve the desired performance are reduced, resulting in a more efficient and cost-effective system.

Therefore, the combination of the backstepping controller and the transition controller is the recommended control strategy for the architecture. This combination leverages the advantages of both controllers and results in a more robust and effective control system.

5.4 Chapter Summary

In HHEA, a transition controller is utilized for motion control during pressure rail switches. Its main objective is to minimize the impact of pressure rail changes on motion tracking while maintaining feasible control input limits. The transition controller is designed to attain a zero-error state at the end of the transition period and subsequently, control is returned to the nominal controller. To achieve this optimally, Least Norm Control is employed. The pressure rail switches are known disturbances that the control input aims to counteract.

A comparison was made between the tracking performance of the nominal controller and the transition controller during a pressure rail switch, in simulation. The results showed that the transition controller improved tracking performance

by sevenfold and reduced the recovery time by 60%. Furthermore, the electric motor torque required by the transition controller was lower than that of the nominal controller. Consequently, the combination of the nominal and transition controllers yields the best motion control results for HHEA.

Chapter 6

Hardware in the Loop Validation

In this chapter, we have developed hardware-in-the-loop (HIL) testbeds, which serve as a platform for experimentally validating the proposed motion control strategy for the Hybrid Hydraulic Electric Architecture (HHEA). The primary objective of this experimental setup is to assess the control performance of the HHEA under different loading conditions by testing its ability to track a desired duty-cycle trajectory on the test actuator.

To achieve this goal, we will be utilizing a HIL testbed, which is a powerful tool that allows for the integration of physical hardware with a computer simulation model. In this way, we can replicate real-world scenarios and test the performance of the HHEA in a controlled environment.

The primary focus of our testing will be on the HHEA's motion control strategy presented in previous chapters, which is a critical component of its overall performance. By subjecting the HHEA to various loading conditions, we can evaluate

its ability to maintain stability and accurately track the desired duty-cycle trajectory. The development of HIL testbed is an essential step in the evaluation of the HHEA's motion control capabilities and represents a critical milestone in the development of this technology. With this platform, we can test and refine the HHEA's performance, ensuring that it meets the demanding requirements of its intended applications.

To thoroughly test the control system of the Hybrid Hydraulic Electric Architecture (HHEA), two single-axis hardware-in-the-loop (HIL) testbeds with 200 and 300 bars maximum pressure capability have been devised. As heavy-duty mobile machinery typically operates at peak pressures of around 300 bars, the second testbed has been specifically tailored to accommodate these conditions. The development of two single-axis HIL testbeds with different maximum pressure ratings enables us to test the HHEA's control performance under varying pressure conditions. This allows us to better understand how the system will perform in real-world scenarios and ensure that it operates optimally in a range of different applications.

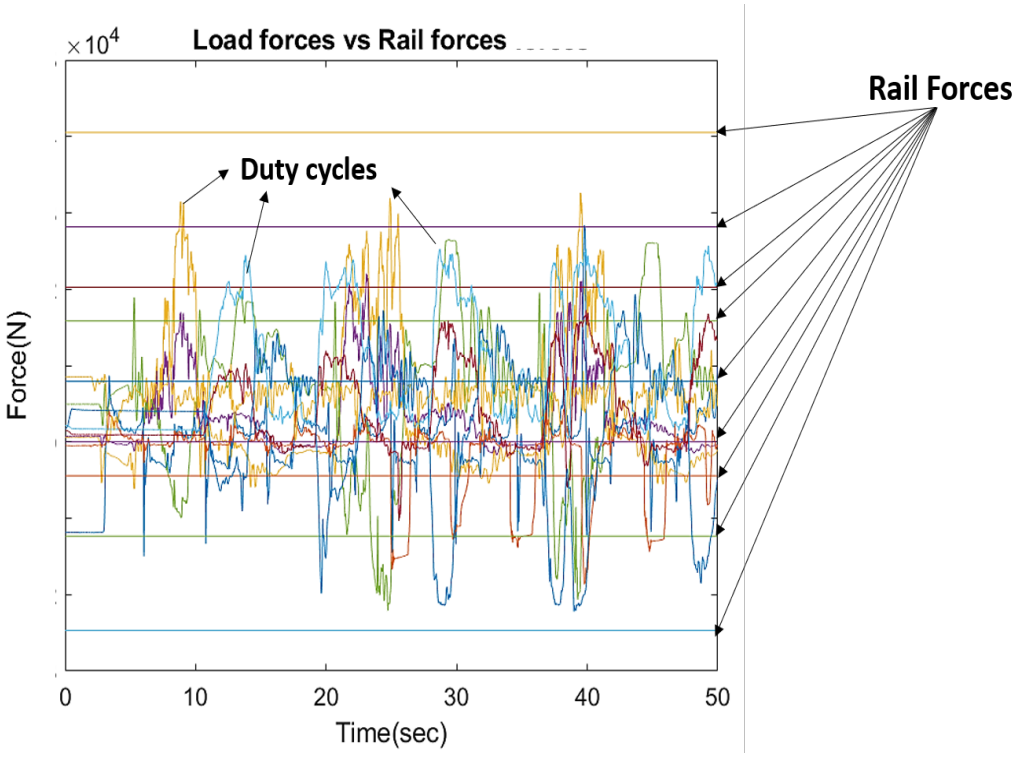

Figure 6.1: Rail forces encompassing the representative duty cycle forces

6.1 Medium pressure test stand

The design of the medium pressure hardware-in-the-loop testbed for the Hybrid Hydraulic Electric Architecture (HHEA) involves the use of three constant common pressure rails. For a single ended double-acting hydraulic cylinder with different cap and rod side areas, we can achieve 9 different hydraulic force combinations. The HHEA actuator is sized such that the rail forces generated by the three pressure rails can encompass load force trajectories from multiple duty cycles provided by an OEM partner. As it can be seen in figure 6.1, the selected actuator encompasses all the duty cycle peak load forces.

The testbed layout can be seen in figure 6.2 and it can be subdivided into three different subsystems [69]. These subsystems are:

1. The Load Emulation Module
2. Hydraulic-Electric Control Module (HECM)
3. Common Pressure Rail Generation Module

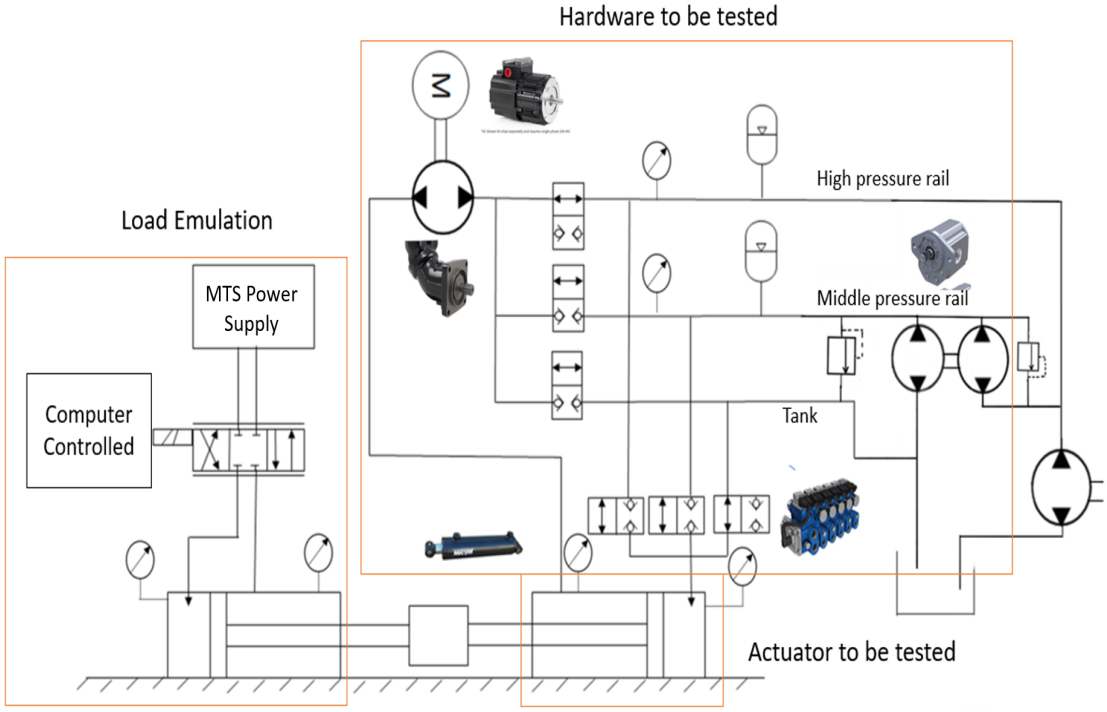

Figure 6.2: Hardware in the Loop testbed layout

These sub-systems interact with each other and form the HIL testbed. The Load Emulation Module is responsible for emulating the physical load on the hydraulic motion control system. This subsystem provides a controlled load to the system, simulating different operating conditions, and testing the system's

response. The Hydraulic-Electric Control Module (HECM) is responsible for regulating the hydraulic pressure and flow to the test actuator. The Common Pressure Rail Generation Module is responsible for generating and maintaining the pressure rails within the system. All the components have been retrofitted to a hydraulic actuator and are mounted on a frame as it can be seen in figure 6.3. To

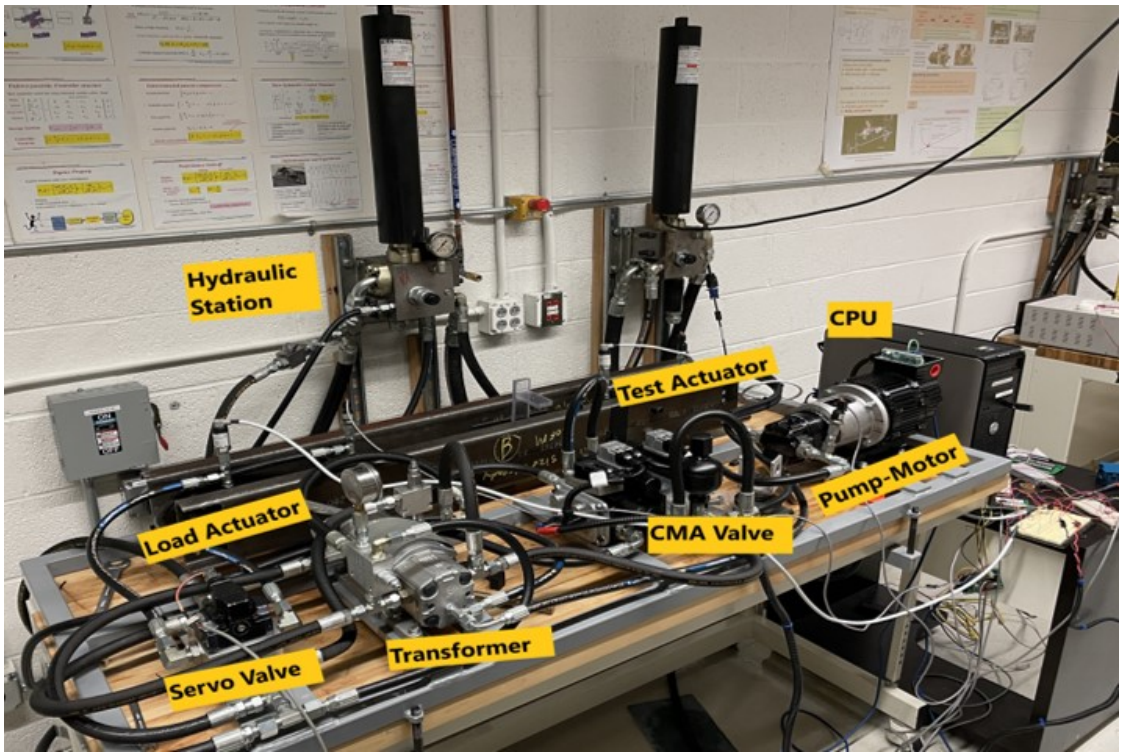

Figure 6.3: Medium pressure hardware in the loop testbed

implement the motion control algorithm on the hardware we use Matlab Simulink Realtime (SLRT). A target PC is used as a dedicated computer that runs the compiled code for the motion control algorithm. This computer is connected to the testbed's hardware and runs in real-time, ensuring that the control signals are sent at precise intervals. By using a dedicated computer for running the motion

control algorithm, we can ensure that the control algorithm is executed at fixed time intervals so that the system responds quickly and accurately to changes in the input signal. The host computer, on the other hand, runs Matlab/Simulink, which is a software tool used for designing, simulating, and implementing control algorithms. The host computer communicates with the target PC to send control signals and monitor the system's performance during testing. The communication between the host computer and the XPC target PC is typically done using a network connection. We have used Humusoft MF634 as a data acquisition system that is used to measure, and record the system's performance parameters and also send various signals to the hardware in real-time. The target computer is able to execute the motion control algorithm with a sample time of 1 ms. To understand the hardware in the loop testbed shown in figure 6.3 the sub-systems are described in detail below.

6.1.1 Load Emulation Module

The Load Emulation module is an important component of the HIL testbed whose purpose is to emulate the varying external load on the actuator. As shown in the circuit diagram in figure 6.2, this module consists of a hydraulic actuator (in-line with a test actuator) and a servo valve. The test-actuator represents the hydraulic actuator of an application being tested and is driven by the motion control algorithm being evaluated. The opposing load emulation actuator, on the other hand, is designed to impart an emulated load on the test-actuator, thereby simulating different operating conditions [27][70]. The actuator sizes have

been carefully selected to enable testing of the scaled versions of OEM-provided test duty cycles on the system. This ensures that the testbed can accurately replicate the conditions under which the hydraulic system would function in real-world applications, allowing for a thorough assessment of the system's performance under practical operating conditions.

To monitor the position of the actuators, a linear optical encoder (US Digital) is used. This provides precise and accurate position measurement, which is important for controlling the motion of the actuators. Finally, pressure measurements are available on both chambers of both actuators. The pressure measurements are used to estimate the load acting on the test actuator.

The load emulator actuator is controlled by an MTS series 252 servo valve, which allows for precise control of the pressures on the rod and cap sides of the hydraulic cylinder. By commanding the servo valve, the pressure can be varied to generate any desired load force on the hydraulic actuator. The MTS series 252 servo valve is a high-performance hydraulic valve that is designed to provide precise and responsive control of hydraulic systems. It uses advanced electro-hydraulic technology to modulate the flow of hydraulic fluid to the actuator, which in turn controls the actuator's position, velocity, and force.

In the Load Emulation Module, the servo valve is used to control the load emulator actuator, which is coupled in line with the test actuator. By varying the pressure on the load emulator actuator, a simulated load can be generated on the test actuator, allowing the motion control algorithm to be tested under different load conditions. While a load cell can be used to measure the applied load force,

the testbed currently uses pressure sensors on the cap and rod sides of the load emulation actuator to estimate the load force. The dynamics of the emulated load force F_L are described by the following equations:

$$\dot{F}_L = \dot{P}_{scap} A_{scap} - \dot{P}_{srod} A_{srod} \tag{6.1}$$

$$\dot{P}_{scap} = \frac{\beta}{V_1}(Q_1 - A_{scap}\dot{x}_c) \tag{6.2}$$

$$\dot{P}_{srod} = \frac{\beta}{V_2}(Q_2 + A_{srod}\dot{x}_c) \tag{6.3}$$

$$Q_1 = \begin{cases} kx_v\sqrt{|P_S - P_{scap}|}sign(P_S - P_{scap}) \ for \ x_v > 0 \\ kx_v\sqrt{|P_{scap} - P_T|}sign(P_{scap} - P_T) \ for \ x_v < 0 \end{cases} \tag{6.4}$$

$$Q_2 = \begin{cases} kx_v\sqrt{|P_{srod} - P_T|}sign(P_{srod} - P_T) \ for \ x_v > 0 \\ kx_v\sqrt{|P_S - P_{srod}|}sign(P_S - P_{srod}) \ for \ x_v < 0 \end{cases} \tag{6.5}$$

Here, P_{scap} and P_{srod} are the cap side and rod side pressure of the load cylinder, A_{scap} and A_{srod} are the cap and rod side area of the load actuator, x_v is the spool displacement, Q_1 and Q_2 are the flow into the cap and the rod side of cylinder respectively, and V_1 and V_2 are the volume on the cap and rod side of the load cylinder, P_S and P_T are the supply and tank pressures, k is the valve constant and x_c is the position of the load cylinder. Assuming that the response of the servo valve is fast enough the control input is spool displacement x_v. Also, note that the position of the test actuator is coupled with the load actuator.

To design the control logic for the load emulation module, we define the desired load force F_d and the error $\tilde{F} := F_L - F_d$. The Lyapunov function V is defined

as:

$$V = \frac{1}{2}\tilde{F}^2 \tag{6.6}$$

The derivative of the Lyapunov function is given by:

$$\dot{V} = \frac{d}{dt}\left(\frac{1}{2}\tilde{F}^2\right) = \tilde{F}(\dot{F}_L - \dot{F}_d) \tag{6.7}$$

where $\dot{F}_d$ is the derivative of the desired load force. To achieve stability in the system, we want to ensure that $\dot{V} \leq 0$ for all time. Therefore, we need to design the control input in such a way that it makes $\dot{V}$ negative definite. Choosing the control input x_v by rearranging the dynamic equations and canceling out the non-linear terms we can show that it satisfies the Lyapunov stability criteria.

$$x_v = \frac{1}{\Gamma}\left(k\dot{x}_c - k^*\tilde{F} + \dot{F}_d\right) \tag{6.8}$$

where k^* is a positive gain and

$$\Gamma = \begin{cases} \frac{k\beta A_{scap}}{V_1}\sqrt{P_S - P_{scap}} - \frac{k\beta A_{srod}}{V_2}\sqrt{P_{srod} - P_T} & for\ x_v > 0 \\ \frac{k\beta A_{scap}}{V_1}\sqrt{P_{scap} - P_T} - \frac{k\beta A_{srod}}{V_2}\sqrt{P_S - P_{srod}} & for\ x_v < 0 \end{cases}$$

By substituting the value of x_v into the load force dynamics equation and simplifying it, we obtain:

$$\dot{F}_L = -k^* \tilde{F} + \dot{F}_d \tag{6.9}$$

On plugging equation (6.9) in equation (6.7) we get:

$$\dot{V} = -k^* \tilde{F}^2 < 0 \tag{6.10}$$

The application of the above controller ensures that the error $\tilde{F}$ approaches zero, resulting in the desired load force F_d being achieved with high precision. To validate the performance of the controller, a simulation was conducted where a duty cycle load force was tracked, utilizing the aforementioned controller. The simulation results are depicted in figure 6.4, which demonstrate that the desired force is tracked consistently throughout the duty cycle.

6.1.2 Hydraulic Electric Control Module

The Hydraulic-Electric Control Module (HECM) is composed of two main components: an electric motor coupled with a hydraulic pump, and a set of switching valves for switching among the different pressure rails. The hydraulic pump is an 8cc gear pump, while the electric motor is a 5kW ClearPath PMAC motor (CPM-MCPV-N1432P-RLN) with integrated power electronics. These two components are mechanically coupled together to work in tandem. Specifically, the hydraulic pump is connected to the rod end of the test actuator on one side, and

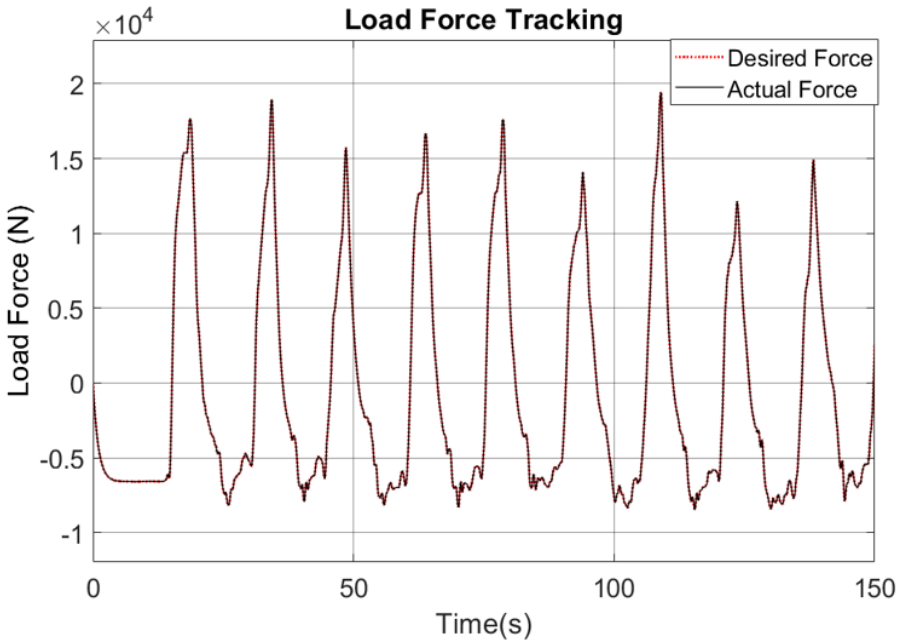

Figure 6.4: Simulation of load force stracking

to switching valves on the other side. Meanwhile, the cap side of the test actuator is directly connected to the switching valves.

Eaton's 2-section CMA-90 valves are used as the switching valves. The CMA valve is an electro hydraulic two stage metering valve that has two independant spools in each worksection. With three pressurized rails and two sections with 4 workports we can achieve all possible switching combinations for the test actuator. One of the sections with two work ports is connected to high-pressure rail and tank, and the other section is connected to middle-pressure rail and tank. The CMA-90 valve utilizes the SAE J1939 protocol for communication over a Controller Area Network (CAN) bus. This protocol is a standardized communication protocol used primarily in heavy-duty commercial vehicles and equipment, and it allows

for reliable, high-speed communication between the different components of the system. We operate the CMA valve in open loop control mode to open the valves faster. To facilitate communication between the CMA-90 valve and a target PC, an Arduino is used as a CAN bridge. The Arduino receives commands serially from the target PC and translates them into CAN messages to open and close the workports within the CMA-90, which connects different pressure rails on both the cap and rod sides of the actuator.

6.1.3 Common Pressure Rail Generation

The Hardware-in-the-Loop (HIL) testbed employs three common pressure rails (CPRs) at 20 MPa, 10 MPa, and tank. However, unlike the actual HHEA (Hybrid Hydraulic and Electric Actuator) shown in figure 2.1 which uses fixed displacement pumps to supply the common pressure rails, the HIL testbed uses a simpler method of generating the CPRs since the primary goal is to test motion control. We use MTS Silent Flow Series 505 hydraulic power supply in the laboratory to feed the highest-pressure rail. There is an accumulator at the hydraulic station shown in figure 6.3 which ensures the pressure of the highest pressure rail remains constant with flow disturbances.

To generate the middle pressure in an efficient manner, the HIL testbed employs a pair of hydraulic gear motors (Danfoss Group 2 8.4cc gear motors) that are coupled together to form a shared output hydraulic transformer, as illustrated in figure 6.5. The transformer is supplied by the highest-pressure rail. To ensure precise pressure regulation, the HIL testbed uses a pressure-reducing valve and

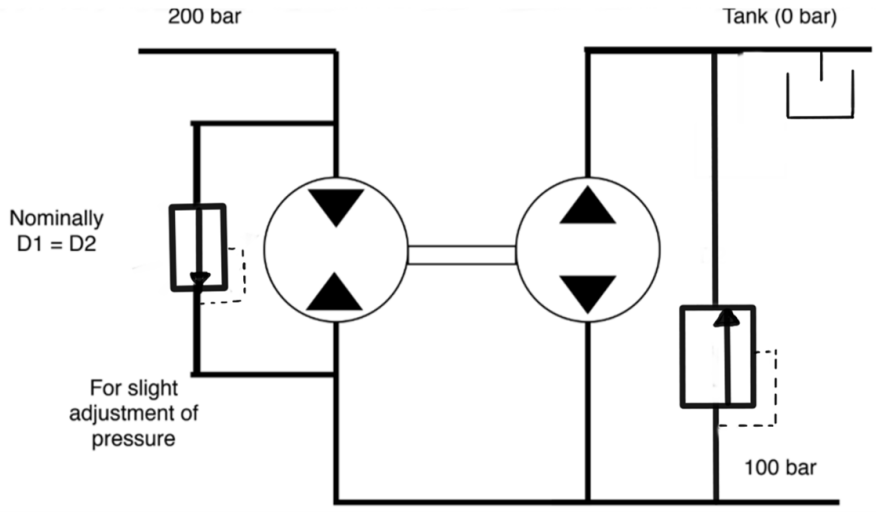

Figure 6.5: Hydraulic Transformer for middle rail generation

a relief valve. The required displacement for both the motor and pump can be found depending on the desired middle rail pressure as:

$$T_1 = T_2 \tag{6.11}$$

$$(P_H - P_M)D_1 = (P_M)D_2 \tag{6.12}$$

$$P_M = \frac{P_H D_1}{D_1 + D_2} \tag{6.13}$$

Here, T_1 and T_2 are the torques across the transformer setup. P_H is the highest rail pressure or the inlet to the transformer and P_M is the required middle-pressure rail. D_1 and D_2 are the displacements for the hydraulic motor and pump respectively. If we choose equal displacements then the middle-pressure rail P_M is half of the highest-pressure rail. The displacement selection also varies on flow requirement from the middle-pressure rail. The majority of the flow on the middle-pressure

line is supplied efficiently using the transformer, with the throttling functions of the reducing and relief valves only being used for small modulation.

6.1.4 Experimental results

Having discussed the control strategy in chapter 4 and chapter 5, it has been successfully implemented on the hardware-in-the-loop testbed, demonstrating its viability and effectiveness in practical testing scenarios. The experiments conducted on this testbed are aimed to illustrate four different pressure rail switch cases, all of which are subject to varying load force. To perform these experiments, trajectory tracking with sinusoidal and trapezoidal cylinder trajectories is utilized as they are quite representative of real-world scenarios. The experiments involve four main switching cases, as outlined below:

1. No pressure rail change
2. Rod side pressure rail change with varying load force
3. Cap side pressure rail change with varying load force
4. Both cap and rod side pressure rail change

The controllers for HHEA are tuned to the best of my knowledge, with the electric motor speed serving as the primary control input. Specifically, the electric motor is operated in torque control mode, wherein a PID controller is used in the inner loop to track a desired reference speed.

Table 6.1: UMN testbed Parameters

Parameter	**Symbol**	**Value**
Cap Area	A_{cap}	0.002 m^2
Rod Area	A_{rod}	0.0012 m^2
HECM pump displacement	D	8 $\frac{cc}{rev}$
e-motor-pump inertia	J	0.0024 Kgm^3
Mass	M	5 Kg
Bulk Modulus	β	$1.3GPa$
velocity error dynamics gain	λ_p	10
Reference velocity error gain	K_v	100
Integral gain	K_I	120000
Pressure feedback gain	λ_3	10^{-10}

No pressure rail switch

This is a nominal case where the pressure rails selected in the rod and cap side do not switch. In this test, a constant load force has been kept as it can be seen in figure 6.7 and the highest pressure rail (18 MPa) on the pump inlet and the cap side of the test actuator has been selected as shown in the figure 6.6. The passivity-based integral back-stepping controller is used for this case. A sinusoidal trajectory has been used to test the trajectory tracking performance. Under the

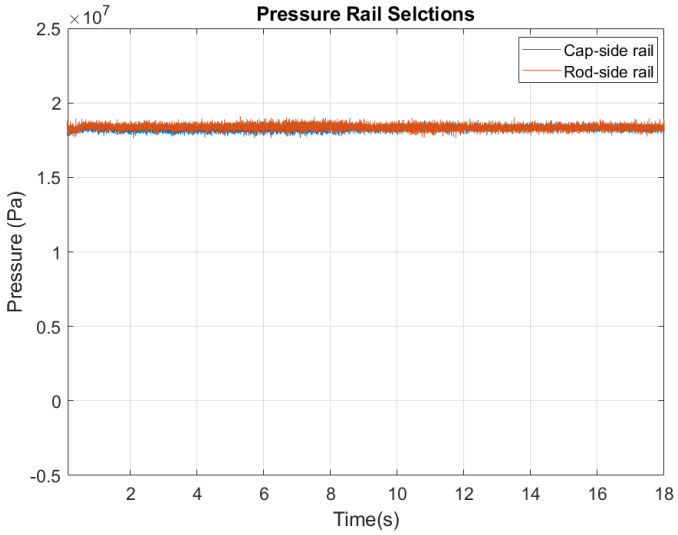

Figure 6.6: Both the pressure rails are set at the highest rail setting

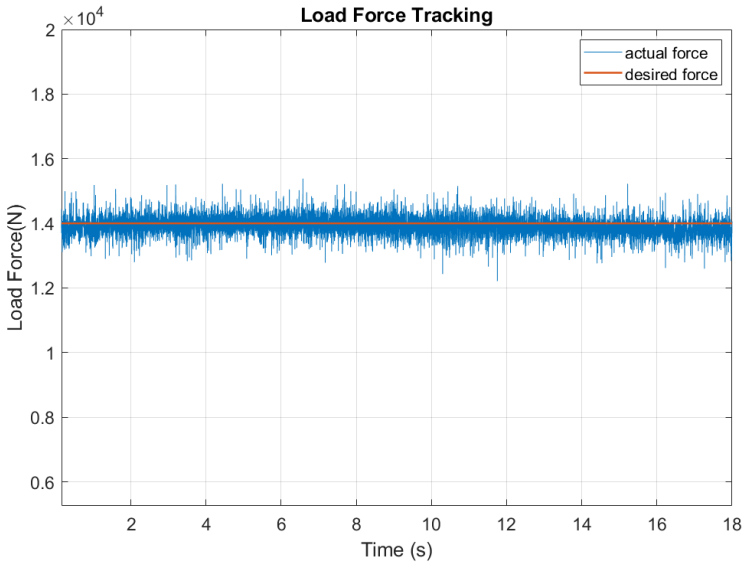

Figure 6.7: Constant load force tracking

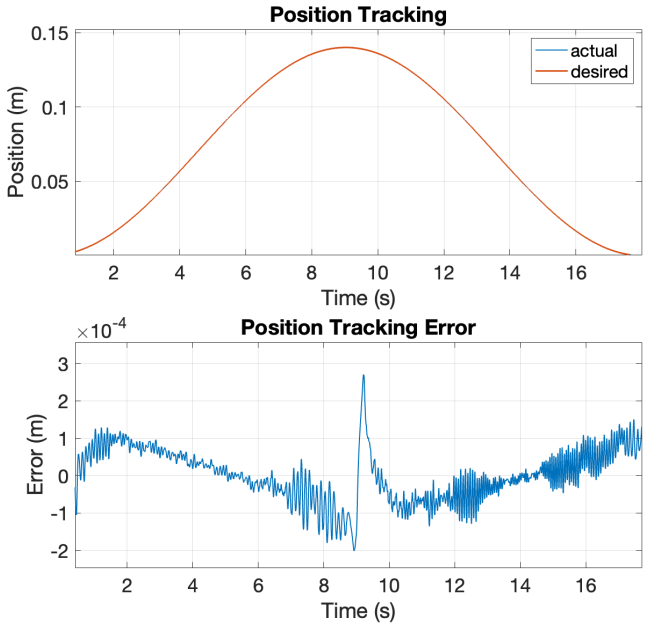

Figure 6.8: Trajectory tracking performance without rail switches

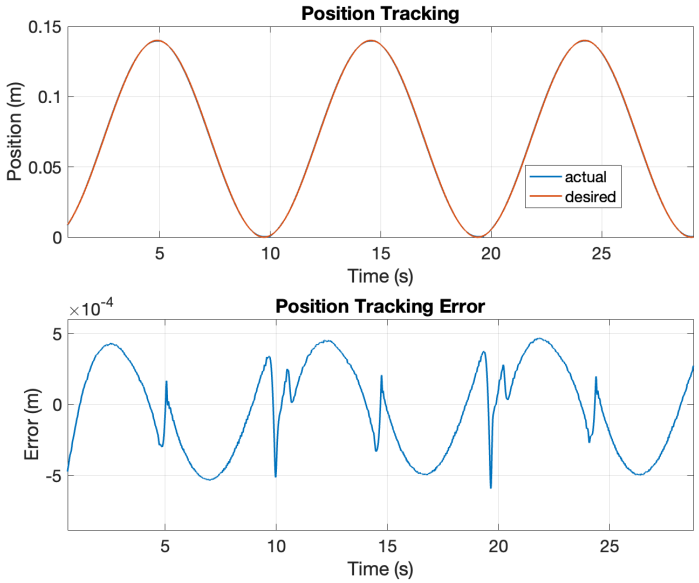

Figure 6.9: Position tracking with no switches for a faster trajectory

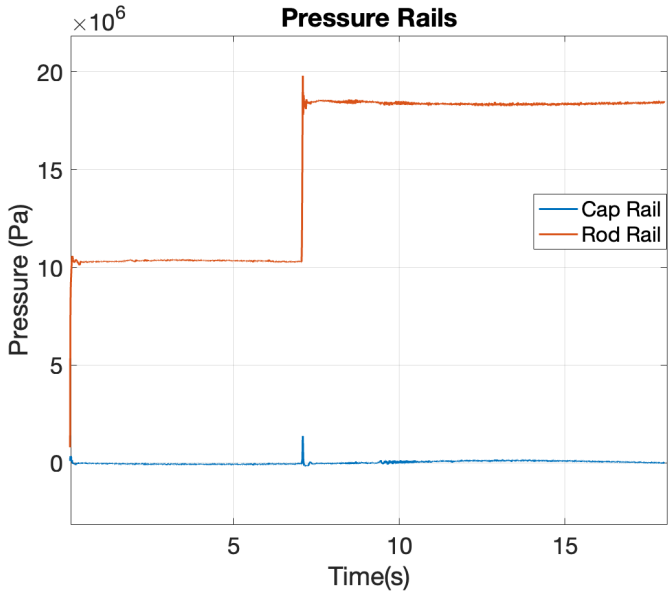

Figure 6.10: Rod side pressure rail switch from middle-pressure rail to high

same setting, a faster trajectory has also been shown to show the effectiveness of the motion control strategy. It can be seen from figure 6.8 that the maximum position tracking error is 0.27 mm and that occurs when the actuator is changing its direction. The tracking performance for the faster trajectory has been shown in figure 6.9 and the maximum error recorded is 0.52 mm. It also occurs at the beginning of the stroke. These tracking errors are within .25% of the stroke. Majority of the operations are done under similar settings (nominal conditions) where the pressure rails are not changing.

Rail switch only on the rod side

In this case, as the load force changes as it can be seen in figure 6.11 a rail change on the rod side is requested to keep the ΔP across the HECM pump/motor small.

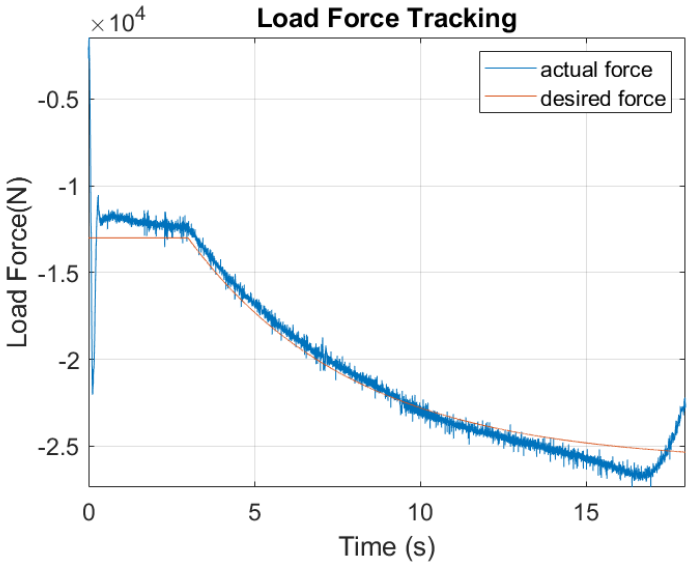

Figure 6.11: Varying load force for rod side rail switch

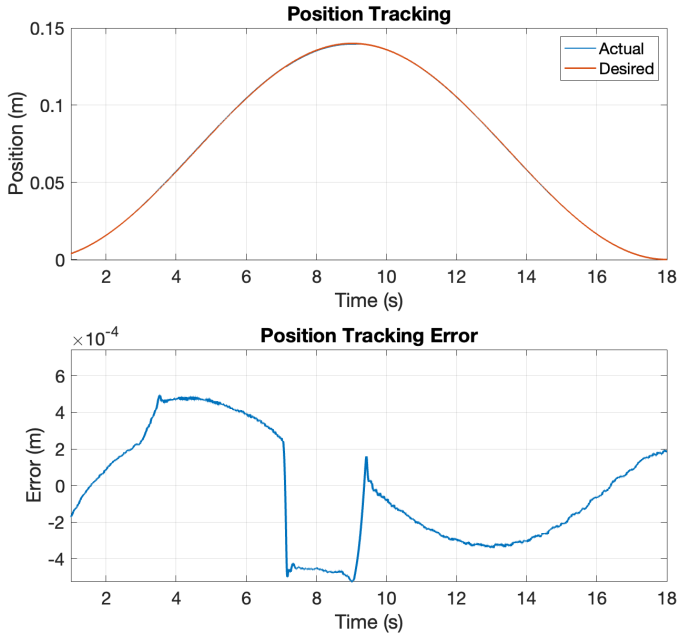

Figure 6.12: Tracking performance with rod side pressure rail switch

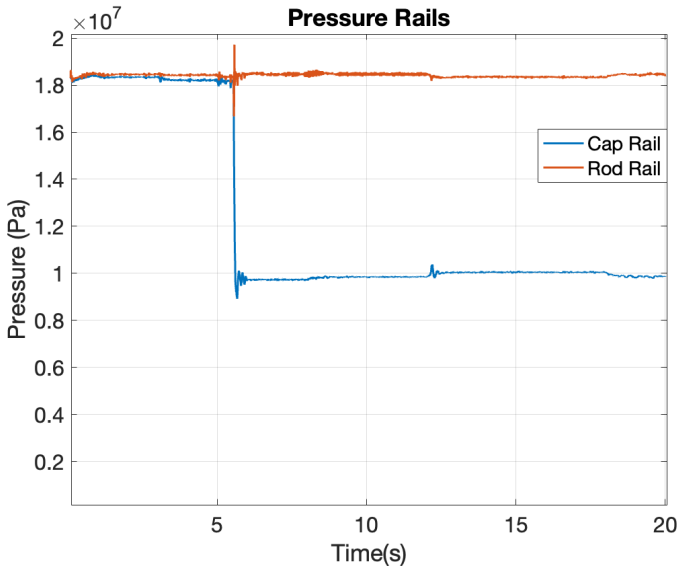

Figure 6.13: Cap side pressure rail switch from high-pressure rail to middle

The rod side pressure rail switches from the middle-pressure rail to high-pressure rail as shown in figure 6.10 and the cap side pressure rail stays constant. It should be noted that the middle-pressure rail is generated by the hydraulic transformer and it does a good job of maintaining the pressure rail. The trajectory tracking performance for a sinusoidal trajectory has been shown in figure 6.12. The switch is requested at 7.5 seconds and the peak error is 0.53mm (0.26% of the stroke) which is observed during the switch.

Rail switch only on the cap side

In this case, the cap side pressure rail switches and the rod side pressure rails are kept constant. The cap side switches from high-pressure rail to middle-pressure rail and the rod side is kept at the highest pressure rail as shown in figure 6.13.

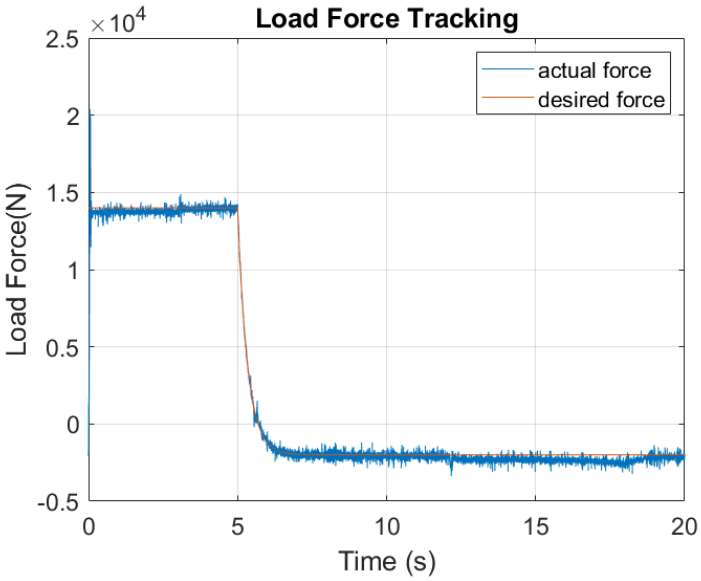

Figure 6.14: Load force tracking for cap side pressure rails switch

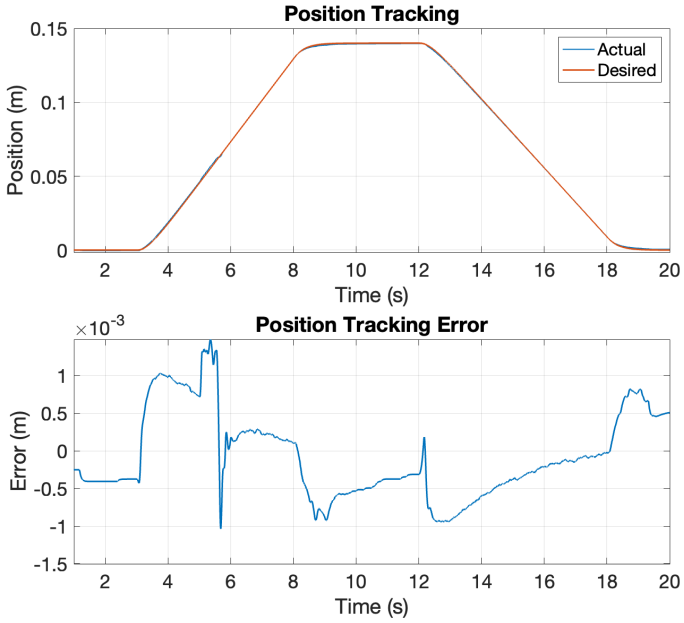

Figure 6.15: Tracking performance with cap side pressure rail switch

Similar to the previous case the switching is triggered based on the load force change as can be seen in figure 6.14. Trajectory tracking performance for a trapezoidal trajectory has been shown in figure 6.15. It can be seen that the maximum tracking error is 1.3 mm and it takes place during the switch which is triggered at 5 sec. A trapezoidal trajectory has been used for this experiment and the switch is timed in the cylinder extension portion of the trajectory.

Rail switch on both cap and rod side

In this case, both the cap and rod side pressure rail switch from middle-pressure rail to high-pressure rail as it can be seen in figure 6.16. This is a challenging case for the nominal controller. Under the same settings, we performed a tracking experiment on a trapezoidal trajectory with just the nominal controller and the combination of both nominal and transition controllers. The transition controller gets activated for 100 ms during the switch and then switches back to the nominal controller (passivity-based back-stepping control). The tracking performance for both the controllers is shown in figure 6.17. The switch is requested at 5.5 seconds and it can be seen from the figure 6.17 that the peak error is 6 mm when only the nominal controller is used. Whereas, the peak error is just 1.8 mm when the transition controller is used during the switch. Also, it can be noted that the transition controller makes the system reach steady state faster than the nominal controller. This demonstrates the uniqueness and effectiveness of the proposed motion control strategy for HHEA.

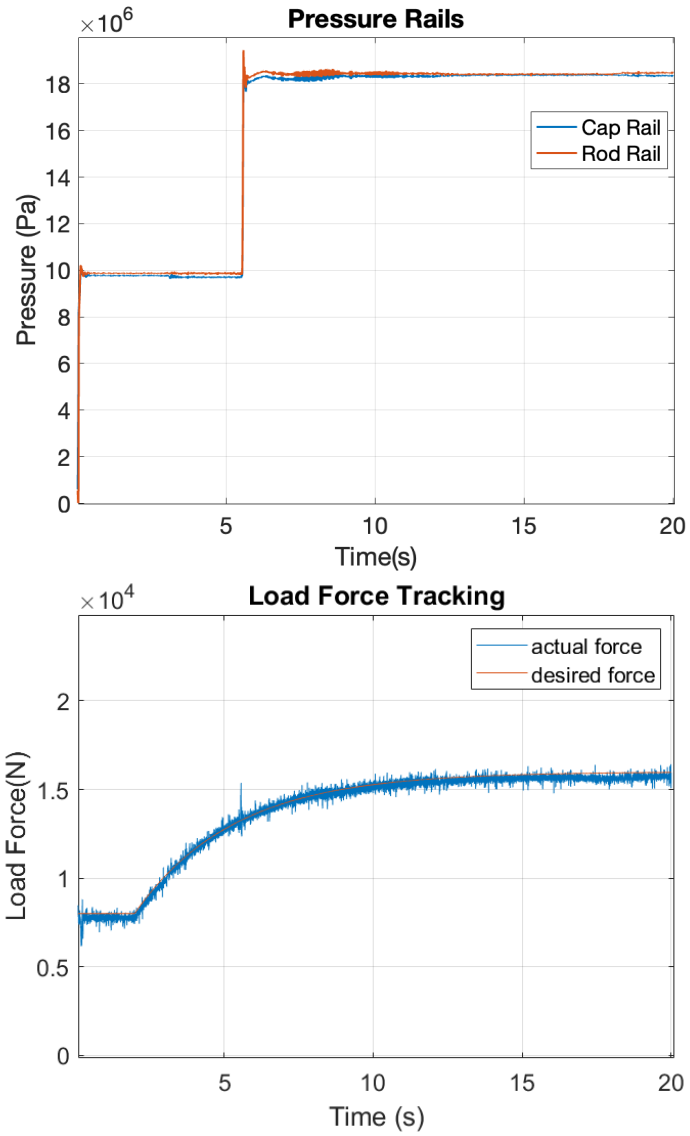

Figure 6.16: Pressure rail switches and load force tracking for cap and rod side switch from middle to high rail

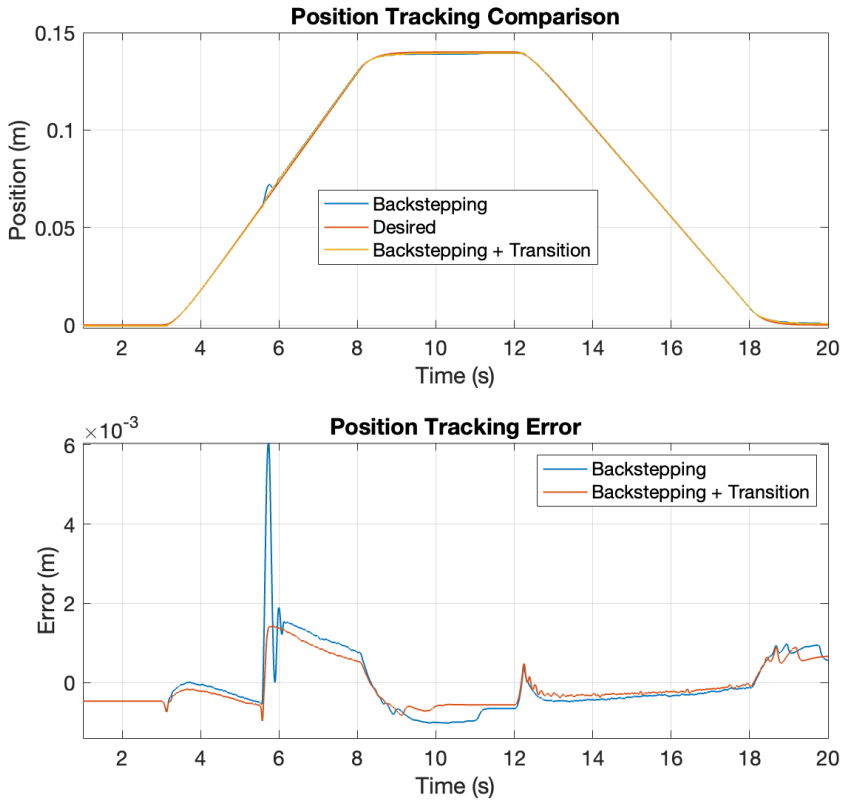

Figure 6.17: Tracking performance comparison for the nominal controller only and combination of nominal and transition controller during both cap and rod side switch

Trapezoidal and sinusoidal trajectories can be a good representation of operation profiles for heavy duty machines like excavators, wheel loaders, etc. But, they are not the real machine drive cycle. The duty cycle has been provided by OEM partners and scaled accordingly. This drive cycle mimics an on-field machine during its everyday operation. The load force is tracked using the load emulation module and it does a good job of generating the load experienced by the machine as it can be seen in figure 6.18.

Multiple pressure rail changes are requested for the varying load as can be seen from figure 6.19, and hence it combines various forms of the switching cases discussed above. The trajectory tracking performance of the proposed motion control strategy for HHEA can be seen in figure 6.20. The maximum error is 2.2

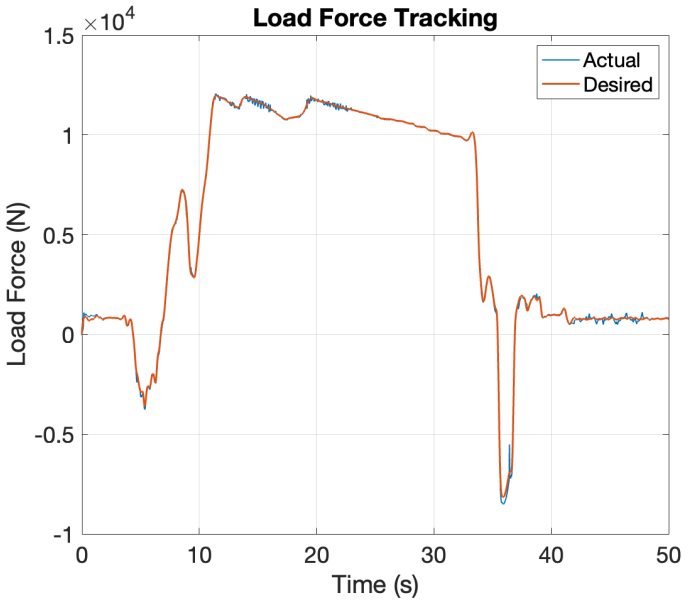

Figure 6.18: Load force tracking for scaled duty cycle

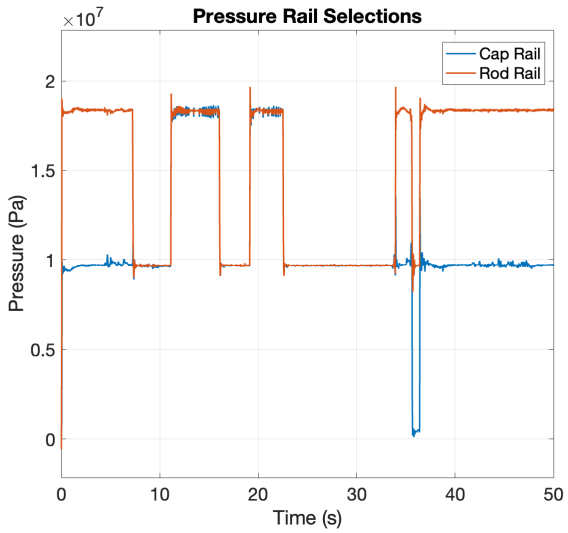

Figure 6.19: Pressure rail selection for scaled duty cycle

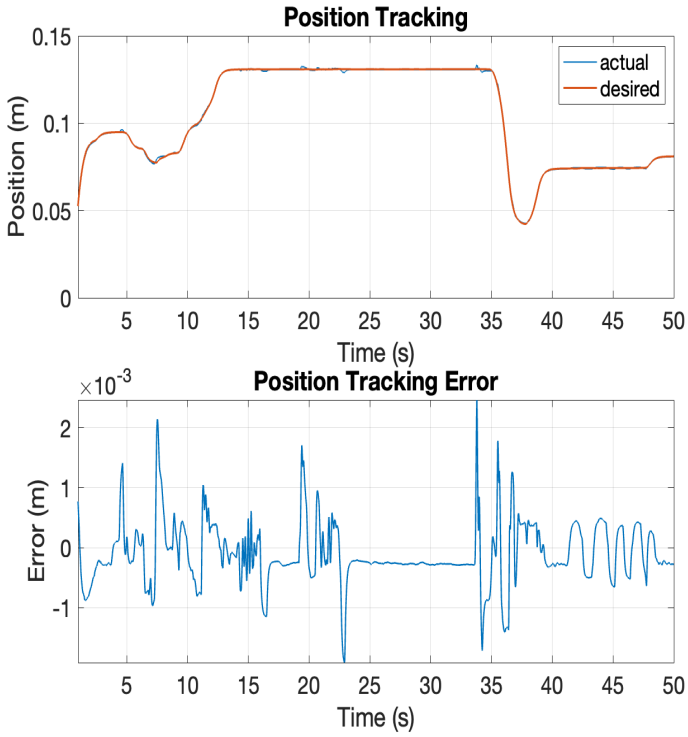

Figure 6.20: Tracking performance for a scaled machine drive cycle

mm and it takes place for a double switching case. This tracking performance validates the use of the proposed motion control strategy during multiple pressure rail switches for HHEA.

6.2 High pressure test stand

Heavy-duty mobile machines typically operate at peak pressure of 300 bar. Therefore, it is crucial to test the control strategy at these high pressures in order to ensure its effectiveness with pressure rail switches. The high-pressure test stand has been built at the Danfoss facility in Eden Prairie to perform these tests. The goal of the high-pressure test stand is similar to the test stand discussed in the previous section, where the trajectory tracking performance of the test actuator is analyzed for the motion control strategy. Specifically, the high-pressure test stand will evaluate the control strategy's effectiveness in high-pressure scenarios with pressure rail switches. The aim of testing the control strategy under high pressure is to validate its performance in real-world applications. This will help to ensure that the control strategy can handle the high-pressure demands of heavy-duty mobile machines in various pressure rail switching scenarios. The results of the high-pressure tests will be critical in determining the effectiveness of the control strategy in practical applications.

6.2.1 Test stand design

The HIL test stand layout shown in figure 6.21 consists mainly of an actuator cylinder coupled mechanically to a load emulation cylinder (26-inches stroke), a variable displacement pump/motor connected to an electric motor, two proportional flow-control valves (PFV), and Eaton's CMA90 electro-hydraulic control valves as denoted by CV-1 and PV1 – PV5. The load cylinder emulates the external loading to the actuator from the test vectors.

The HECM's electric motor driven pump is Danfoss's 72400 servo-controlled variable displacement piston pump/motor with 49 cubic centimeters (cc) total displacement. The pump is modified to facilitate a four-quadrant operation and the axis is mechanically coupled to a 5.6kW 3-phase 230VAC electrical motor (model number in appendix A), as per HECM design. The pump's inlet is connected to the HECM pressure rails using switching valves and the pump's outlet is used to control the actuator cylinder's motion. During the test, however, the pump displacement will be fixed.

CMA90 electro-hydraulic control valve is selected to control hydraulic pressures on the bench due to its compact and modular design, which also provides independent meter-in and meter-out capability by leveraging integrated pressure and spool position sensors and onboard electronics. In the configuration shown in figure 6.21, the CMA valve system consists of an inlet control module CV1 that is connected to a hydraulic pressure source, that controls a common inlet pressure for the work sections, denoted by PV1-PV5. Each PV section consists of a pair of three-position three-way valves, denoted by A and B in figure 6.21,

which controls the outlet pressures or flows independently. Reference pressures or flow for a specific PV section can be sent to CMA90 via CAN J1939 communication protocols from a controller. The functions of each specific valve section are shown in figure 6.22. The sections associated with maintaining pressure in the rails use pressure feedback control to regulate the opening of the spool based on the desired pressure of the three rails. This allows for precise pressure regulation of all three rails. Meanwhile, two other sections of the CMA valves are responsible for rail switching and operated using open loop PWM position control. This is done to move the spool as quickly as possible to minimize switching times. For load control, one of the work sections is connected to the tank, while the other is operated in pressure control mode. This configuration is determined by whether the load applied to the test actuator is pushing or pulling.

The two Danfoss's SBV11-8-C proportional flow-control valves (PFV-1 and PFV-2) in figure 6.21 are utilized as On-Off valves and are controlled via analog inputs. The three HECM rail pressures, namely the low, medium, and high pressures, are controlled via PV1-A, PV2-A, and PV2-B respectively. These controlled rail pressures are connected to the inlet of the variable displacement pump through six On-Off valves, namely PFV-1 (Rod-Med), PFV-2 (Cap-Med), PV3-A (Rod-High/Low), PV3-B (Rod-High/Low), PV4-A (Cap-High/Low) and PV4-B (Cap-High/Low). Note that PV3 and PV4 sections of the CMA are utilized as On-Off valves. The load cylinder Cap and Rod pressures are controlled by PV5-A and PV5-B.

The whole setup is designed to be fitted within a 3-foot by 6-foot bench top.

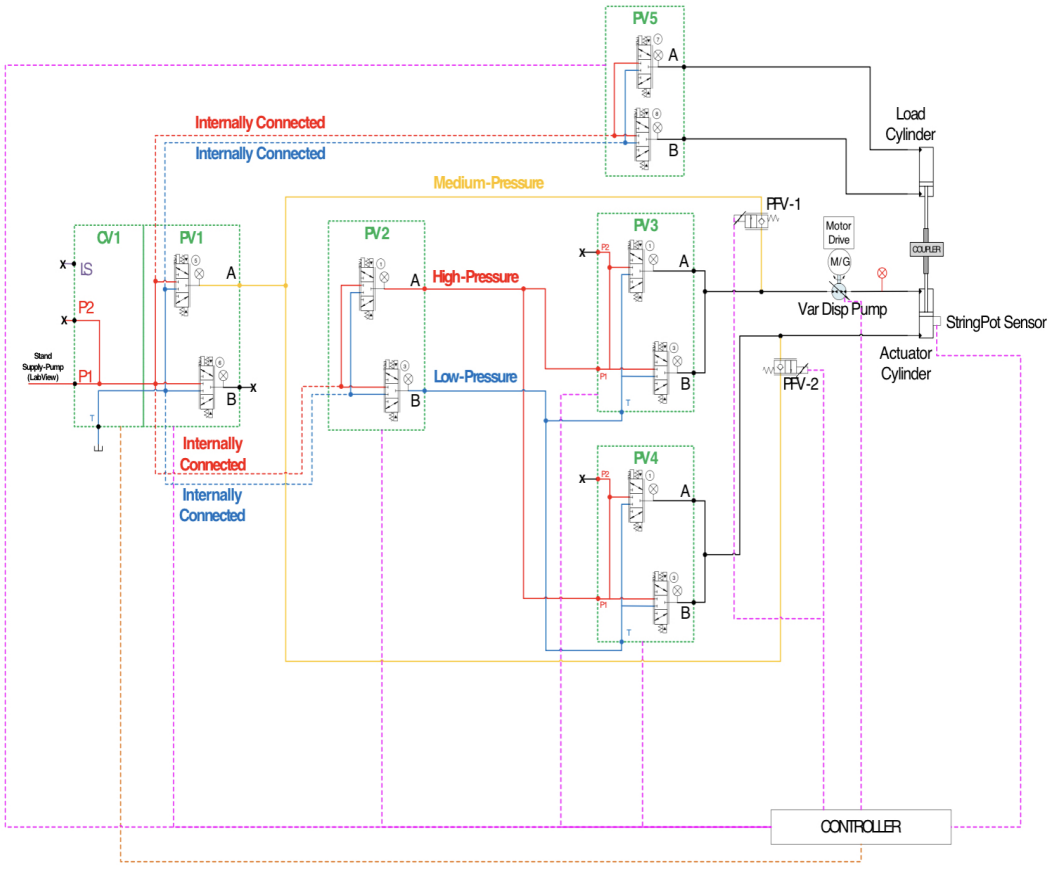

Figure 6.21: Test stand for validating the control performance on high-pressure environment at Danfoss (provided by Danfoss)

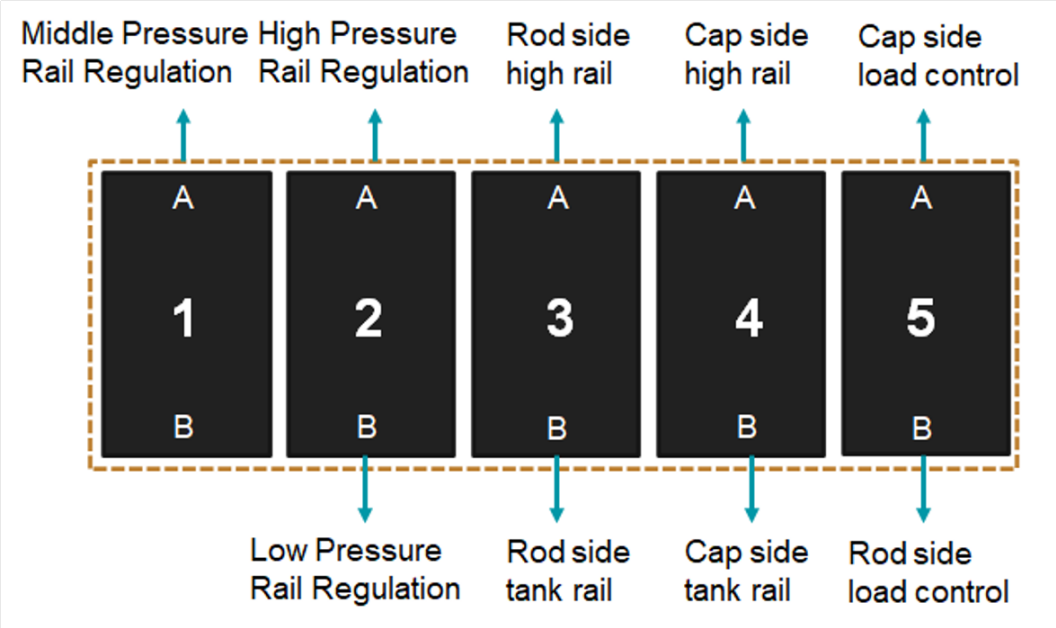

Figure 6.22: Tasks for individual work ports of the CMA valve

The test setup is kept inside a closed chamber and the hydraulic power can only be activated when the chamber is closed. The setup can be seen in figure 6.23

Just like the previous testbed we are using Matlab Simulink Realtime (SLRT) to run our motion control software. We have used Humusoft MF634 as our data acquisition board. The instrumentation setup as it can be seen in figure 6.24 has been kept outside the testing chamber. The CMA valves are controlled using an Arduino which acts as a CAN bridge between the target computer and the CMA valves. The CMA valve utilizes a pressure control mode to maintain a desired pressure level in the system. In order to achieve this, the desired pressure level must be encoded in a CAN message, which is then sent to the valve for processing. If the pressure level is constant, the message is fixed, as the rail pressure value does not change. However, for load control, the desired pressure

level is variable and must be encoded in real-time. To accomplish this, the desired pressure value is sent from the Simulink environment as two 8-bit bytes. These values are interpreted as ASCII symbols by the Arduino, which then typecasts them into integer values. The encoding of the pressure value is performed within the Arduino, and the resulting CMA message with the pressure control mode is sent to the valve for processing.

By utilizing this process, the CMA valve is able to achieve precise pressure control, even in applications where the desired pressure level may vary over time. The use of CAN messages and specialized encoding techniques enables the valve to process and respond to changes in pressure quickly and effectively, ensuring reliable and accurate control over pressure levels in the system.

In the Simulink environment, the decision for rail change is made by tracking the rail IDs to determine which pressure line needs to be closed or opened. Once these decisions have been made, they are encoded as characters and sent to the Arduino for processing. The Arduino then acts as a slave, using the character data to select the correct message and trigger the appropriate actions within the CMA valve. By utilizing this setup, the CMA valve is able to control a majority of its functions through a compact, efficient setup.

6.2.2 Experimental Results

Commissioning

The testbed has been commissioned by operating in all 4 quadrants where the test cylinder is extending or retracting under passive and overrunning load. A

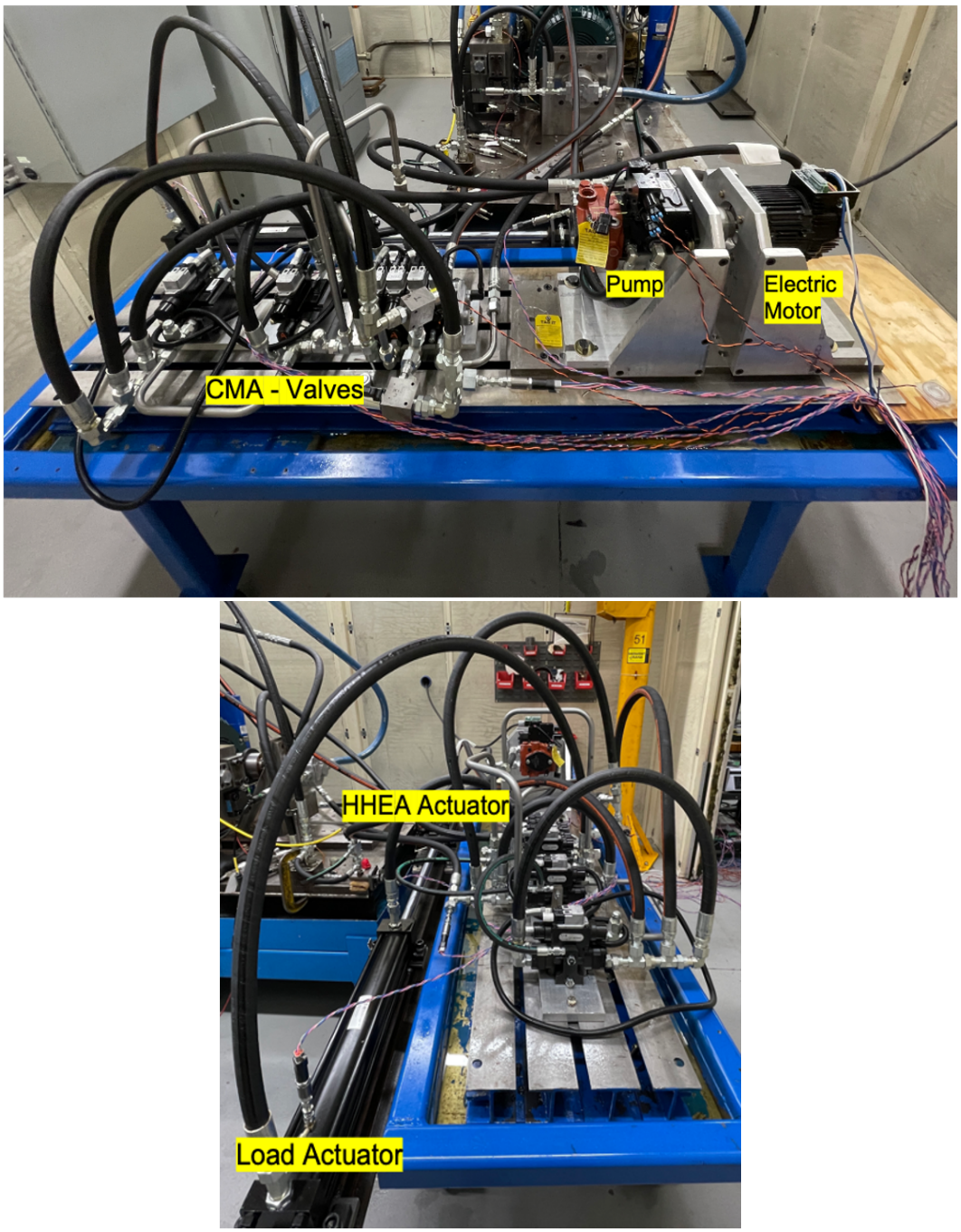

Figure 6.23: High-pressure testbed built-in Danfoss facility

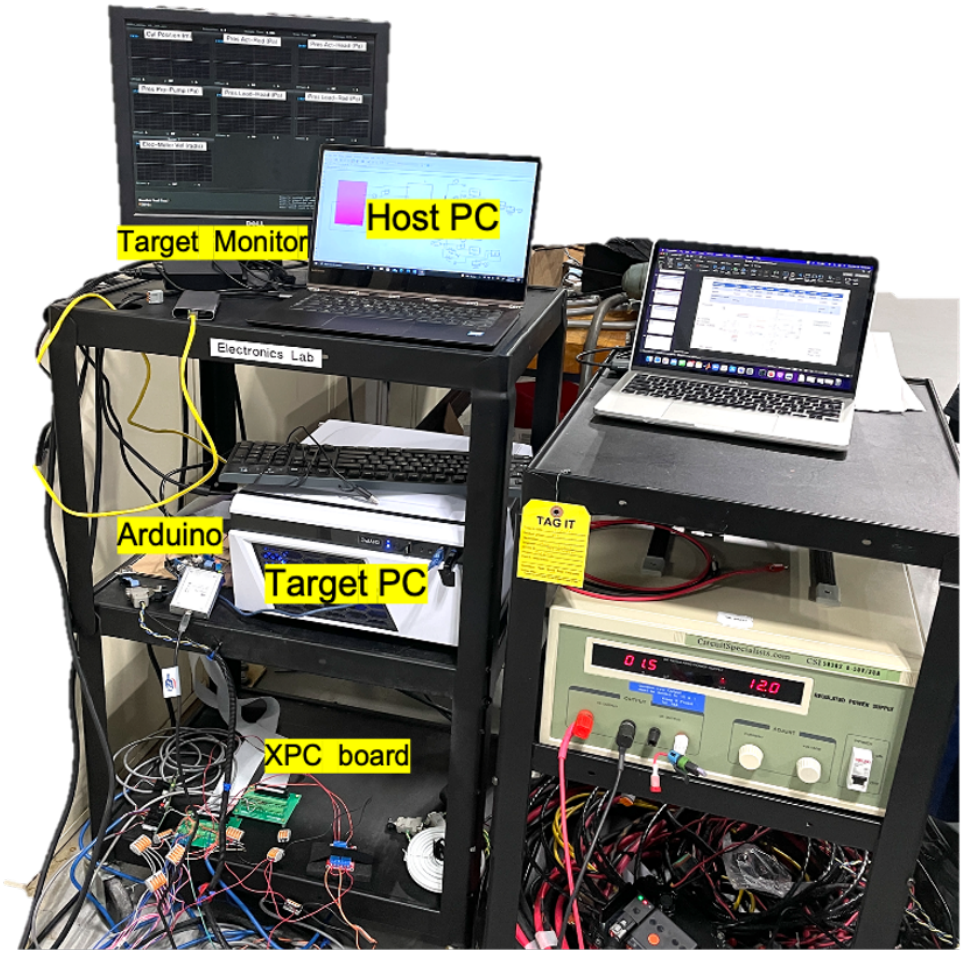

Figure 6.24: High-pressure test stand instrumentation

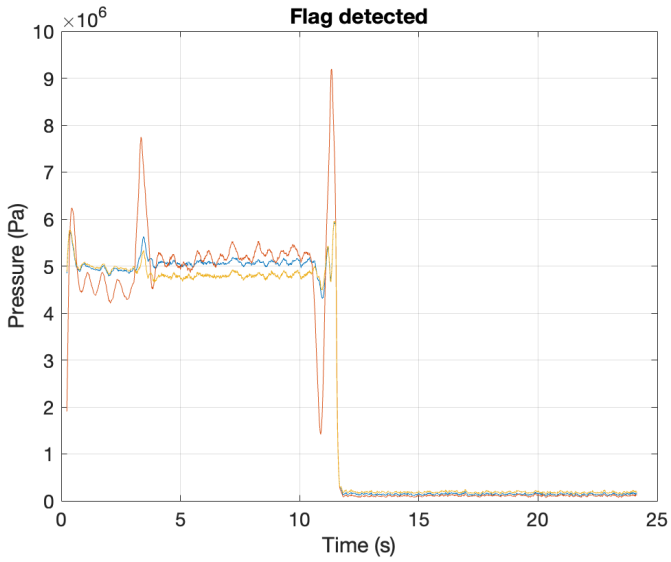

Figure 6.25: Cap and rod side pressure rails along with rod side actuator pressure is relieved as safety flag is triggered

safety system has been established to ensure the reliable and secure operation of the software. This system comprises of multiple safety checks that are designed to detect any anomalies in specific parameters such as pressure differential across the electric motor, load force, and defective pressure signals. Whenever a safety flag is raised, the entire system automatically enters a standby mode, whereby all valves open to the tank at approximately 1 bar, and the electric motor is disabled. This effectively releases any built-up pressure in the system and maintains the torque limit for the electric motor, preventing sudden high regenerative loads.

To accommodate electric regenerative load from the ClearPath electric motor in the HEMC for up to 400 Watts, a fan-cooled shunt is also employed. In a sample scenario, as illustrated in figure 6.25, the pressure difference across the HECM pump/motor and the cap side pressure of the actuator is continuously

monitored. When the pressure difference exceeds the electric motor's regenerative capabilities, a reliable safety system comes into action. It automatically relieves the system pressure, safeguarding all components from potential damage.

Control testing

Successive versions of the controllers were implemented starting with a feedforward PID controller with no rail switches, to using the backstepping controller and the transition controller in the presence of varying loads, rail switchings, and high-pressure operation. In all these cases reference speed for the electric motor has been used as the control input and the internal speed loop of the motor is used to track the reference. A trapezoidal trajectory was adopted throughout the process as a prevalent trajectory in motion planning.

Constant pressure rail selections

The first tests were performed under a constant load of 4000N and the pressure rails of the cap and rod side were set at 50 bar. The tests are to establish the performance of the baseline backstepping controllers. Sample results using a PID with a feedforward controller and a backstepping controller are shown in figure 6.26 where The PID controller exhibits position errors in the range of 5-10mm whereas the backstepping controller exhibits improved performance with errors in the range of 5mm which is within the range of the sensor noise.

The nominal controller's performance was assessed under a sinusoidal load variation as depicted in the accompanying figure 6.27. The results indicate that

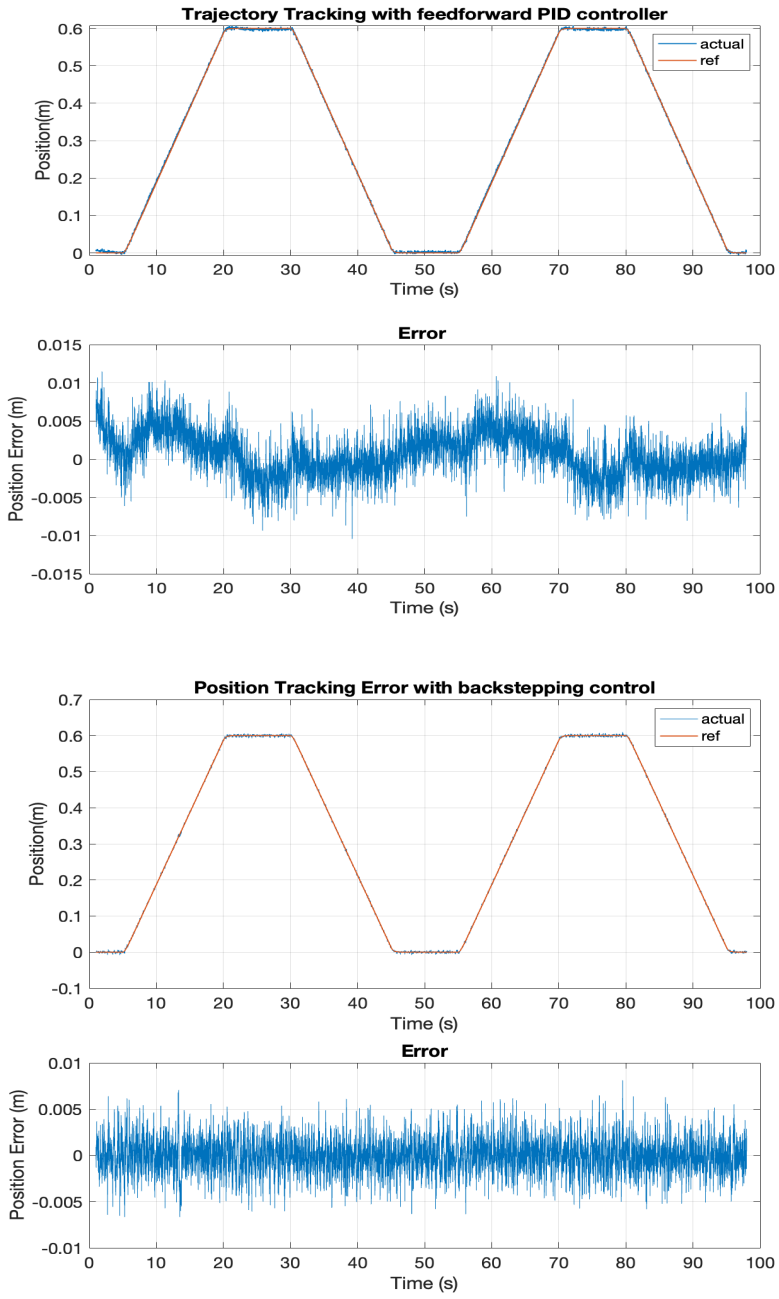

Figure 6.26: Position tracking performance under constant load (4000N) and no rail switching (50bar) (top): PID with feedforward controller, and (bottom): Backstepping controller

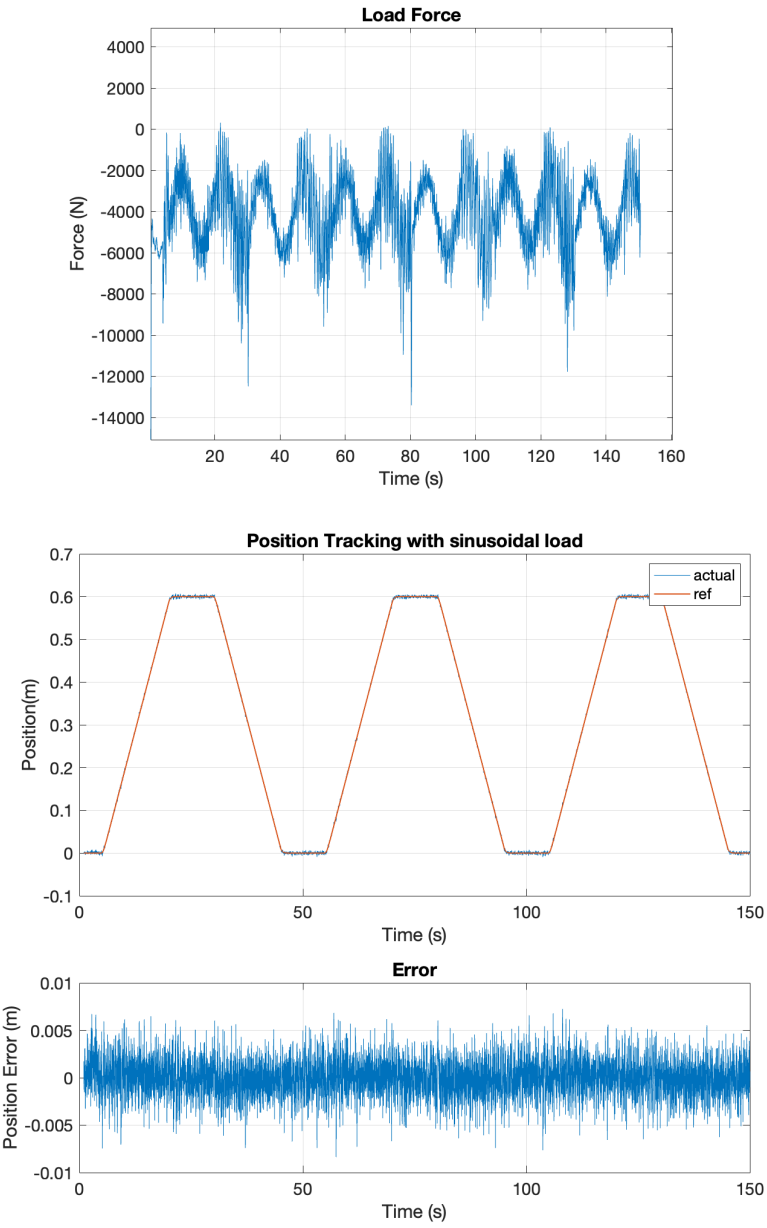

Figure 6.27: Tracking performance under varying load force and no pressure rails switching (50bar)

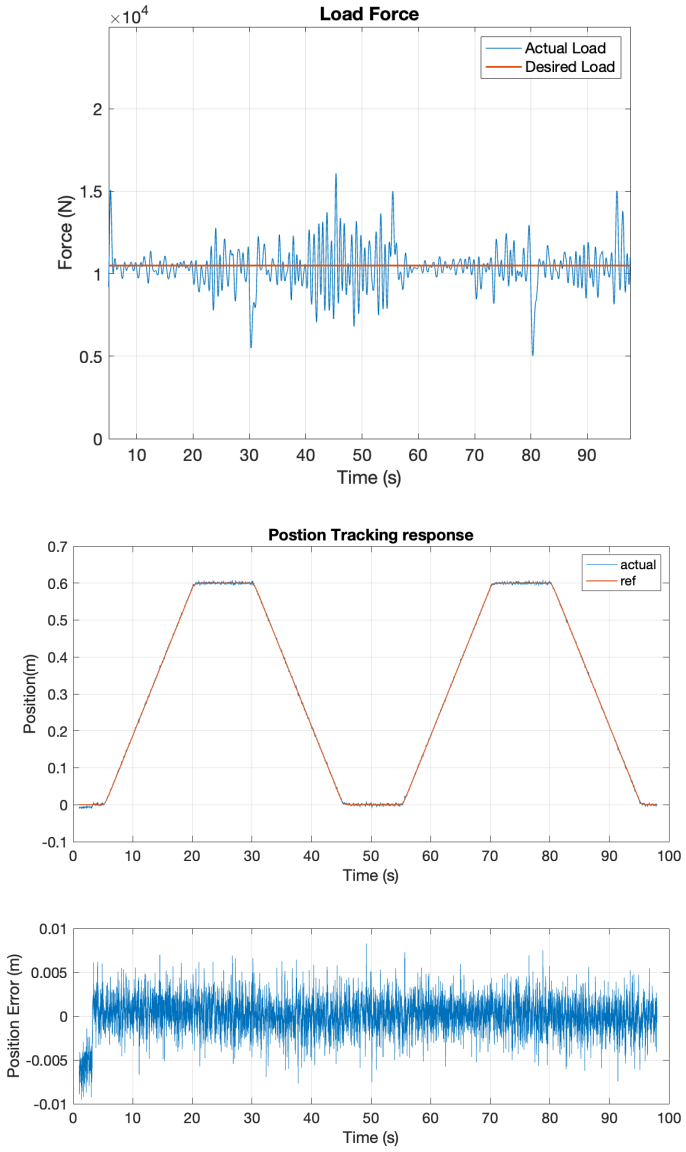

Figure 6.28: Tracking performance with a higher constant load of 10kN and 100 bar pressures were selected on both sides of the actuator

the tracking performance remains consistent despite the presence of load fluctuations.

Control performance with 100 bar pressure (the middle-pressure rail was selected on both sides of the actuator) and with a constant load of 10kN was tested next. Figure 6.28 shows the position tracking performance.

Rod side pressure rail switch

After successfully demonstrating the efficacy of the backstepping controller in the absence of pressure rail switching, the investigation proceeded to evaluate the impact of switching on the system's performance and assess the effectiveness of the transition controller in mitigating any adverse effects. The first switching scenario examined involved the activation of the rod-side switch. In order to increase the severity of the switch, a constant load force was maintained during testing as shown in figure 6.29, and the switch was made from 100 bar to 150 bar on the rod side at 30 sec. This led to a higher pressure differential across the HECM pump as it can be seen from figure 6.30. Initially, during the pressure rail buildup phase, the electric motor was disabled, resulting in an error due to a pressure mismatch caused by the load. However, after 6 seconds, when the electric motor was enabled and the controller activated, the error was corrected, and the actuator returned to its desired position as it can be seen in figure 6.29. The load was configured such that during actuator extension, the electric motor functioned as a motor. However, during retraction, with a pressure difference of 50 bar, the electric motor acted as a generator. This caused the motor to stop

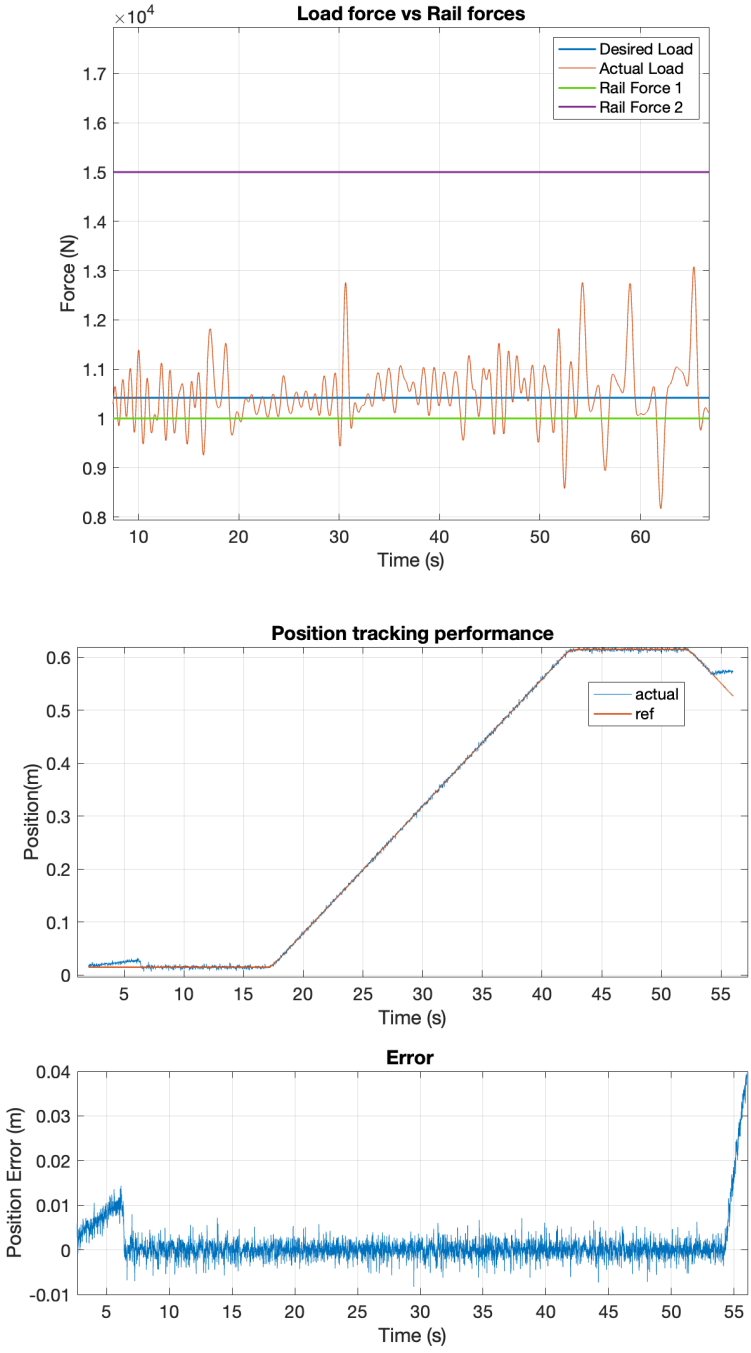

Figure 6.29: Load force and position tracking performance for rod side switching case

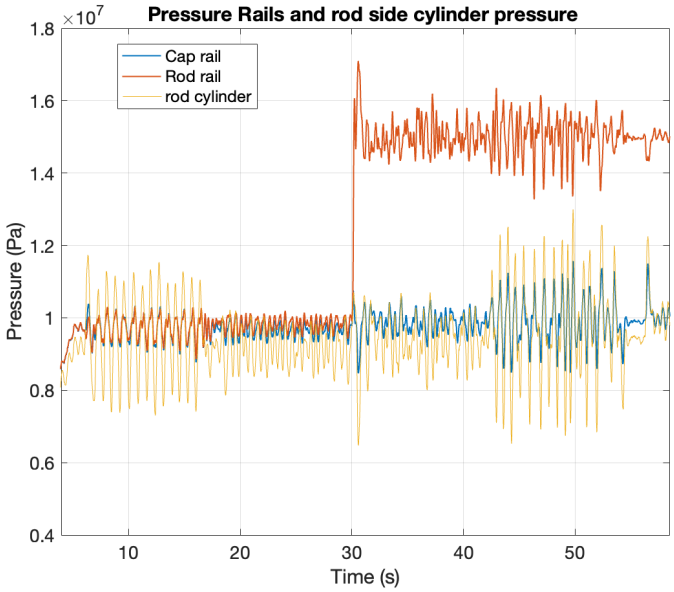

Figure 6.30: Pressure rail switch on the rod side

during retraction at 55 sec due to its limitation of handling a 30 bar pressure drop across the pump when undergoing regeneration.

figure 6.30 illustrates the pressure rail switches and the rod side chamber pressure to show the pressure differences across the HECM pump after switching. The tracking performance (shown in figure 6.29) despite sudden pressure rail change is similar to previous cases.

Both cap and rod side switch

The subsequent objective was to exhibit switching on both the cap and rod sides to 300 bar, which constitutes the highest pressure rail. The outcomes of this task are demonstrated in figure 6.32, where the switch occurred at t=60sec. In this double-switching scenario, the rail switch was devised in response to the varying

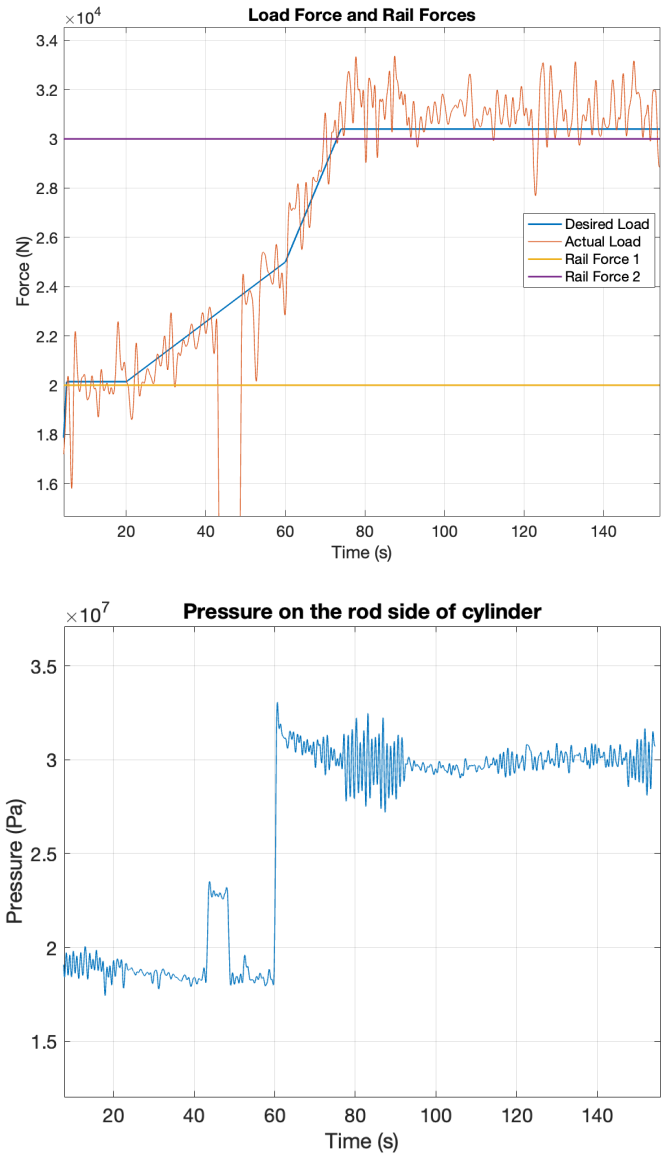

Figure 6.31: Load force and rod side cylinder pressure for a double switching case

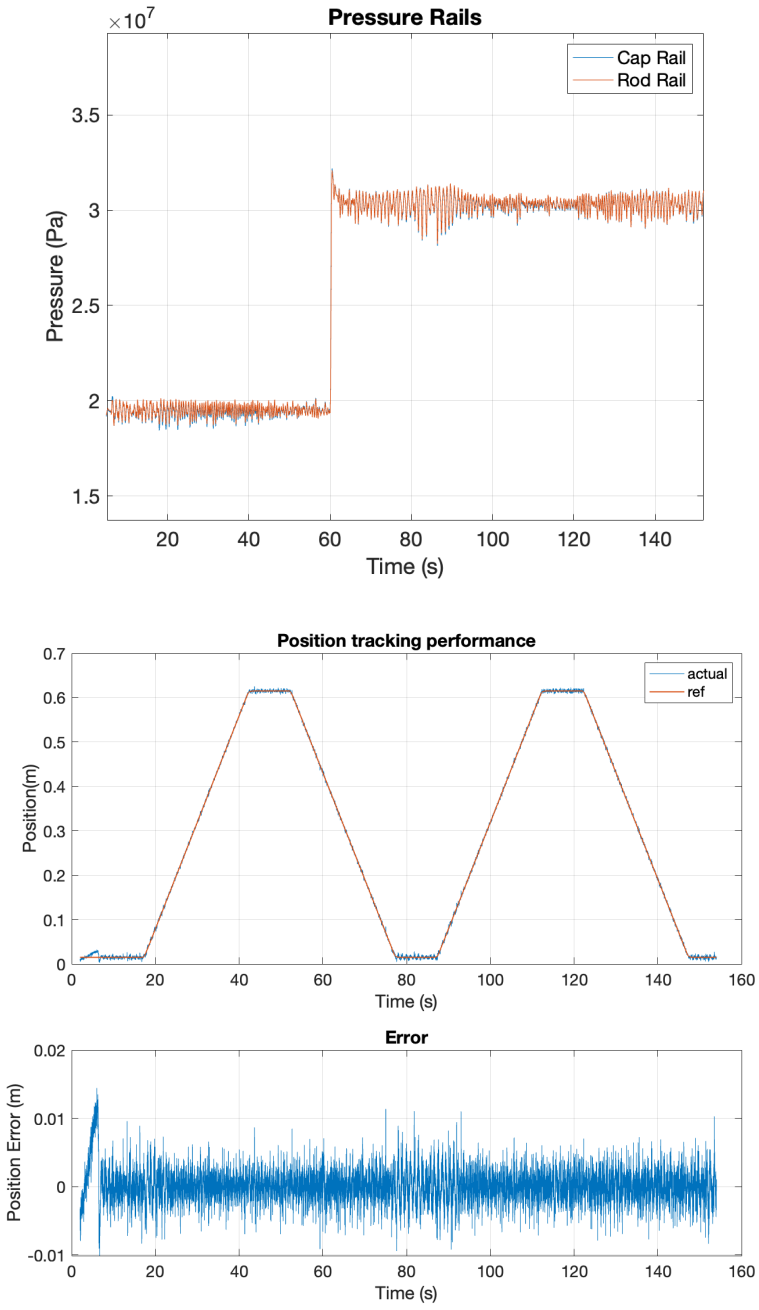

Figure 6.32: Pressure rails and tracking performance with double switch case

load force to curtail the required electric motor torque as shown in figure 6.31. The decision to switch is made when the load force is almost halfway between the two rail forces. Between 45 to 50 seconds, the load force experienced a drop, and the rod-side pressure was increased by the HECM unit to compensate for the load reduction without any effect on the tracking performance.

The desired trajectory, depicted in figure 6.32, consists of two trapezoidal segments. The first trapezoid illustrates the switching at 60 seconds, while the second trapezoid demonstrates the complete duty cycle tracking with 300 bar (highest pressure rails) on both cap and rod sides. As previously observed, tracking error remains insignificant despite rail switching on both sides of the actuator to high pressure.

Multiple switches

The final experiment involved multiple double rail switches during both the retraction and extension phases of the duty cycle. Specifically, the switching involved a change from high (300 bar) to mid-rail (200 bar) on both cap and rod sides during the extension phase and a change from mid to high-rail during the retraction phase. The desired load force has been designed such that the rail changes would take place when the load force becomes closer to either of the two rail forces at 35 and 60 seconds as shown in figure 6.33. Just like in the previous case, the HECM unit increases the rod side chamber pressure to counter sudden drops in load forces which act as a disturbance to the system. Results presented in figure 6.34 indicate that the tracking error remained low, with no significant

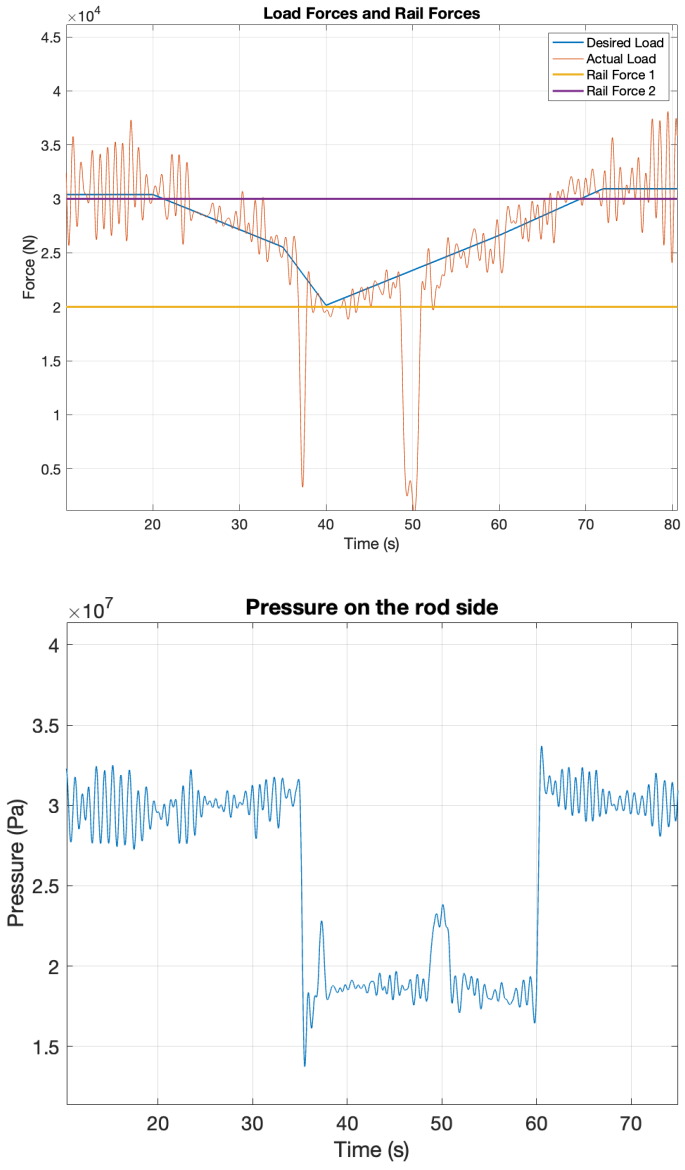

Figure 6.33: Load force and rod side cylinder pressure for multiple switch case

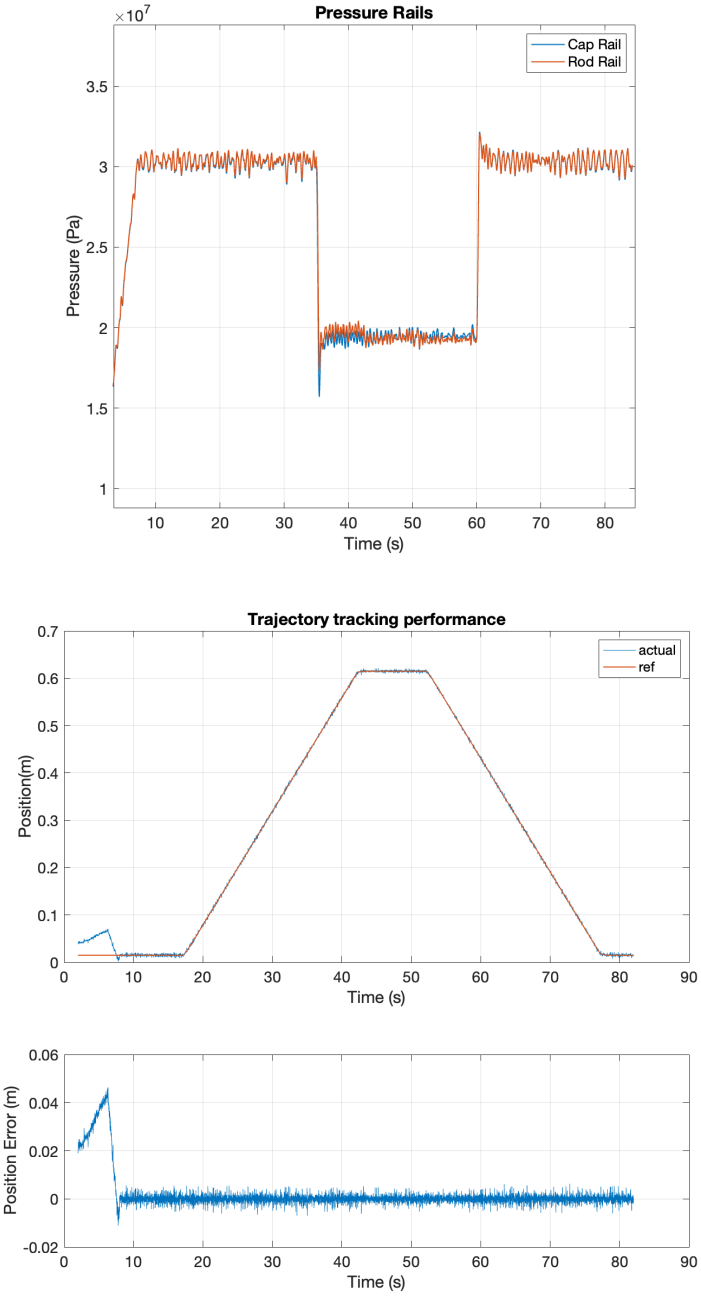

Figure 6.34: Pressure rails and tracking performance with 2 different switches

increase in error magnitude as a result of the rail switches. Overall, the findings suggest that the backstepping controller with the transition controller effectively mitigated the effects of rail switching, even in complex cases involving multiple switches.

6.3 Discussion

The effectiveness of the motion control strategy has been demonstrated on two different testbeds, despite some differences between them. In the UMN testand the maximum position tracking error is less than 0.5mm under nominal operating conditions and less than 2 mm when pressure rail switches take place. For the high pressure teststand under both nominal operating conditions and with pressure rail switches the maximum tracking error is below 5 mm. While the overall design of the testbeds may be similar, there are notable distinctions that could impact performance. For instance, the high pressure test stand employs a variable displacement HECM pump, which is operated at 25% displacement for the tests, leading to reduced efficiency. Additionally, the cylinder sizes in the high pressure test stand are larger, indicating there is more volume in the chamber. Furthermore, the hose sizes in this test stand are significantly bigger than in the UMN test stand. Despite these variations, the nominal controller has been shown to be equally effective in both test stands in tracking a reference trajectory, even in the presence of fluctuating load forces, small pressure ripples on pressure rails, and pressure rail switches. These results illustrate the robustness of the controller

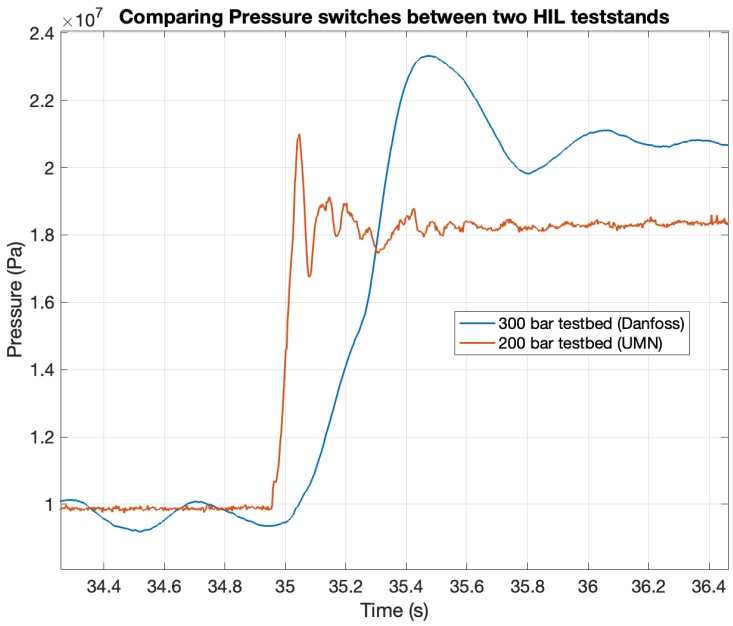

Figure 6.35: Comparison of pressure rail switch between two testbeds

and its potential to perform effectively across varying conditions.

The high pressure test stand and the UMN test stand have different resistance to pressure rail switches, as can be seen in the results. To understand why, a comparison of pressure rail switches on the cap side of both test actuators is shown in figure 6.35. The same switching valve and switching mode (PWM) were used for both testbeds, and the initial delays were adjusted to make the switch at the same time for a better comparison. It can be seen that it takes more time for the pressure to rise and reach a steady state in the high pressure test stand, compared to the UMN test stand. The UMN test stand takes 50-60 ms to reach the desired rail pressure, while the high pressure test stand takes 400-500 ms to reach the desired pressure.

This is because the volume between the switching valve and the actuator which mainly comprises of actuator volume and line volume is almost 15-20 times more in the high pressure test stand than in the UMN test stand. The rate of change of pressure decreases as the volume increases, which helps the controller better deal with the switches and has minimal effect on tracking during switches due to slower transients. However, there is a tradeoff, as the pressure takes more time, there are potentially more throttling losses. So, there is more throttling with the high pressure test stand, but the UMN test stand is more efficient and difficult to control during switches, hence a small loss in tracking during control is observed. Nevertheless, the controller does an excellent job of reducing the tracking loss during the pressure rail even when the rate of pressure change is very fast, proving that the controller is robust and effective in both testbeds.

6.4 Chapter summary

The proposed motion control strategy for the Hybrid Hydraulic Electric Architecture (HHEA) has been experimentally validated using two Hardware-in-the-loop (HIL) testbeds capable of handling pressures of up to 200 bar and 350 bar. The primary objective of this experimental setup was to evaluate the HHEA's controllability under different loading conditions by testing its ability to track a desired duty-cycle trajectory on the test actuator.

The experiment involved validating both the nominal and transition controllers. The passivity-based backstepping controller consistently demonstrated

a tracking error of less than 1 mm when the pressure rails were not switching. On the other hand, the least norm transition control reduced the tracking error compared to the passivity-based backstepping controller from 6 mm to 1.8 mm. Additionally, the motion control strategy was applied to a representative duty cycle where multiple pressure rail switches occurred, and the maximum tracking error was 2.2 mm when both cap and rod side pressure rails switched. The maximum position tracking error for the high pressure teststand is less than 5 mm for all different cases which involves varying load force, single pressure rail switches and multiple pressure rail switches. Furthermore, a comparison was made between the backstepping controller and a feedforward PID controller, and the backstepping controller was shown to have better tracking performance.

Despite differences between the two testbeds, the motion control strategy was successfully validated for both, demonstrating its versatility and robustness in diverse scenarios. The effect of pressure rail switching was observed to have a more significant impact on the medium-pressure testbed compared to the high-pressure testbed. This discrepancy is attributed to the higher chamber volume in the latter, which leads to longer switching times (50 ms to 450 ms) and increased switching losses.

Overall, the experimental results demonstrate the effectiveness of the proposed motion control strategy for the HHEA and its ability to achieve precise tracking control under different loading conditions and pressure rail switches.

Chapter 7

Human in the Loop Validation

Off-highway vehicles such as bulldozers, excavators, and wheel loaders are important machines that are used in a variety of industries, including construction, mining, and agriculture. These vehicles are known for their ability to operate in rough and challenging environments, and they are used to move heavy loads, excavate earth, and perform other tasks that require significant power and maneuverability.

As of now, the majority of these machines are operated by skilled human operators who are trained to control them in a safe and efficient manner. This means that any new architecture for these vehicles must be tested for its motion control performance with human operators. The motion control problem in this sense refers to the ability of a machine to accurately and reliably move and position itself in response to commands from an operator.

Until now in this thesis, it has been assumed that both the load force trajectory

and actuator trajectories are available, which allows for offline computation of the decision to choose pressure rails based on the available load force. Additionally, the desired reference position velocity is also assumed to be available. However, this assumption is no longer valid when the desired reference is generated from the command given by the operator. As a result, the future duty cycle is unknown, which poses a significant challenge for the system. Furthermore, the decision to choose the pressure rails needs to be made in real-time since the load force is generated by how the operator uses the machine. This necessitates a dynamic decision-making process that adapts to changing conditions.

This chapter showcases the implementation of the motion control strategy using HHEA on a 2-DOF backhoe arm, which is operated by a human operator. The boom and stick actuators of the backhoe arm are retrofitted with HHEA, and a 2-degree-of-freedom joystick is employed to control the boom and stick motion. The majority of the off-highway machines currently in use rely on open loop control structure and operator feedback to complete the loop. For HHEA both open-loop and closed-loop response is studied with operator feedback.

The load force in a hydraulic machine is dependent on the operator's interaction with the machine and the environment. This implies that the pressure rail switches need to be able to respond in real-time to the operator's usage. In order to achieve this, a real-time rail switching strategy has been formulated based on rail forces. This strategy is designed to switch the pressure rails in real time based on the operator's usage of the machine, albeit the strategy being sub-optimal in terms of energy usage.

Off-highway mobile machines, such as backhoes, are typically operated by highly skilled and experienced operators. However, the availability of these operators can be scarce, which can limit the productivity of these machines. To address this issue, a coordinated control strategy has been developed to simplify the motion control of the backhoe arm and make it more intuitive for human operators of varying skill levels. The coordinated control strategy discussed in this chapter is designed to streamline the operation of the backhoe arm, making it easier for operators to control and reduce the amount of training required to operate the machine effectively.

The goal of this chapter is to demonstrate the effectiveness of the motion control strategy for HHEA with a human operator and an effort to improve human interaction with the architecture. The chapter follows a logical progression, beginning with a detailed exploration of the human-in-the-loop testbed design. This comprehensive discussion sets the foundation for the subsequent development of a real-time control strategy. Notably, the strategy enables the operator to effectively operate the backhoe using a joystick, a key aspect of the research. Building upon the successful implementation of the control strategy, the chapter then delves into exploring methods to make the control of backhoe arms more intuitive using the existing human-machine interface.

7.1 Human in loop testbed design

The backhoe arm shown in figure 7.3 is equipped with three hydraulic linear actuators, each of which provides a distinct degree of freedom. Specifically, the boom, stick, and bucket actuators are responsible for controlling vertical movement, horizontal extension/retraction, and bucket opening/closing, respectively, and are in conventional machines regulated using spool valves. However, this approach results in significant energy loss due to throttling. To address this problem, the Hybrid Hydraulic Electric Architecture has been implemented specifically for the boom and stick actuators of the backhoe arm, as illustrated in figure 7.1. Both actuators' rod chambers are connected to an electric motor and pump combination. Along with a pump and electric motor combination, a 5 section Danfoss CMA valve (switching valve) is used to form the Hydraulic Electric Control Module (HECM). The 5-section CMA valve is designed to serve two functions: generating the middle-pressure rail and switching pressure rails for both actuators. One of the work ports functions in pressure control mode to generate the middle-pressure rail, while the other four sections are operated in PWM mode to switch among three pressure rails on both the cap and rod ends of the two actuators. The external hydraulic power supply is responsible for generating both the high-pressure line and the tank line. This testbed demonstrates how the HECM can be retrofitted to a hydraulic actuator making the Hybrid Hydraulic Electric Architecture flexible to implement on an existing machine.

Motivation for the Hybrid Hydraulic Electric Architecture is enable electrification without needing very large electric components Therefore, the sizing of the

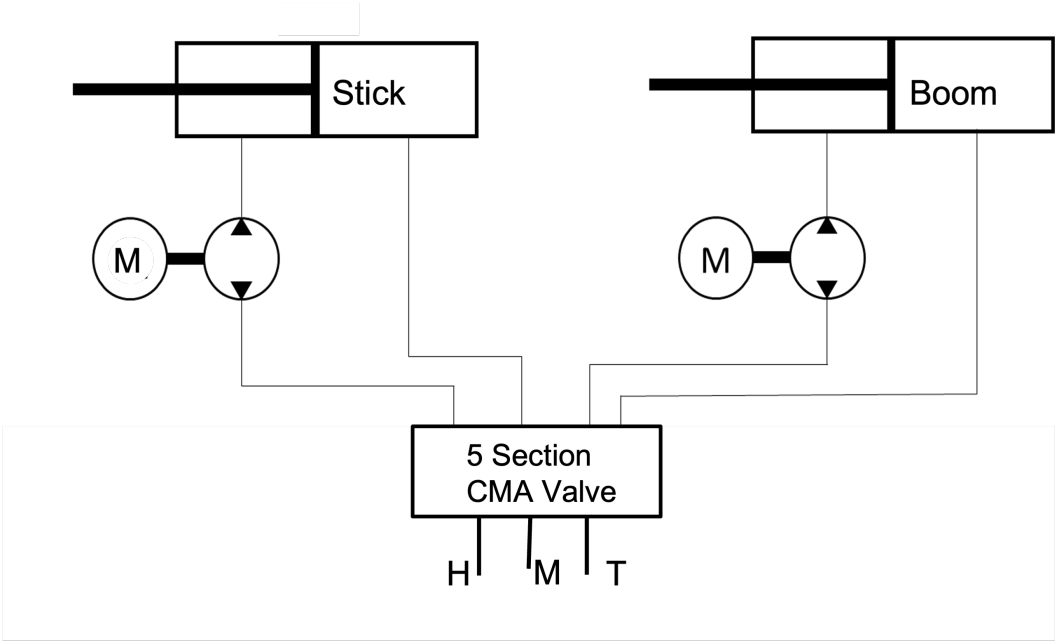

Figure 7.1: Backhoe stick and boom actuator with HHEA implementation

HECM (Hybrid Electric Control Module) components plays a crucial role in the success of this architecture. Since the testbed involves retrofitting the existing backhoe arm actuators, the sizing of the components revolves around the dimensions of the boom and stick actuators. The rail forces required for these actuators can be calculated based on the three pressure rails (100 bar, 50 bar, and tank) and the dimensions of the hydraulic actuators (cap and rod side area). The nine possible combinations of rail forces for the boom and stick cylinders are shown in figure 7.2.

The electric motor is responsible for supplying half of the difference between consecutive pressure rail forces. Consequently, the torque capacity of the electric motor has been sized to meet half of the maximum force difference between two

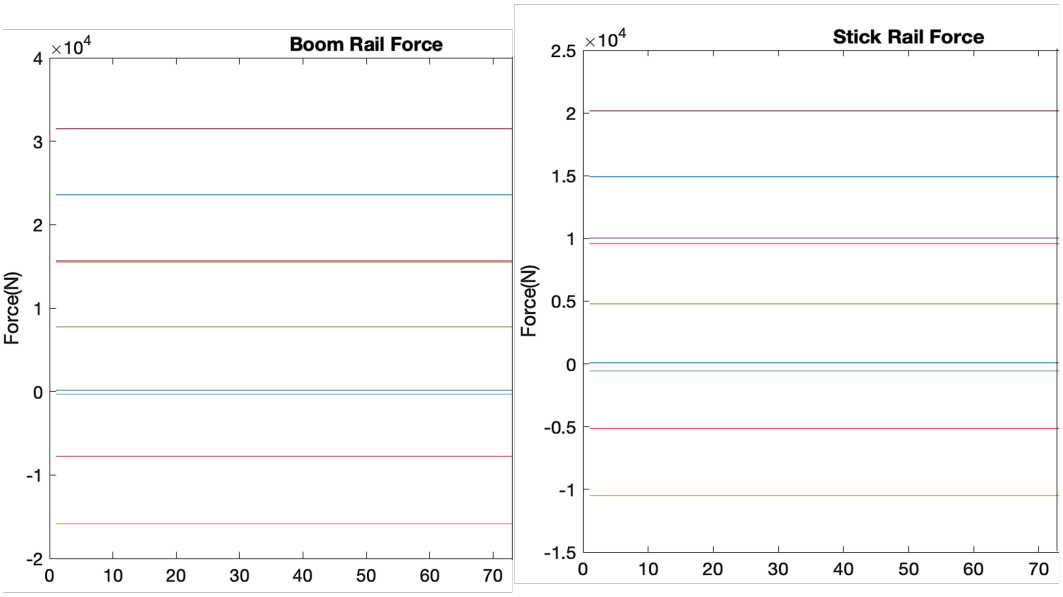

Figure 7.2: Backhoe stick and boom actuator pressure rail forces

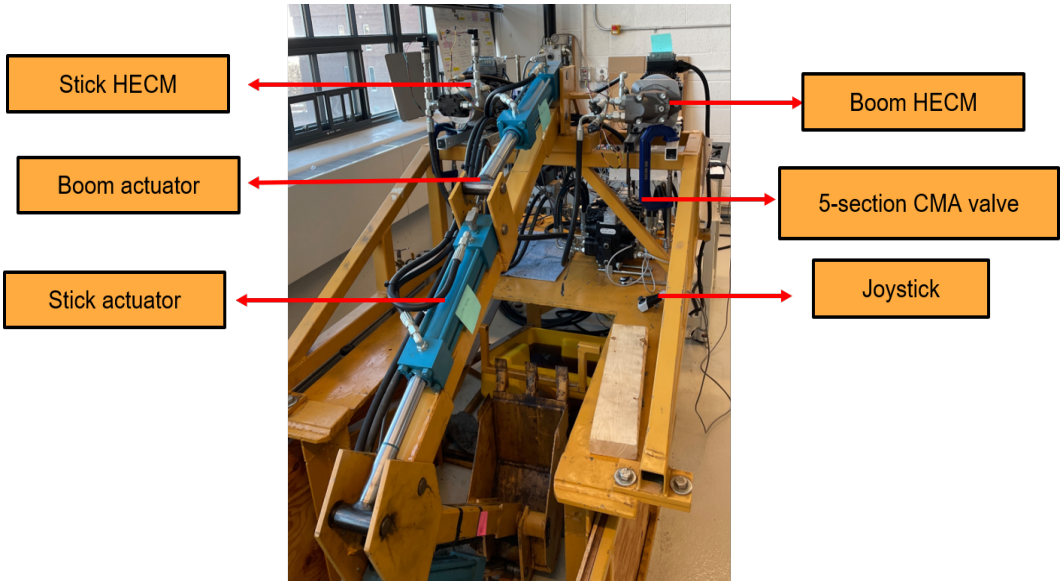

Figure 7.3: Backhoe testbed with Hybrid Hydraulic Electric Architecture

consecutive rails. It is worth noting that the motor has been sized with an additional 10-15% margin to account for cavitation effects. The maximum flow rate required to achieve a full stroke of 8 inches within a 3-second timeframe has been assumed as the maximum flow requirement. Electric motors can operate at higher speeds than pumps, therefore the maximum speed of the e-motor-pump unit is limited by the maximum speed of the pump itself (sizing details in appendix A). With the maximum flow requirement and the operating speed of the pump, the displacement of the pump can be calculated. The hardware used in the retrofitting is listed in table A.4. In figure 7.3, the backhoe arm retrofitted with HECM and equipped with a 2-degree-of-freedom joystick is depicted. The motion of the stick and boom actuators is controlled by an analog 2-DOF joystick. While according to SAE and ISO conventions, boom and stick controls are typically assigned to separate joysticks, for the purpose of this testbed, since only two actuators have been retrofitted, the controls have been consolidated onto one joystick to ensure more intuitive interaction.

7.2 Control design

The Hybrid Hydraulic Electric Architecture (HHEA) requires a two-tiered controller design, consisting of both a high-level and a low-level controller. The high-level controller's objective is to minimize system losses by selecting appropriate pressure rails on both the cap and rod sides, given the limited torque availability.

However, this pressure rail optimization is performed offline, which makes it challenging to implement in real-time scenarios where the pressure rails must adapt to changing system conditions. To address this issue, a real-time rail-switching strategy has been developed and validated experimentally on the backhoe testbed.

Meanwhile, the low-level controller is responsible for the motion control of the HHEA. This controller uses position, velocity, and load force references, which are pre-defined based on a specific machine's duty cycle. However, during real-world operation, these reference trajectories are generated in real time by the operator. To address this challenge, a control strategy has been devised to enable the low-level controller to generate the reference trajectories in real time and utilize them for motion tracking.

7.2.1 Realtime switching

The Hybrid Hydraulic Electric Architecture relies heavily on efficient switching among the pressure rails to minimize the size of the electric component and maximize fuel savings. As discussed in chapter 2, the high-level controller plays a critical role in selecting the pressure rails based on the system's performance and prior knowledge of the duty cycle and component operational zones. This requires the optimization process to be computed offline over the entire drive cycle. However, future drive cycle information is unavailable when a human operator drives these mobile machines. Therefore, a real-time pressure rail switching strategy is necessary to drive the system with reduced electric component sizes.

The system incorporates three pressure rails on both the cap and rod sides,

providing a total of nine possible rail force options. To ensure efficient operation within the limits of the electric motor torque, the decision to switch between pressure rails is based on the load acting on the actuator. The actuator load force is measured by utilizing pressure sensors on both the cap and rod sides of the actuator. The load force is compared with each of the nine rail forces to determine the most suitable combination of pressure rails. A cost function is formulated using the absolute difference between the rail forces and the actuator load, aiming to minimize the cost function by selecting the rail force that is closest to the actuator load. This approach enables downsizing of the electric motor. The decision to choose the nearest rail force is assessed at each time step, except during a switching decision where it is evaluated after the switching period concludes. Let F_{Rails} represent the set of all possible forces and the load force F_L is given by:

$$F_L(t) = P_c(t)A_c - P_r(t)A_r \tag{7.1}$$

where $P_c(t)$, $P_r(t)$ are the pressure measuremnts on the cap and rod side of the actuator and A_c, A_r are the cap and rod side areas respectively. The selected rail force F_* that minimzes the cost function is given as :

$$F_* = \arg \min_{F_{\mathrm{R}} \in F_{Rails}} \left[Cost(F_R, F_L) \right] \tag{7.2}$$

Nominally, the cost function is the absolute difference between the rail force F_R and the load force F_L. However, if the chosen rail force leads to cavitation, the

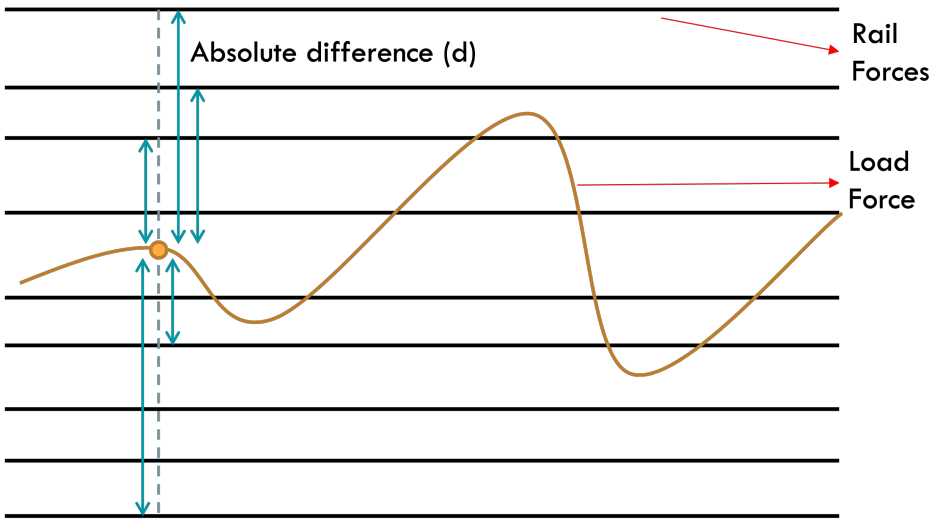

Figure 7.4: Realtime pressure rail switch

cost associated with that rail force is set to infinity, rendering it infeasible. Hence

$$Cost(F_R, F_L) = \begin{cases} |F_R - F_L| & \text{No cavitation} \\ \infty & \text{if } F_R \text{ leads to cavitation.} \end{cases} \tag{7.3}$$

In this way, the optimization process avoids choosing a set of pressure rails that leads to cavitation. A switching penalty can also be added to reduce frequent switching. It is important to note that this approach represents a sub-optimal solution since the decision to switch is based on minimizing the size of the electric motor, rather than on the objective of minimizing losses in the system. In contrast, offline optimization techniques, such as [48] developed by Siefert and Li involve a more comprehensive analysis that considers a broader range of factors when making switching decisions, resulting in the identification of the optimal solution

that minimizes energy use.

7.2.2 Reference tracking

The HHEA requires precise control of its hydraulic actuators to accomplish tasks performed by mobile off-road machines. To achieve this, the HHEA motion control design and strategy have been developed and explained in the two previous chapters: Nominal Control (chapter 4) and Transition Control (chapter 5). The primary objective of the HHEA motion control design is to track a desired reference position, which in the previous chapters is known beforehand. To achieve this, a feedback control design is implemented for the nominal control, where the current system state and the desired reference position are used to compute the control action. This controller does not rely on any future drive cycle information. On the other hand, the transition controller does rely on future reference trajectories for a brief period. The purpose of the transition controller is to smoothly handle pressure rail switches encountered in HHEA's operating modes. During this brief period, the reference trajectories are used to compute the final state based on the future drive cycle information, and the actuator achieves the final state at the end of the transition period.

In real-time operation, the reference trajectories are generated based on the operator's input via the joystick. The joystick has two degrees of freedom that are linearly mapped to the desired cylinder velocities. The reference cylinder velocities are integrated over time to obtain position references. The operator uses visual feedback to change the reference for the controller, completing the human-in-loop

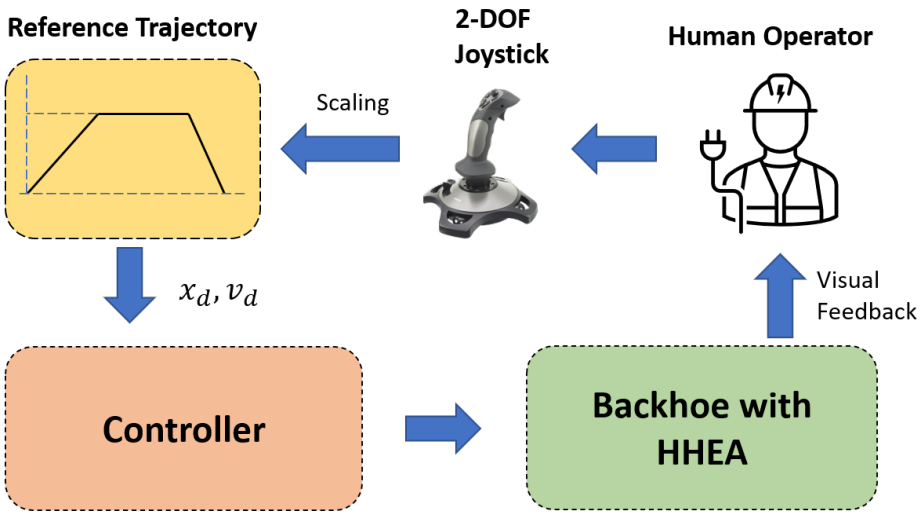

Figure 7.5: Backhoe setup control framework

control system as it can be seen in figure 7.5. Passivity-based integral backstepping controller (discussed in chapter 4) is used in between pressure rail switches and the Least Norm controller (chapter 5) is used during a pressure rail switch.

For the computation of the Least Norm Control during the transition period (100 ms), the pressure rail switches are modeled as a first-order filter using the old and new rail selection. The velocity reference and the load forces are assumed to be constant during the transition period as the transition period is short. These assumptions would enable scaling the Least Norm Control solution as described in chapter 5 for different rail switches.

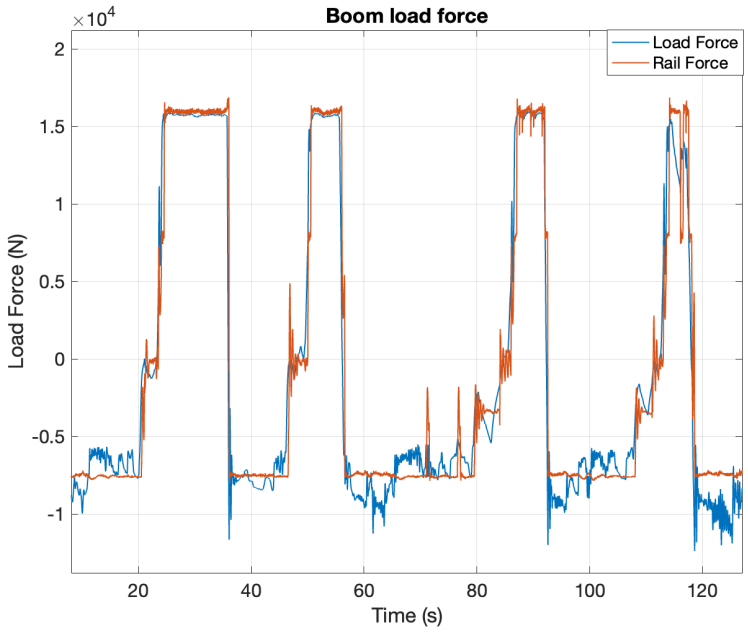

Figure 7.6: Load force vs Rail force with three pressure rails (50 bar, 25 bar, tank)

7.2.3 Results

Real-time rail switching

The real-time pressure rail switching strategy discussed in the above section is demonstrated on the backhoe testbed retrofitted with HHEA (figure 7.3). In this particular experiment, the external loading on the boom actuator undergoes variation as the operator pushes the bucket against the ground, aiming to lift the backhoe frame.

As depicted in figure 7.6, the load exerted on the boom actuator undergoes dynamic changes throughout the course of the experiment. Initially, before the bucket makes contact with the ground, the load on the boom actuator is solely

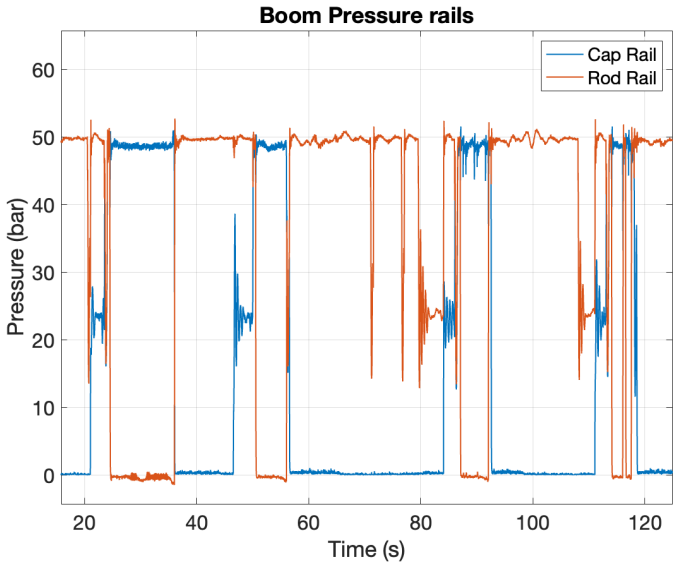

Figure 7.7: Pressure rails switches on the cap and rod side of the boom actuator

due to the force of gravity. However, once the bucket hits the ground, a reaction load is generated, which acts on the boom cylinder. As the frame continues to lift, the load on the boom actuator eventually stabilizes and remains constant. The pressure rail switching strategy uses the pressure rail switches as shown in figure 7.7 to provide the majority of the load force hydraulically. Overall, this experiment demonstrates the effectiveness of the real-time pressure rail switching strategy as the external load changes.

Open loop vs Closed loop tracking

An experiment is conducted to test the performance of open loop control with the passivity-based backstepping control for the backhoe testbed with the open loop control design being the baseline. In this experiment, the operator uses the

joystick to move the backhoe stick back and forth from a fully extended to a fully retracted position without triggering any pressure rail switches. For the open-loop control design, the 2-dof joystick was utilized to control the speed of the electric motor for both stick and boom HECM. The joystick was linearly mapped to the electric motor speed reference, and the motor was controlled by its inbuilt speed control to track the speed reference.

The velocity tracking performance of the stick cylinder for both the controllers is presented in figure 7.8. As expected, the backstepping controller performed better in tracking the reference signal. The user input delay was estimated to be 150 ms for the open-loop control and 80 ms for the backstepping control indicating that the backstepping control is much more responsive. The delay is determined by computing the normalized cross-correlation between each pair of signals at all possible delays. Then the estimated delay is reported by identifying the shift for which the normalized cross-correlation had the largest absolute value. The backstepping controller also performs better than the open loop controller in tracking the reference velocity set by the operator.

Reference tracking with rail switches

The objective of this experiment is to assess the motion control performance of the backhoe testbed in the presence of pressure rail switches. The backhoe arm's boom and stick actuators are controlled using a 2-degree-of-freedom (2-dof) joystick, which establishes a velocity reference based on the joystick's position. The operator concurrently manipulates both the stick and boom actuators, while the

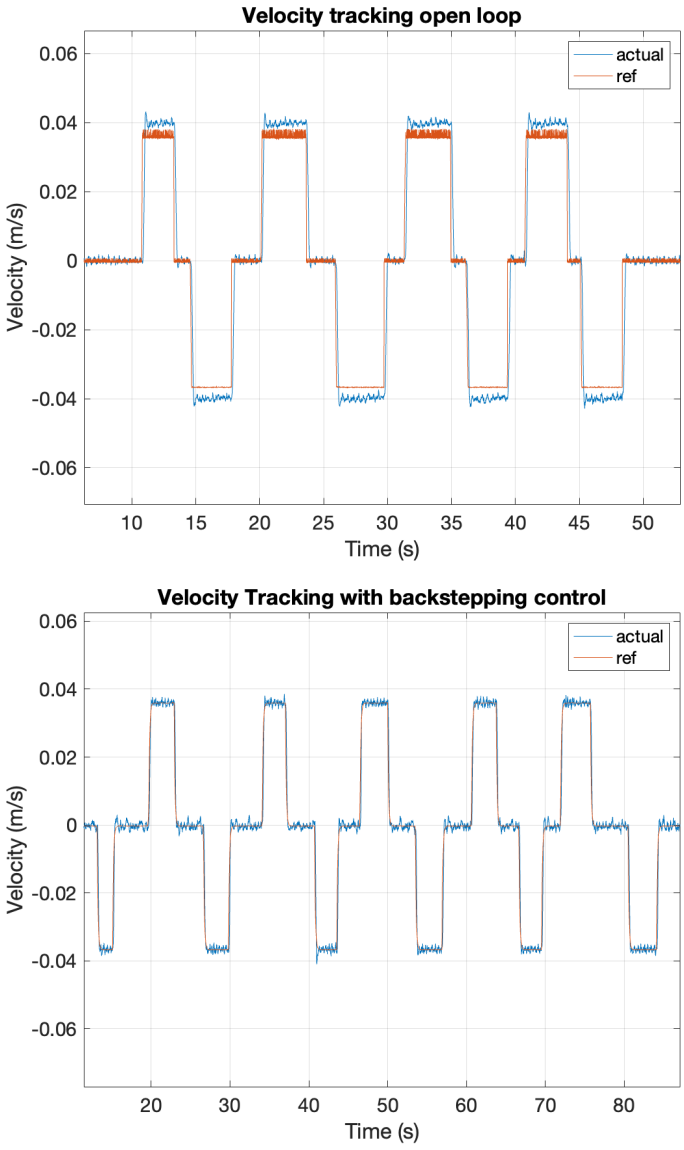

Figure 7.8: Open loop vs Closed loop velocity control for stick actuator

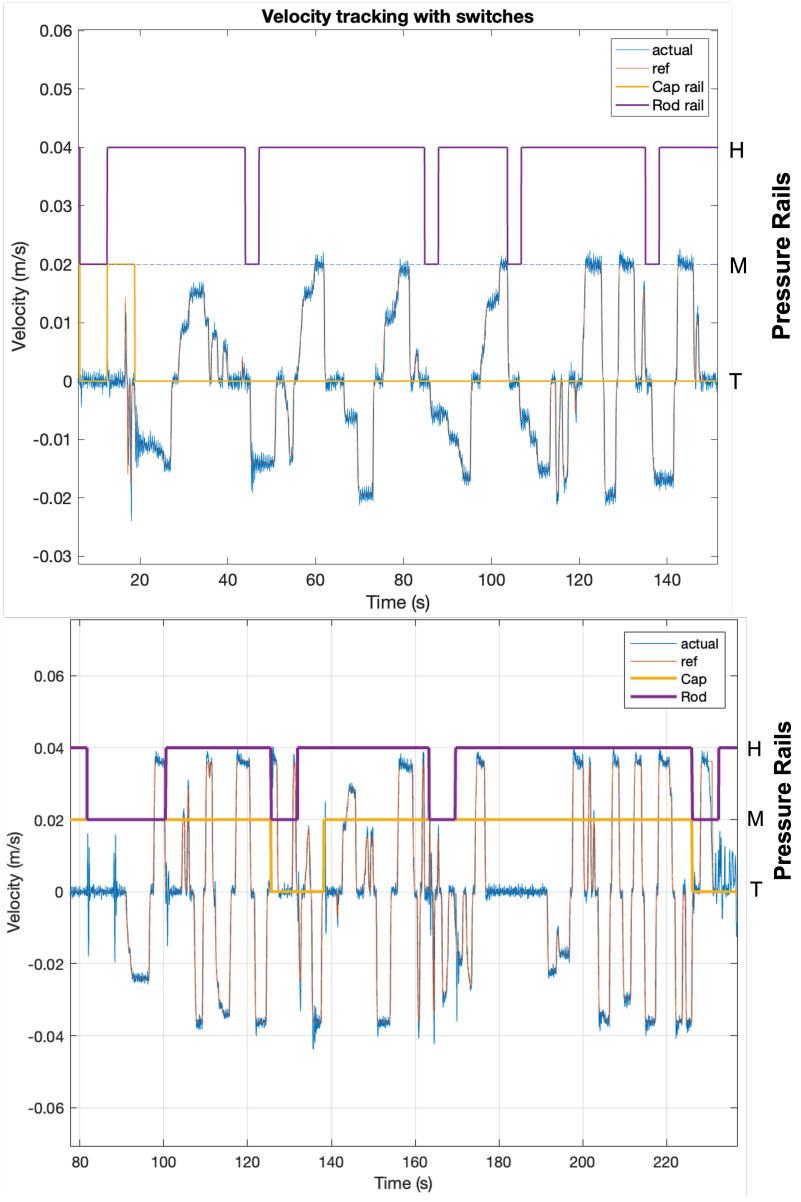

Figure 7.9: Velocity tracking for the boom (top) and stick actuator (bottom)

real-time rail switching strategy triggers the pressure rail switches to accommodate changes in the load acting on these actuators.

As depicted in figure 7.9, both the stick and boom actuators effectively track the reference velocity. The figure also illustrates the pressure rail selections made on both the cap and rod sides for each actuator. Notably, the impact of the switching process on the boom actuator is minimal due to its significant inertia, which inherently provides damping and reduces velocity spikes during the switching events. In contrast, the stick actuator, having lower inertia, experiences greater tracking loss during specific switches (max velocity error 0.01 m/s), resulting in a few velocity spikes. It is important to highlight that despite the slight tracking deviations and velocity spikes observed in the stick actuator during certain switches, the overall motion control algorithm and real-time pressure rail switching strategy employed for operating the backhoe yield excellent tracking performance for both the stick and boom actuators.

7.3 Human machine interaction

Off-highway mobile machines such as backhoes, excavators, and bulldozers are critical equipment in the construction industry. However, operating these machines requires specialized skills that can only be acquired through rigorous training and hands-on experience. Skilled operators are essential for the efficient and safe operation of these machines, which in turn impacts the productivity, quality, and safety of construction projects.

Despite the crucial role played by skilled operators, the construction industry is facing a looming shortage of such skilled laborers. Finding a skilled operator can be quite challenging and expensive for construction companies. Currently, the human-machine interface for these machines requires the use of two 2-degree-of-freedom joysticks to command the motion of four degrees of freedom. However, most of the tasks these machines perform require the simultaneous use of multiple degrees of freedom, making the precise operation of these machines a challenge that requires practice.

To address this issue, reducing the complexity of the operation of these machines can allow even amateur operators to perform the required tasks. The ultimate goal for the human-machine interface is to simplify the operation of the machine and make it more intuitive and user-friendly, reducing the amount of training needed to operate it effectively. By achieving this goal, operators of varying skill levels can perform complex tasks with ease, improving efficiency, reducing errors, and increasing productivity. One of the potential ways of making the existing human-machine interface easier to operate is by coordinating the motion of multiple degrees of freedom to perform specific tasks. In this section, we will go through step by step process of developments made in the human-machine interface of the backhoe to make the controls easier to operate.

7.3.1 Cartesian workspace operation

Tasks for manipulators are frequently defined in Cartesian space, as they offer several advantages over individual joint motions. One significant advantage is

the ease of perceiving and conceptualizing the end effector's motion when tasks are specified in Cartesian coordinates. This allows the operator to control the movement of the backhoe by specifying a desired velocity at the end effector (bucket joint), which is then translated into the appropriate joint velocities to achieve the desired movement. However, the end effector movement is in Cartesian space, while the stick and actuator movements are mapped to joint space and the motion controller also works in the joint space. This requires a kinematic mapping between the Cartesian and joint spaces of the backhoe to translate the desired end effector velocities into the appropriate joint velocities. In the backhoe testbed, joint angle sensors are not available, and therefore the joint angles need to be kinematically estimated from the actuator positions.

Figure 7.10 defines the geometry of the backhoe for boom and the stick actuator to calculate joint angles q_1 and q_2. Using cosine law a geometric mapping can be obtained to convert actuator position to joint angles and vice versa. The kinematic parameters used are shown in table A.1 in the Appendix.

1. Calculating joint angle for boom actuator where x_{booom} is the boom actuator position and $l_{boom,retracted}$ is the fixed retracted length of the boom cylinder:

$$d_2 = x_{boom} + l_{boom,retracted} \tag{7.4}$$

$$cos(\theta_A) = \frac{-d_2^2 + d_1^2 + d_3^3}{2d_1 d_3} \tag{7.5}$$

$$q_1 = \pi - \theta_3 - \theta_A - \theta_{CB} \tag{7.6}$$

Here θ_3 and θ_{CB} are constants and θ_A depends on x_{booom}.

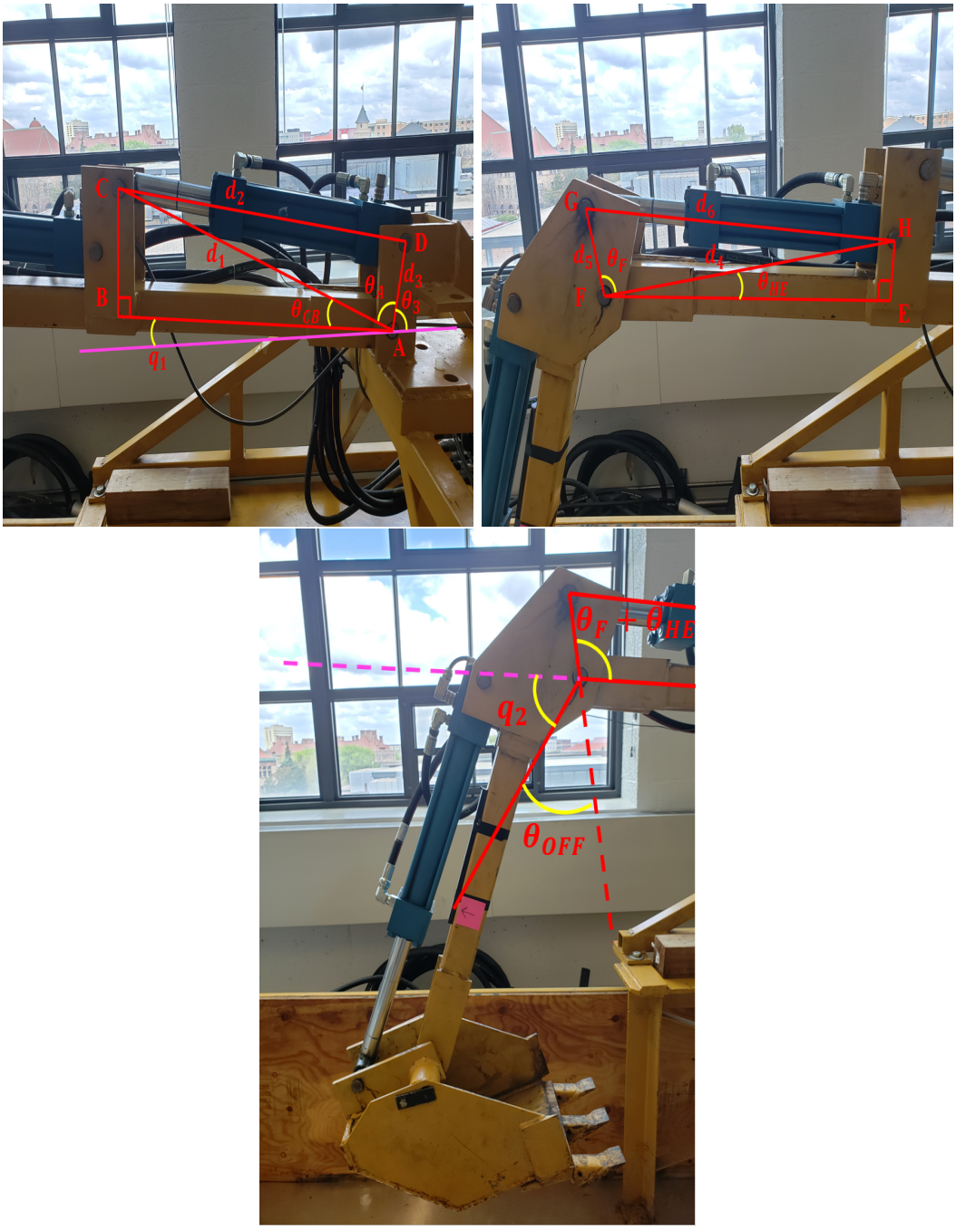

Figure 7.10: Geometric definitions for the backhoe boom and stick actuator [8]

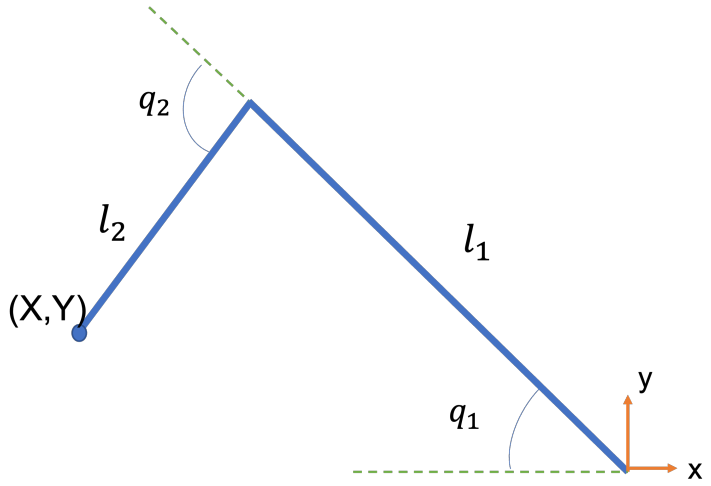

Figure 7.11: Backhoe skeletal diagram in cartesian frame with joint angles

2. Calculating joint angle for stick actuator where θ_{HE}, θ_{OFF} are constants and θ_F depends on stick actuator position x_{stick}:

$$d_6 = x_{stick} + l_{stick,retracted} \tag{7.7}$$

$$cos(\theta_F) = \frac{-d_6^2 + d_4^2 + d_5^3}{2d_4d_5} \tag{7.8}$$

$$q_2 = \theta_F + \theta_{HE} - \theta_{OFF} \tag{7.9}$$

3. The inverse relation between joint angles and actuator positions is given as:

$$x_{boom} = \sqrt{d_1^2 - d_3^2 - 2d_1d_3cos(\pi - \theta_3 - \theta_{CB} - q_1} - l_{boom,retracted} \tag{7.10}$$

$$x_{stick} = \sqrt{d_4^2 - d_5^2 - 2d_4d_5cos(q_2 - \theta_{HE} - \theta_{OFF}} - l_{stick,retracted} \tag{7.11}$$

The backhoe arm can be modeled as a 2-degree-of-freedom robot arm in Cartesian space, as illustrated in figure 7.11. The joint angles shown in the figure determine the position and orientation of the arm's end effector, which can be calculated using forward kinematics. Specifically, the end effector's coordinates can be obtained as a function of the joint angles, and are expressed as:

$$X = -l_1 cos(q_1) - l_2 cos(q_2 - q_1) \tag{7.12}$$

$$Y = l_1 sin(q_1) - l_2 sin(q_2 - q_1) \tag{7.13}$$

The end effector velocity in cartesian space v_x and v_y (same as $\dot{X}$ and $\dot{Y}$) can be mapped to the joint velocities in joint space using the Jacobian matrix (J). The Jacobian matrix is a function of the joint angles and describes the sensitivity of the end effector's position and orientation to changes in the joint angles. The relationship can be described as :

$$\begin{bmatrix} v_x \\ v_y \end{bmatrix} = J \begin{bmatrix} \dot{q}_1 \\ \dot{q}_2 \end{bmatrix} \tag{7.14}$$

$$J = \begin{bmatrix} l_1 sin(q_1) + l_2 sin(q_1 - q_2) & -l_2 sin(q_2) - l_2 \\ l_1 cos(q_1) + l_2 cos(q_1 - q_2) & -l_2 cos(q_2) - l_2 \end{bmatrix} \tag{7.15}$$

Here $\dot{q}_1$ and $\dot{q}_2$ can be expressed in terms of stick and boom actuator position and velocities and it can be obtained by differentiating q_1 and q_2 from equation (7.6) and equation (7.9). When the joystick positions are set to the desired values of v_x and v_y, (7.14) can be used to command the end effector without focusing on

individual actuator motions.

7.3.2 Pressure feedback design

The joystick control discussed so far is based solely on a velocity reference independent of the load that the machine experiences while attempting to track the reference. This can be dangerous to both the machine and its environment. A possible solution involves employing a haptic joystick to convey the load experienced by the machine through haptic feedback. However, an alternative method is to introduce force feedback directly into the generation of the reference velocity. This can be achieved without resorting to haptic interfaces, offering a simpler and more cost-effective solution. In this scheme, the operator can switch to this mode as needed.

To illustrate this concept, consider the scenario where the machine encounters an external load. Let $q_x \in \Re^2$ be actuator space coordinates (x_stick, x_boom), and $X \in \Re^2$ be the workspace (end effector) coordinates. Assume that the velocity command derived solely from the joystick position is denoted as $v_{d,X}$. When there's an external load (F_X) in Cartesian coordinates, the reference velocity is adjusted as follows:

$$v_{ref,X}(t) = v_{d,X}(t) - \gamma \cdot F_X(t) \tag{7.16}$$

where γ is a positive gain. Consequently, when the machine confronts an external load, it naturally slows down due to the modification of the reference velocity. If the operator wishes to operate at higher speeds, they must actively work to

increase the $v_{d,X}$ command. This velocity adjustment in equation (7.16) can also be expressed in terms of actuator coordinates:

$$v_{ref,q_x} = J^{-1}(q_x)v_{d,X} - \gamma \left[J^{-1}(q_x)J^{-T}(q_x)\right] F_{q_x} \tag{7.17}$$

Here, $J(q_x)$ represents the Jacobian, linking velocities and forces between actuator and Cartesian coordinates. The relationships between actuator forces (F_{q_x}) and Cartesian forces (F_X) are given by:

$$\dot{x} = J(q_x)\dot{q}_x \qquad \dot{q}_x = J^{-1}(q_x)\dot{x}$$
$$F_{q_x} = J^T(q_x)F_x; \qquad F_x = J^{-T}(q_x)F_{q_x}$$

This approach was implemented on a backhoe testbed, where the backhoe arm was used to lift the setup's body by pushing against the ground. Figure 7.12 provides a visual comparison of velocity references with and without force feedback and the load force acting on the lift actuator. Notably, as the external load increases, the velocity reference incorporating force feedback adapts to the load force, decreasing the velocity. This adaptation prevents rapid upward movement, enabling more controlled interaction with external forces.

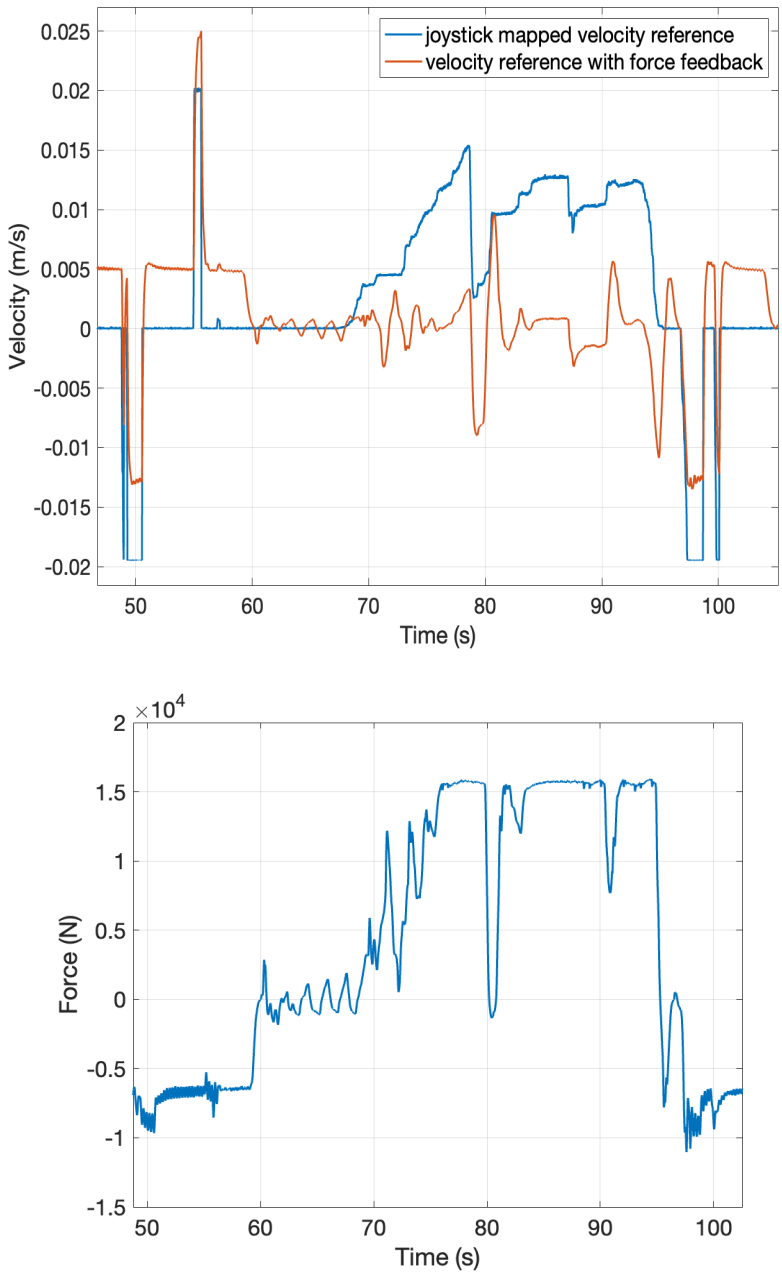

Figure 7.12: Velocity reference with force feedback and load force on boom actuator

7.3.3 Velocity Field Control

Coordinating multiple degrees of freedom in complex machines, such as the backhoe, is a challenging task that requires extensive experience. The operational tasks performed by off-road machines often involve a significant amount of repetition. For instance, consider the dig-lift-dump cycle. To aid inexperienced operators in carrying out such tasks, which typically involve coordinating the movements of various components, we can represent these tasks as velocity fields. By defining a desired velocity for each conceivable machine position, a velocity field can guide the machine to naturally adopt the necessary motion for the task at hand.

The field of robotic manipulators has seen a wide application of velocity field control techniques. One notable development in this area is the passive velocity field control (PVFC) approach, which was introduced by Li et al. [71] for contour following tasks in mechanical manipulators. In order to improve tracking performance, Li et al. later extended this approach by introducing an adaptive version that estimates the system's inertial parameters in real-time [72]. When a velocity field encoding does not exist for a particular contour, Li et al. [73] has developed a suspension technique that defines a velocity field on a manifold related to the configuration manifold of the system. This enables PVFC to be applied even in situations where a velocity field is not explicitly defined for the contour.

Kapitanyuk et al. [74] presents a novel approach for path-following control of nonholonomic mobile robots using a guiding vector field algorithm. The proposed algorithm generates a smooth vector field that guides the robot along the desired path while avoiding obstacles in the environment. The algorithm is based on

the idea of representing the path as a set of waypoints and generating a vector field that smoothly connects these waypoints. The vector field is designed to be attractive towards the path and repulsive away from obstacles. The algorithm uses a potential function to compute the vector field, which ensures that the robot follows the path while avoiding obstacles. They have formulated vector field designs for elliptical and Cassini Oval contours.

Treadway et al. [75] presents a study on the application of vector field control methods for controlling the motion of discretely variable passive robotic devices. The authors focus on devices that can switch between discrete configurations, such as origami-inspired robots. They use a switching function to smoothly transition between different vector fields as the robot changes its configuration. The authors evaluate the proposed approach through simulations and experiments on a prototype origami-inspired robot. The results show that the approach is effective in controlling the motion of the robot and in smoothly transitioning between different vector fields as the robot switches its configuration.

The majority of the work done in velocity field control has been implemented on robotic arms, teleoperation robots, passive walkers, etc. There have been very few implementations in off-road mobile machines. Zhang et al. [76] presents a study on trajectory planning and autodig for hydraulic excavators. The authors propose a new approach for trajectory planning and auto dig, which uses a combination of inverse kinematics and fuzzy control. The trajectories are time dependent making it difficult to change the digging rate or course on the fly. Iwano et al. [77] present a new approach to semi-autonomous control of a leader-follower

excavator system by proposing the use of admittance control to achieve synchronization and autonomy while incorporating bifurcation and stagnation for human interface. They have defined a velocity field for a digging task following two separate trajectories. In this case, human input is only required to change different digging paths or to come to a stop. With the existing human-machine interface available in off-road mobile machines it is possible to recalibrate the function of the joysticks to make the control of a specific task more intuitive by using velocity field control.

This section showcases the implementation of the velocity field control approach on the backhoe testbed. Specifically, a circular contour following task is employed to demonstrate the effectiveness of this control strategy. The operator utilizes the joystick to adjust both the rate of contour following and perform normal contour adjustments. This approach significantly simplifies the control of the backhoe when traversing complex contours, as the operator can concentrate on guiding the overall movement of the backhoe rather than managing individual actuator velocities.

Contour following with speed adjustment

An example task is for the end-effector to move along a circular path. For this example task, the velocity field is defined based on the distance of the end effector from the center of the circular contour. As it can be seen in the figure 7.13 the distance d from the center of the circle divides the cartesian space into 3 different zones. If the end effector is far from the contour then the field's velocity moves

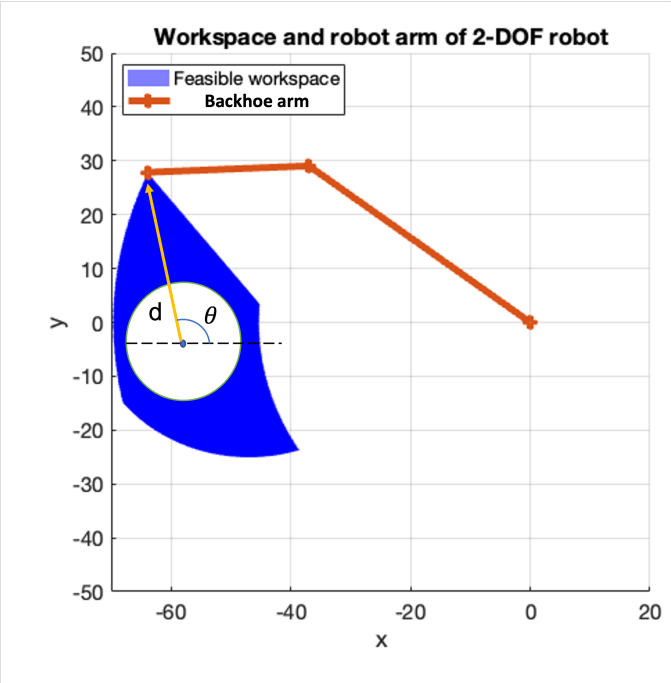

Figure 7.13: Backhoe workspace with circular contour

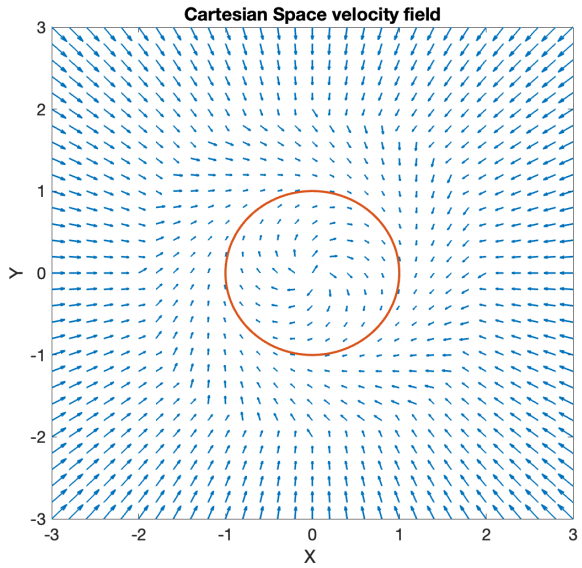

Figure 7.14: Velocity field for circular contour tracking

the end effector towards the contour in the radial direction based on the position of the end effector being outside or inside the contour. As the end effector approaches closer to the circle then the field contains both tangential and radial velocity components. If the end effector is on the circle there is only a tangential component - to move along the circle. The field in x direction (v_x) and y direction (v_y) can be defined as:

For $d > r + \delta$ or $d < r - \delta$

$$v_x = cos(\theta)\frac{r-d}{r} \tag{7.18}$$

$$v_y = sin(\theta)\frac{r-d}{r} \tag{7.19}$$

For $r - \delta \leq d \leq r + \delta$

$$v_x = cos(\theta)\frac{r-d}{r} - sin(\theta) \tag{7.20}$$

$$v_y = sin(\theta)\frac{r-d}{r} + cos(\theta) \tag{7.21}$$

Let x_c and y_c be the center of the circular contour and r be the radius of the circle. Then the distance d and angle θ can be defined as $\sqrt{(X-x_c)^2 + (Y-y_c)^2}$ and $\arctan(\frac{Y-y_c}{X-x_c})$. δ is the tolerance for a smooth transition. The spatial velocity field converging to a circular contour has been shown in figure 7.14. The velocity field associated with the circular contour is used as a reference for the end effector velocity (v_x, v_y). This velocity is then converted to joint velocity, and subsequently

used to determine the reference joint angle. The joint angles are then converted to position references for the actuators. The motion controller is then used to track the given reference trajectory. The joint velocity is given by :

$$\begin{bmatrix} \dot{q}_1 \\ \\ \dot{q}_2 \end{bmatrix} = \alpha J^{-1} \begin{bmatrix} v_x \\ \\ v_y \end{bmatrix} \tag{7.22}$$

In this particular context, the parameter α represents the gain that governs the rate at which the contour is traversed. It determines the speed of traversal along the contour. By mapping one of the degrees of freedom of the joystick linearly to α, the operator gains control over the traversal speed. When the joystick is in the neutral position, α is set to 0, resulting in no traversal along the contour. The maximum value of α is determined by the desired maximum traversal speed. This means that the operator only needs to manipulate the joystick to moderate the speed of traversal, without the need to control multiple degrees of freedom simultaneously.

This approach simplifies the task for the operator by reducing the control effort to a single degree of freedom. It allows the operator to focus on adjusting the traversal speed without being burdened by the complexities of coordinating multiple movements. As a result, the operator can achieve smoother and more efficient traversal of the contour.

To demonstrate the effectiveness of this approach, an experimental implementation is showcased in figure 7.15, where only one degree of freedom of the joystick

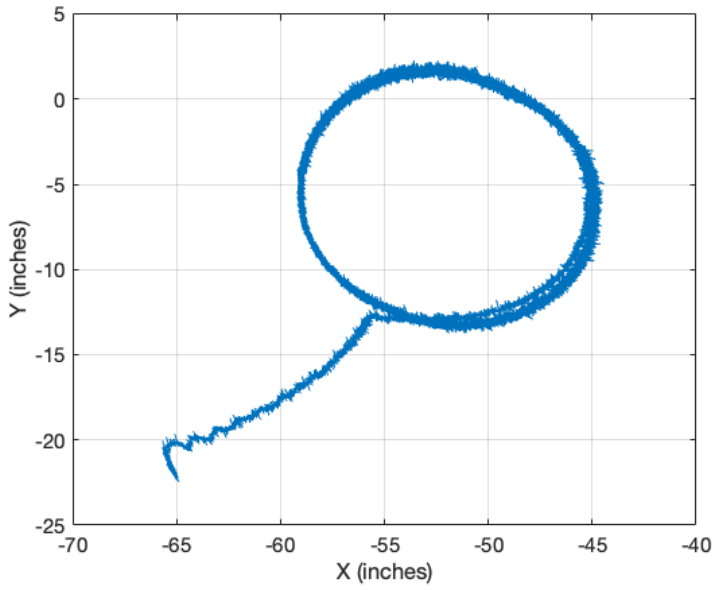

Figure 7.15: Experimentally validating velocity field control for circular contour

is utilized to traverse a circular contour. By simplifying the control task and enabling intuitive adjustment of the traversal speed, this approach enhances the operator's experience and facilitates more effective contour traversal for novice operators.

Normal contour adjustment

The circular contour serves as the nominal trajectory that the operator will follow for the majority of the task. However, it is possible that the operator may need to deviate from this path based on the interaction with the environment and task requirements. Therefore, the operator needs the ability to move normally to the nominal contour. To achieve this, a normal velocity field can be added such

that, when required, the operator can enable the field to make the end effector move normally to the nominal contour. The joystick can be utilized to control the rate or extent of the deviation from the circular contour. This provides the operator with the flexibility to make necessary adjustments during the task while still maintaining the overall trajectory.

To demonstrate this concept, we use the Cartesian space circular contour task demonstrated in previous sub section. Let $v_f(q) \in \Re^2$ be velocity field for the nominal contour task as described in equation (7.18) and equation (7.20). Now, let $v_{fn}(q) \in \Re^2$ be a normal velocity field (not shown) such that the inner product between them is $\langle v_f(q), v_{fn}(q) \rangle = 0$, $\forall q$. The resultant reference velocity to be tracked is defined as:

$$v_{d,x} = \alpha(t) v_f(q) + \beta(t) v_{fn}(q) \tag{7.23}$$

where $\alpha(t)$ and $\beta(t)$ correspond to the vertical and horizontal positions of a joystick control, respectively. These parameters act as scaling factors applied to the nominal and normal velocity fields. Consequently, by manipulating the joystick in the vertical direction ($\alpha(t)$), the operator can easily adjust the speed of following the intended circular trajectory. Conversely, if the operator wishes to divert from the predefined circular path, the joystick can be maneuvered horizontally ($\beta(t)$) to activate the orthogonal field. This dynamic feature empowers the operator with complete control over the machine's behavior. Such a design allows for seamless transitions between maintaining the circular trajectory and veering away from it, granting the operator a high degree of flexibility and responsiveness in their interactions with the machine.

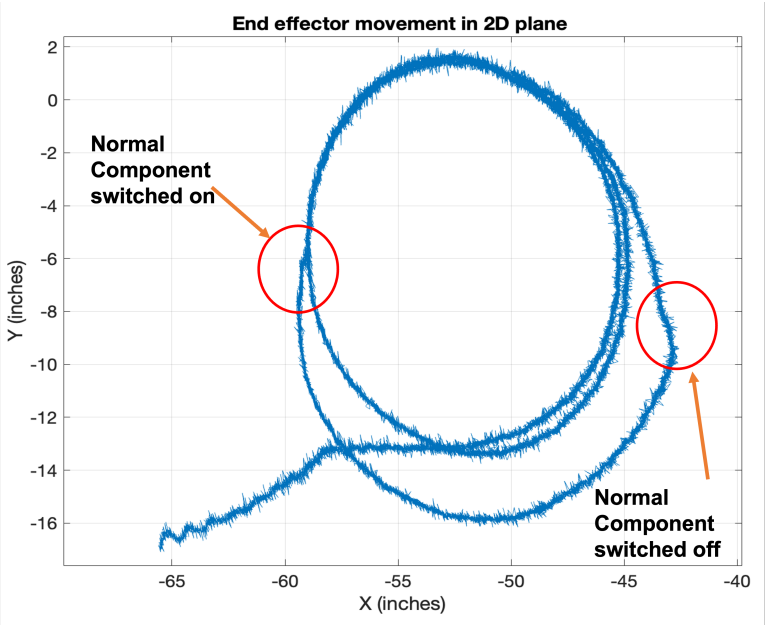

Figure 7.16: Demontrating intended deviation from the nominal trajectory

To illustrate this concept, an experimental demonstration is presented in figure 7.16 for the backhoe arm. It showcases how an operator can intentionally deviate from the nominal trajectory and then smoothly return to following the intended contour. This capability provides the operator with greater flexibility and control over the task, allowing for making changes to the trajectory on the fly without needing to stop.

Overall, Velocity field control can be utilized to enhance the interaction with off-road mobile machines, thereby making it easier to operate these machines. While the example shown was for a circular trajectory, this concept can be extended to any parametrized trajectory. A skilled operator can perform the task while their motion is captured, and the trajectory can be encoded in a velocity field. This enables a novice operator to perform the same task without having

to control multiple degrees of freedom. This approach simplifies the task for the operator, reduces the risk of errors, and improves the efficiency of the operation. Overall, this demonstrates the potential for using velocity field control as a tool for improving the operation of off-road mobile machines.

7.4 Chapter summary

The Hybrid Hydraulic Electric Architecture has been retrofitted to the boom and stick actuators of a backhoe arm. The motion of these actuators is controlled by a 2-degree-of-freedom joystick that is operated by a human operator. Unlike the previous chapter, where the future drive cycle data was known beforehand, for human-in-the-loop systems the control decisions need to be made based on present information. To address this challenge, a real-time rail switching algorithm has been developed that chooses pressure rails based on the proximity of the load force to the rail forces. If the selected pressure rails cause cavitation, the next closest rail force is used. For motion control, the joystick is mapped to a velocity reference, which is then fed to the developed motion control strategy that includes passivity-based backstepping control and least norm control for pressure rail switches. As the operator changes the joystick position, a velocity reference is sent to the motion control algorithm to track the desired reference. Experimental results have demonstrated that the real-time rail switching strategy is effective and the tracking performance, even with pressure rail switches, is impressive. There is a user delay of 80 ms between the joystick command and the actuator

response which is quite impressive for off-road mobile machines. Off-road machines typically require skilled operators to operate the human-machine interface. To simplify the operation of mobile machines, efforts have been made to modify the functions associated with the existing human-machine interface. One such effort is the demonstration of velocity field control, which enables a novice operator to use the joystick to change the rate of following a circular contour or make slight adjustments to the trajectory without having to coordinate multiple degrees of freedom. This approach makes controlling multiple degrees of freedom tasks easier, and hence a novice operator can perform such tasks with reduced risks, improved efficiency, and productivity.

Chapter 8

Conclusion

8.1 Research summary and contributions

The Hybrid Hydraulic Electric Architecture has been shown to save more than 55-70% of energy as compared to the Load Sensing system. However, while energy savings are critical, precise motion control is extremely crucial for off-road mobile machines as the utility of the vehicles depends on this. Various control system designs have been reviewed in chapter 1, but the HHEA has unique requirements as it involves pressure rail switches. Therefore, it is essential to carefully design and optimize the control system for the HHEA architecture to ensure precise and reliable motion control. In this thesis, a control strategy for HHEA architecture has been developed and successfully implemented on various hardware in the loop test stands.

The control strategy for the HHEA architecture involves a high-level controller

and a low-level controller. The high-level controller is responsible for optimizing the pressure rail choices to increase the energy-saving potential for the architecture. On the other hand, the low-level controller is responsible for the motion control of the multi-degree-of-freedom actuators. The primary objective of the motion control for HHEA is to track a desired position or velocity reference trajectory set by the operator using the HECM's electric motor torque as the control input. Two different controllers have been designed for two different operational zones. A nominal controller is designed for the duration between two pressure rail switches, and a transition controller is designed to handle pressure rail switches. The nominal controller is based on Passivity-based Backstepping Integral Control, which ensures the robustness of the system while providing accurate tracking of reference trajectories. The transition controller, on the other hand, is based on Least Norm Control, which minimizes the control input required to achieve a desired final state during a pressure rail switch.

The nominal controller formulated in (chapter 4) has demonstrated excellent tracking performance (under 0.1 mm peak tracking error), provided there are no restrictions on the electric motor torque. However, when the torque of the electric motor is saturated, the backstepping controller experiences tracking loss during pressure rail switches (peak tracking error 7mm during a switch). Thus, a separate controller has been developed in this thesis which has been formulated in chapter 5, to manage pressure rail switches. The transition controller reduces the peak error during a switch from 7 mm to 1mm while also reducing the control effort. The

recommended control strategy for this system is a combination of the passivity-based backstepping controller as the nominal controller and the least norm control as the transition controller. By leveraging the strengths of both controllers, this strategy creates a more robust and effective control system overall.

Two hardware-in-the-loop testbeds were constructed to validate the motion control strategy for the Hybrid Hydraulic Electric Architecture (HHEA). The maximum pressure rails for the two testbeds were set at 200 bar and 300 bar, respectively. The transformer setup employed to generate the middle pressure rail is a unique approach that is highly effective in maintaining rail pressure without throttling. Additionally, the load emulation module used to generate dynamic load forces on the test actuator has been effectively able to track desired duty cycles.

Compared to a feedforward PID controller, the nominal controller has demonstrated superior tracking performance by reducing the maximum tracking error from 10 mm to 5 mm. In all experimental tests, the nominal controller has consistently achieved a tracking error of less than 0.5% of stroke under nominal conditions, demonstrating the robustness of the control design. Furthermore, the least norm control strategy for transition control has been successfully applied in both isolated and multiple pressure rail switch cases. The tracking performance is improved when the transition controller is used during a pressure rail switch. In the experimental results presented in the thesis, the maximum tracking error has been reduced by more than 3 times when the transition controller is used during pressure rail switches (for 200 bar test stand). In the high-pressure test stand,

the impact of pressure rail switches is found to be relatively minimal due to the considerably slower dynamics of these switches compared to the 200-bar test stand (almost 10 times slower). This difference in dynamics is primarily attributed to the larger chamber volume present in the actuators of the high-pressure test stand. However, it's important to note that while the pressure rail switching dynamics are slower, this also results in higher switching losses.

Both testbeds have demonstrated the functionality and controllability of the HHEA architecture, along with the effectiveness of the motion control strategy under varying loading conditions. These test results are a stepping stone toward the commercialization of this architecture. The validation of the control strategy in the HHEA testbeds showcases the potential of this technology and provides a promising foundation for further development and commercialization.

The flexibility of the Hybrid Hydraulic Electric Architecture (HHEA) has been also demonstrated by retrofitting the system onto a backhoe, where the throttling valve used for actuation was replaced. A 2-degree of freedom joystick has been utilized to control the boom and stick actuators of the backhoe. However, since the future duty cycle trajectories are unknown when a human operator controls the actuators, a real-time switching algorithm has been developed to make pressure rail switching decisions based on the present load acting on the cylinder. While this approach is sub-optimal and doesn't consider energy-saving potential, it aims to make switching decisions based on the electric motor torque availability. The joystick commands from the operator are mapped into velocity references for the boom and stick actuators, which are then fed into the motion control strategy.

The motion controller is capable of tracking the reference velocity commanded by the operator for both boom and stick actuators with an 80 ms user-perceived delay. It's worth noting that the boom actuator, due to its higher inertia, is more tolerant to pressure rail switches causing smaller tracking errors than the stick actuator. Overall, the human-in-the-loop validation highlights the potential of the HHEA for use in real-world scenarios and its ability to adapt to different operating commands set by the user.

Off-road mobile machines can be challenging to operate when it comes to performing tasks that require controlling multiple degrees of freedom. The current human-machine interface for these machines is often complicated and difficult to manage. To simplify these coordinated tasks, velocity field control has been implemented. One example of this is demonstrated in a circular contour tracking task for the bucket. With velocity field control, the operator only needs to use a joystick to adjust the tracking rate or make slight adjustments to the circular nominal trajectory. They don't need to worry about controlling individual actuators to achieve the contour, as the system takes care of this automatically. Overall, velocity field control makes the execution of coordinated tasks more intuitive and easier to operate. It simplifies complex machine interfaces and streamlines the operator's actions, allowing them to focus on the task rather than struggle with the machine controls.

The Hybrid Hydraulic Electric architecture has tremendous potential to electrify off-road mobile machines in a cost-effective way. However, the controllability of the system is critical to the utility of mobile machines. This thesis has been

able to retire the risks associated with the controllability of HHEA by making these specific contributions:

1. Building a dynamic model for the HHEA system and developing a control strategy that enables precise motion control of actuators. This control strategy leverages passivity-based backstepping control design and least norm control to solve motion control challenges associated with HHEA.

2. Validating the motion control performance of the control strategy using a hardware-in-the-loop testbed with varying operating conditions. This helps to demonstrate the effectiveness of the control strategy in controlled simulated environments.

3. Investigating human-machine interaction for HHEA by building a human-in-the-loop testbed to understand real-world operation with human operators. This research provides insights into how operators interact with the HHEA system and how the system can be made more intuitive to control.

The work showcased in this thesis has so far resulted in the publication of three conference papers. The development of the transition control approach, detailed in chapter 5, has been published in a conference paper [66]. Additionally, The experimental results of the nominal controller shown in chapter 6 have been published in [69]. The findings pertaining to the validation of human-in-the-loop interactions and the endeavors aimed at enhancing the human-machine interface for off-road machinery, as presented in chapter 7 have been published in a peer-reviewed conference paper [78]. These publications highlight the progress and

importance of the research presented in this thesis.

8.2 Future work recommendation

The Hybrid Hydraulic Electric architecture is a relatively new technology, and the work done in a limited time has shown tremendous potential. However, there is still a significant amount of future work that needs to be done to optimize the system further and unlock its full potential.

1. To further establish the credibility of HHEA's energy-saving claims, conducting a demonstration of its benefits on a full-size off-road machine would provide tangible evidence and solidify its position as an effective solution for reducing energy consumption in heavy machinery. The HHEA system model presented in this thesis is considered a medium-fidelity model. While it provides valuable insights, it does have some limitations. One limitation is that it fails to accurately capture the pressure spikes that occur during a switch between pressure rails. Additionally, the model assumes constant pressure rails without considering the dynamics of accumulators. By developing a high-fidelity model, a more comprehensive understanding of the HHEA system dynamics can be achieved. Although the passivity-based backstepping controller, which utilizes integral control to reduce modeling uncertainties, is a robust control strategy, it requires an accurate estimation of cylinder friction to function optimally. Therefore, incorporating an adaptive parameter and friction estimator can enhance the robustness of the controller and

improve its ability to handle varying levels of friction, ultimately increasing its effectiveness in controlling the system.

2. The current transition control system has been shown to be effective in reducing tracking errors during pressure rail switches. However, there is still room for improvement. To enhance the system, a more accurate estimation of the pressure profile during a pressure rail switch is necessary to estimate the final state. It is worth noting that the assumption of a first-order hold on load force during the transition period may not be valid for a fast dynamic duty cycle with a longer transition period. Therefore, exploring the use of Closed-Loop Least Norm Control can make the transition control strategy more robust. Furthermore, the estimation of the duty cycle can be improved by implementing a Model Predictive Controller. This approach can lead to a more accurate estimation of the end states over the prediction horizon for the transition control system.

3. The current real-time rail switching algorithm has been designed to make switching decisions based on load force proximity to a rail force. However, it lacks an energy-saving optimization mechanism. To improve the algorithm, stochastic optimization methods should be explored to reduce losses in the system in real time, leading to more efficient energy usage. By incorporating these methods, the real-time rail switching algorithm can make optimal rail switching decisions based on energy-saving optimization, while ensuring that the size of the electric components is small. Currently, the load force is

estimated from the pressure measurements which can be noisy. The sliding mode can be used to estimate the external load forces more accurately [79]. In addition to the above consideration, it is important to explore the impact of the motion control algorithm on energy efficiency. One aspect to investigate is the accuracy of estimated energy consumption and losses using a static model. How does this static model compare to a dynamic model or experimental results that incorporate the actual control system dynamics? This empirical analysis can provide a clearer understanding of the control system's real impact on energy consumption, enabling us to fine-tune and improve the control strategy for better overall performance.

4. In a HHEA system, switching losses account for a significant portion of the total losses, approximately 25%. These switching losses are composed of throttling and compressibility losses. To decrease throttling losses, the valve opening and closing speed should be increased to reduce the time during which the valves are partially open. This technique can help minimize the duration of throttling losses. To reduce compressibility losses, implementing softswitching in HHEA can be explored [80][81][82].Softswitching involves raising the chamber pressure to the rail pressure before opening the valve to minimize compressibility losses. By adopting softswitching, switching losses can be reduced, and control becomes more straightforward as the rate of pressure change during the switch is regulated using this technique.

5. The human-machine interface proposed in this thesis is an effective means

of simplifying controls for novice operators. However, encoding the velocity field for different trajectories may require significant effort. It should be noted that the scope of the thesis has been limited to modifications within the existing interface (joysticks). A promising opportunity for further improvement could be to completely overhaul the interface, replacing joysticks with manipulators that can mimic all degrees of freedom. Additionally, exploring visual and haptic cues to guide operators could improve overall performance. The effectiveness of the velocity field control proposed in this thesis has not been tested. Therefore, a test study could be planned to evaluate the system. In this study, a skilled operator could perform a task, and then the same task could be performed by multiple novice operators, with productivity compared to the skilled operator. This type of study could provide valuable validation of the system and help identify areas for further improvement.

References

[1] R. Rahmfeld, M. Ivantysynova, and J. Weber, "Displacement controlled wheel loader–a simple and clever solution," in *Proceedings of the 4th International Fluid Power Conference, Dresden, Germany*, 2004, pp. 23–24.

[2] K. Heybroek, "Saving energy in construction machinery using displacement control hydraulics: Concept realization and validation," Ph.D. dissertation, Linköping University, 2008.

[3] W. Shen, H. Huang, Y. Pang, and X. Su, "Review of the energy saving hydraulic system based on common pressure rail," *IEEE Access*, vol. 5, pp. 655–669, 2017.

[4] V. Milo, H. Murrenhoff, and R. Leifeld, "STEAM – a hydraulic hybrid architecture for excavators," in *10th International Fluid Power Conference*, 2016.

[5] G. Xiaofan, L. Jacob, and A. Vacca, "A variable pressure multi-pressure rail system design for agricultural applications," *Energies*, vol. 15, no. 17, 2022. [Online]. Available: https://www.mdpi.com/1996-1073/15/17/6173

[6] P. Li, J. Siefert, and D. Bigelow, "A hybrid hydraulic-electric architecture (HHEA) for high power off-road mobile machines," *Proceedings of the ASME/BATH 2019 Symposium on Fluid Power and Motion Control FPMC2019*, 10 2019. [Online]. Available: https://www.osti.gov/biblio/1547072

[7] J. Siefert and P. Y. Li, "Optimal control and energy-saving analysis of common pressure rail architectures: HHEA and STEAM," in *BATH/ASME 2020 Symposium on Fluid Power and Motion Control*, ser. Fluid Power Systems Technology, 09 2020, v001T01A050. [Online]. Available: https://doi.org/10.1115/FPMC2020-2799

[8] R. Reich, "Point-and-follow gesture control of hydraulic arm using infrared camera feedback," Honor's Thesis, Department of Mechanical Engineering, University of Minnesota, 2019.

[9] L. Love, E. Lanke, and P. Alles, "Estimating the impact (energy, emissions and economics) of the US fluid power industry," *Oak Ridge National Laboratory (ORNL), TN*, 2012.

[10] M. Thornton, M. Ratcliff, and K. Kelly, "Off-road vehicle decarbonization and energy systems integration: R&d gaps and opportunities," National Renewable Energy Lab.(NREL), Golden, CO (United States), Tech. Rep., 2022.

[11] D. Padovani, M. Rundo, and G. Altare, "The Working Hydraulics of Valve-Controlled Mobile Machines: Classification and Review," *Journal of*

Dynamic Systems, Measurement, and Control, vol. 142, no. 7, 03 2020, 070801. [Online]. Available: https://doi.org/10.1115/1.4046334

[12] H. Pedersen, T. Andersen, and M. Hansen, "Load sensing systems - a review of the research contributions throughout the last decades," in *International Fluid Power Conference, Dresden, Germany*, 01 2004, pp. 125–139.

[13] R. Hippalgaonkar, M. Ivantysynova, and J. Zimmerman, "Fuel savings of a mini-excavator through a hydraulic hybrid displacement controlled system," in *Proceedings of the 8th International Fluid Power Conference, Dresden, Germany*, 2012, pp. 26–28.

[14] R. Ivantysyn and J. Weber, "Open circuit displacement control in a 300 t mining excavator," *ATZoffhighway worldwide*, vol. 10, pp. 48–53, 06 2017.

[15] J. Zimmerman and M. Ivantysynova, "Displacement controlled wheel loader - a simple and clever solution," in *Proceedings of the 12th Scandinavian International Conference on Fluid Power. Tampere, Finland,*, 2011.

[16] W. Shen, J. Jiang, X. Su, and H. Karimi, "Energy-saving analysis of hydraulic hybrid excavator based on common pressure rail," *The Scientific World Journal*, vol. 2013, pp. 560–694, 09 2013.

[17] S. Lee, "System configuration and control using hydraulic transformers," PhD Dissertation, Department of Mechanical Engineering, University of Minnesota, 2018.

[18] P. Gagnon, "Configuration and performance of hydraulic transformer power distribution systems," M.S. Thesis, Department of Mechanical Engineering, University of Minnesota, 2016.

[19] S. Li and P. Y. Li, "Passivity based backstepping control for trajectory tracking using a hydraulic transformer," in *ASME/BATH 2015 Symposium on Fluid Power and Motion Control*. American Society of Mechanical Engineers, 2015, p. V001T01A064.

[20] S. Lee and P. Y. Li, "Supervisory control for a switched mode hydraulic transformer," in *BATH/ASME 2018 Symposium on Fluid Power and Motion Control*. American Society of Mechanical Engineers, 2018.

[21] ——, "Passive control of a hydraulic human power amplifier using a hydraulic transformer," in *ASME 2015 Dynamic Systems and Control Conference*. American Society of Mechanical Engineers, 2015, pp. V002T27A004–V002T27A004.

[22] P. Y. Li, J. Siefert, and D. Bigelow, "A hybrid hydraulic-electric architecture (HHEA) for high power off-road mobile machines," in *BATH/ASME 2019 Symposium on Fluid Power and Motion Control*. American Society of Mechanical Engineers, 2019.

[23] D. Lewis, D. Lawhorn, and D. M. Ionel, "On the feasibility of electrification for large mobile cranes," in *2020 9th International Conference on Renewable Energy Research and Application (ICRERA)*, 2020, pp. 467–470.

[24] L. Schmidt, S. Ketelsen, M. H. Brask, and K. A. Mortensen, "A class of energy efficient self-contained electro-hydraulic drives with self-locking capability," *Energies*, vol. 12, no. 10, p. 1866, 2019.

[25] A. Niraula, S. Zhang, T. Minav, and M. Pietola, "Effect of zonal hydraulics on energy consumption and boom structure of a micro-excavator," *Energies*, vol. 11, p. 2088, 08 2018.

[26] S. Zhang, T. Minav, and M. Pietola, "Improving efficiency of micro excavator with decentralized hydraulics," in *ASME/BATH 2017 Symposium on Fluid Power and Motion Control*, 10 2017.

[27] S. Qu, D. Fassbender, A. Vacca, and E. Busquets, "A high-efficient solution for electro-hydraulic actuators with energy regeneration capability," *Energy*, vol. 216, p. 119291, 2021. [Online]. Available: https://www.sciencedirect.com/science/article/pii/S0360544220323987

[28] S. Qu, F. Zappaterra, A. Vacca, Z. Liu, and E. Busquets, "Design and verification of an open-circuit electro-hydraulic actuator system with an integrated electro-hydraulic unit," in *The 13th International Fluid Power Conference*, vol. 1, 6 2022. [Online]. Available: https://www.osti.gov/biblio/1872901

[29] D. Padovani, S. Ketelsen, D. Hagen, and L. Schmidt, "A self-contained electro-hydraulic cylinder with passive load-holding capability," *Energies*, vol. 12, p. 292, 01 2019.

[30] P. Casoli, F. Scolari, C. M. Vescovini, and M. Rundo, "Energy comparison between a load sensing system and electro-hydraulic solutions applied to a 9-ton excavator," *Energies*, vol. 15, no. 7, 2022. [Online]. Available: https://www.mdpi.com/1996-1073/15/7/2583

[31] H. Merritt, *Hydraulic Control Systems*. New York, NY: John Wiley & Sons, Inc., 1966.

[32] Y. Lin, "Controller design for hydraulic position control systems," Ph.D. dissertation, The University of Saskatchewan, 2011.

[33] L. Duc Hanh, K. K. Ahn, B. K. Nguyen, and W. Jo, "Trajectory control of electro-hydraulic excavator using fuzzy self tuning algorithm with neural network," *Journal of Mechanical Science and Technology*, vol. 23, pp. 149–160, 07 2009.

[34] T. N. Van, H. Q. Tran, V. X. Ha, C. Ha, and P. H. Minh, "Fuzzy feedback control for electro-hydraulic actuators," *Intelligent Automation and Soft Computing*, vol. 36, no. 2, pp. 2441–2456, 2023. [Online]. Available: http://www.techscience.com/iasc/v36n2/51147

[35] T. Andersen, M. Hansen, H. Pedersen, and F. Conrad, "Comparison of linear controllers for a hydraulic servo system," *Proceedings of the JFPS International Symposium on Fluid Power*, vol. 2005, 01 2005.

[36] M. Wang, Y. Wang, R. Yang, Y. Fu, and D. Zhu, "A sliding mode control strategy for an electrohydrostatic actuator with damping variable

sliding surface," *Actuators*, vol. 10, no. 1, 2021. [Online]. Available: https://www.mdpi.com/2076-0825/10/1/3

[37] H. M. Kim, S. H. Park, J. H. Song, and J. S. Kim, "Robust position control of electro-hydraulic actuator systems using the adaptive back-stepping control scheme," *Proceedings of the Institution of Mechanical Engineers, Part I: Journal of Systems and Control Engineering*, vol. 224, no. 6, pp. 737–746, 2010. [Online]. Available: https://doi.org/10.1243/09596518JSCE980

[38] M. Choux and G. Hovland, "Adaptive backstepping control of nonlinear hydraulic-mechanical system including valve dynamics," *Modeling Identification and Control*, vol. 31, pp. 35–44, 01 2010.

[39] P. Y. Li and K. Krishnaswamy, "Passive bilateral teleoperation of a hydraulic actuator using an electrohydraulic passive valve," *International Journal of Fluid Power*, vol. 5, no. 2, pp. 43–55, 2004.

[40] T. Nguyen, N. Doan, H. Park, and K. K. Ahn, "Trajectory control of an electro hydraulic actuator using an iterative backstepping control scheme," *Journal of Mechatronics*, vol. 29, pp. 96–102, 11 2014.

[41] G. Yang and J. Yao, "Nonlinear adaptive output feedback robust control of hydraulic actuators with largely unknown modeling uncertainties," *Applied Mathematical Modelling*, vol. 79, pp. 824–842, 2020. [Online]. Available: https://www.sciencedirect.com/science/article/pii/S0307904X19306626

[42] S. Zhang, S. Li, and F. Dai, "Integral sliding mode backstepping control of an asymmetric electro-hydrostatic actuator based on extended state observer," in *First International Electronic Conference on Actuator Technology: Materials, Devices and Applications*, vol. 64, 11 2020, p. 13.

[43] P. Y. Li and M. Wang, "Natural storage function for passivity-based trajectory control of hydraulic actuators," *IEEE/ASME Transactions on Mechatronics*, vol. 19, no. 3, pp. 1057–1068, July 2014.

[44] M. Wang and P. Y. Li, "Passivity based adaptive control of a two chamber single rod hydraulic actuator," in *2012 American Control Conference (ACC)*. IEEE, 2012, pp. 1814–1819.

[45] X. Zhang, S. Qiao, L. Quan, and L. Ge, "Velocity and position hybrid control for excavator boom based on independent metering system," *IEEE Access*, vol. 7, pp. 71 999–72 011, 2019.

[46] M. D. Elton, "Matching feedback with operator intent for effective human-machine interfaces," Ph.D. dissertation, Georgia Institute of Technology, 2012.

[47] P. Y. Li, "Hybrid hydraulic-electric architecture (HHEA) for mobile machines (DOE DE-0008384 Final Report)," 7 2022. [Online]. Available: https://www.osti.gov/biblio/1878730

[48] J. Siefert and P. Y. Li, "Optimal operation of a hybrid hydraulic electric architecture HHEA for off-road vehicles over discrete operating decisions," in *2020 American Control Conference (ACC)*, 2020, pp. 3255–3260.

[49] A. Khandekar, J. Wills, M. Wang, and P. Y. Li, "Incorporating valve switching losses into a static optimal control algorithm for the hybrid hydraulic-electric architecture (HHEA)," in *Fluid Power Systems Technology*, vol. 85239. American Society of Mechanical Engineers, 2021, p. V001T01A046.

[50] M. Vukovic, "STEAM: A mobile hydraulic system with engine integration," in *ASME/BATH 2013 Symposium on Fluid Power and Motion Control*, 10 2013.

[51] G. R. Bohach, Nishanth, E. Severson, and J. D. Van de Ven, "Modeling and Optimization Study of a Tightly Integrated Rotary Electric Motor-Hydraulic Pump," in *ASME/BATH 2019 Symposium on Fluid Power and Motion Control*, ser. Fluid Power Systems Technology, 10 2019, v001T01A010. [Online]. Available: https://doi.org/10.1115/FPMC2019-1626

[52] F. Nishanth, G. Bohach, M. M. Nahin, J. Van de Ven, and E. L. Severson, "Development of an integrated electro-hydraulic machine to electrify off-highway vehicles," *IEEE Transactions on Industry Applications*, vol. 58, no. 5, pp. 6163–6174, 2022.

[53] J. Siefert and P. Y. Li, "Optimal control of the energy-saving hybrid hydraulic-electric architecture HHEA for off-highway mobile machines,"

IEEE Transactions on Control Systems Technology, vol. 30, no. 5, pp. 2018–2029, 2022.

[54] R. Ding, X. Bing, J. Zhang, and M. Cheng, "Bumpless mode switch of independent metering fluid power system for mobile machinery," *Automation in Construction*, vol. 68, pp. 52–64, 08 2016.

[55] I. Malloci, L. Hetel, J. Daafouz, C. Iung, and P. Szczepanski, "Bumpless transfer for switched linear systems," *Automatica*, vol. 48, p. 1440–1446, 07 2012.

[56] G. Herbst, "Practical active disturbance rejection control: Bumpless transfer, rate limitation, and incremental algorithm," *IEEE Transactions on Industrial Electronics*, vol. 63, no. 3, pp. 1754–1762, 2016.

[57] K. Heybroek and J. Sjöberg, "Model predictive control of a hydraulic multichamber actuator: A feasibility study," *IEEE/ASME Transactions on Mechatronics*, vol. 23, no. 3, pp. 1393–1403, 2018.

[58] Y. Zhao, J. Zhao, J. Fu, Y. Shi, and C. Chen, "Rate bumpless transfer control for switched linear systems with stability and its application to aero-engine control design," *IEEE Transactions on Industrial Electronics*, vol. 67, no. 6, pp. 4900–4910, 2020.

[59] Y. Shi and X.-M. Sun, "Bumpless transfer control for switched linear systems and its application to aero-engines," *IEEE Transactions on Circuits and Systems I: Regular Papers*, vol. 68, no. 5, pp. 2171–2182, 2021.

[60] D. Zheng and A. Alleyne, "Modeling and control of an electro-hydraulic injection molding machine with smoothed fill-to-pack transition," *Journal of Manufacturing Science and Engineering*, vol. 125, p. 154, 02 2003.

[61] A. van der Schaft, *L2-Gain and Passivity Techniques in Nonlinear Control*, 3rd ed. Springer Publishing Company, Incorporated, 2016.

[62] D. Koditschek, "The application of total energy as a lyapunov function for mechanical control systems," *Contemporary Mathematics, American Mathematical Society, 1989*, vol. 97, 02 1989.

[63] R. Ortega, *Passivity-based control of Euler-Lagrange systems : mechanical, electrical and electromechanical applications*. Springer, 1998.

[64] M. Wang and P. Y. Li, "Displacement control of hydraulic actuators using a passivity based nonlinear controller," in *ASME 2012 5th Annual Dynamic Systems and Control Conference joint with the JSME 2012 11th Motion and Vibration Conference*. Ft. Lauderdale, FL, 2012, dSCC2012-MOVIC2012-8784.

[65] Y. Tan, J. Chang, H. Tan, and J. Hu, "Integral backstepping control and experimental implementation for motion system," in *Proceedings of the 2000. IEEE International Conference on Control Applications. Conference Proceedings (Cat. No.00CH37162)*, 2000, pp. 367–372.

[66] A. Chatterjee and P. Y. Li, "Motion control of hydraulic actuators in the presence of discrete pressure rail switching," in *2020 IEEE/ASME International Conference on Advanced Intelligent Mechatronics (AIM)*, 2020, pp. 1956–1961.

[67] J. B. Rosen, H. Park, and J. Glick, "Total least norm formulation and solution for structured problems," *SIAM Journal on Matrix Analysis and Applications*, vol. 17, no. 1, pp. 110–126, 1996. [Online]. Available: https://doi.org/10.1137/S0895479893258802

[68] F. M. Callier and C. A. Desoer, *Linear system theory*. Springer Science & Business Media, 2012.

[69] A. Chatterjee and P. Y. Li, "HIL testbed and motion control strategy for the hybrid hydraulic electric architecture (HHEA)," in *ASME/BATH 2021 Symposium on Fluid Power and Motion Control*, 2022.

[70] B. Helian, Z. Chen, and B. Yao, "Energy-saving and accurate motion control of a hydraulic actuator with uncertain negative loads," *Chinese Journal of Aeronautics*, vol. 34, 01 2021.

[71] P. Y. Li and R. Horowitz, "Passive velocity field control of mechanical manipulators," *Robotics and Automation, IEEE Transactions on*, vol. 15, no. 4, pp. 751–763, 1999.

[72] P. Li, "Adaptive passive velocity field control," in *Proceedings of the American Control Conference*, vol. 2, 07 1999, pp. 774 – 779 vol.2.

[73] P. Li and R. Horowitz, "Passive velocity field control (PVFC). part ii. application to contour following," *IEEE Transactions on Automatic Control*, vol. 46, no. 9, pp. 1360–1371, 2001.

[74] Y. A. Kapitanyuk, A. V. Proskurnikov, and M. Cao, "A guiding vector-field algorithm for path-following control of nonholonomic mobile robots," *IEEE Transactions on Control Systems Technology*, vol. 26, no. 4, pp. 1372–1385, 2018.

[75] E. Treadway and R. B. Gillespie, "Vector field control methods for discretely variable passive robotic devices," *IEEE Transactions on Robotics*, vol. 37, no. 2, pp. 375–389, 2021.

[76] B. Zhang, S. Wang, Y. Liu, and H. Yang, "Research on trajectory planning and autodig of hydraulic excavator," *Mathematical Problems in Engineering*, vol. 2017, pp. 1–10, 05 2017.

[77] K. Iwano and M. Okada, "Semi-autonomous control of leader-follower excavator using admittance control for synchronization and autonomy with bifurcation and stagnation for human interface," in *2020 IEEE/RSJ International Conference on Intelligent Robots and Systems (IROS)*, 2020, pp. 11 525–11 530.

[78] A. Chatterjee and P. Y. Li, "Human-in-the-loop motion control of a two-dof hydraulic backhoe powered by the hybrid hydraulic electric architecture

(HHEA)," in *ASME/BATH 2023 Symposium on Fluid Power and Motion Control*, no. FPMC2023-111819, 2023.

[79] M. Ruderman, L. Fridman, and P. Pasolli, "Virtual sensing of load forces in hydraulic actuators using second-and higher-order sliding modes," *Control Engineering Practice*, vol. 92, 09 2019.

[80] A. Yudell and J. D. Van de Ven, "Soft switching in switched inertance hydraulic circuits," *Journal of Dynamic Systems, Measurement, and Control*, vol. 139, 05 2017.

[81] M. B. Rannow and P. Li, "Soft switching approach to reducing transition losses in an on/off hydraulic valve," *Journal of Dynamic Systems, Measurement, and Control*, vol. 134, pp. 613–620, 01 2009.

[82] B. Beckstrand and J. D. Van de Ven, "Experimental validation of a soft switch for a virtually variable displacement pump," *ASME/BATH 2014 Symposium on Fluid Power and Motion Control, FPMC 2014*, 09 2014.

Appendix A

Parameters and Intrumentation

Table A.1: Backhoe Kinematics

Parameter	**Symbol**	**Value**
Length of link 1	l_1	47 in
Length of link 2	l_2	24 in
Refer to figure 7.10	d_1	23.56 in
Refer to figure 7.10	d_3	5.08 in
Refer to figure 7.10	d_4	21.87 in
Refer to figure 7.10	d_5	4.59 in
Refer to figure 7.10	θ_{CB}	17.28 deg
Refer to figure 7.10	θ_{HE}	10.54 deg
Refer to figure 7.10	θ_{OFF}	33.43 deg
Continued on next page		

Table A.1 – continued from previous page

Parameter	Second column	Third column
Refer to figure 7.10	θ_3	80.07 deg in
length of the retracted boom	$l_{boom,retracted}$	20.25 in
length of the retracted stick	$l_{stick,retracted}$	20.25 in

Table A.2: Instrumentation for UMN testbed

Device	Specification	Manufacturer
Data Acquisition Card	Analog and digital I/O	Humusoft, MF-634
Pressure Sensors	3000 psi	Honeywell
Encoders	Optical 40000 cont/rev	US Digital
Switching Valves	120 lpm 16 bar ΔP	CMA-90
Electric motor	3ph-230 V, 5KW	Clearpath MCPV
Servo Valve	9.5 lpm	Moog (760C261A)
Gear pump	8.4 cc, 3000 rpm	Eaton
OPAM	100mA output current	LM 7171
Hydraulic Cylinder	2 in Bore, 8 in stroke	WEN
CAN Interface	ATmega2560 microcontroller	Arduino MEGA
Coupling	L-100 jaw coupling	Lovejoy

Continued on next page

Table A.2 – continued from previous page

Device	Specification	Manufacturer
Hydraulic Transformer	8 cc, 3000 rpm	Danfoss
Regen Shunt	250W Continuous	Teknic RES-225
Serial Board	3.3-5V	RS232 board
A-D Converter	(15-30V), (0-10V,4-20mA)	Teknic ASU-FR510

Table A.3: Instrumentation for high pressure testbed

Device	Specification	Manufacturer
DAQ	Analog and digital I/O	Humusoft, MF-634
Pressure Sensors	350 bar	Wika
Hydraulic pump	49 cc variable	Eaton 72400 Series
Switching Valves	90 lpm 16 bar Δ P	CMA-90
Electric motor	3ph-230 V, 5KW	Clearpath MCPV
Switching Valve	60 lpm, 16 bar drop	Eaton SiCV
Gear pump	8.4 cc, 3000 rpm	Eaton
Hydraulic Cylinder	1.38in Rod, Cap 3.25in	Eaton
CAN Interface	ATmega2560 microcontroller	Arduino MEGA
Coupling	L-100 jaw coupling	Lovejoy

Continued on next page

Table A.3 – continued from previous page

Device	Specification	Manufacturer
Relay Board	0-5 V 2 channel	Hiletgo
Regen Shunt	250W Continuous	Teknic RES-225
Serial Board	3.3-5V	RS232 board
A-D Converter	(15-30V),(0-10V,4-20mA)	Teknic ASU-FR510

Table A.4: Instrumentation for backhoe testbed

Device	Specification	Manufacturer
Data Acquisition Card	Analog and digital I/O	NI
Pressure Sensors	3000 psi	Honeywell
Switching Valves	120 lpm 16 bar ΔP	CMA-90 5 section
Boom electric motor	3ph-230 V, 5KW	Clearpath MCPV
Stick electric motor	3ph-230 V, 986 W	Clearpath MCPV
Axial piston pump	10 cc, 3000 rpm	Parker F-11
Gear pump	3.3 cc, 3000 rpm	Danfoss
Boom Cylinder	2.5 in bore, 1.75 in rod	Eaton
Stick Cylinder	2 in bore, 1.375 in rod	Eaton
CAN Interface	ATmega2560	Arduino MEGA

Continued on next page

Table A.4 – continued from previous page

Device	Specification	Manufacturer
Coupling	L-100 jaw coupling	Lovejoy
Regen Shunt	250W Continuous	Teknic RES-225
Serial Board	3.3-5V	RS232 board
A-D Converter	(15-30V),(0-10V,4-20mA)	Teknic ASU-FR510